Autonomous Control and Membrane Maintenance Optimization of Photovoltaic Reverse Osmosis Systems

by

Aditya Sarvanand Bhujle

Bachelor of Science with Honors, Mechanical Engineering and Business Economics & Management
California Institute of Technology, 2010

Submitted to the Department of Aeronautics and Astronautics
in Partial Fulfillment of the Requirements for the Degree of
Master of Science in Aeronautics and Astronautics

at the

MASSACHUSETTS INSTITUTE OF TECHNOLOGY

February 2013

Signature of Author: .....
Department of Aeronautics and Astronautics
January 29, 2013

Certified by: .....
Richard M Wiesman
Professor of the Practice of Mechanical Engineering
Thesis Supervisor

Accepted by: .....
Eytan H. Modiano
Professor of Aeronautics and Astronautics
Chair, Committee on Graduate Students

Autonomous Control and Membrane Maintenance Optimization of Photovoltaic Reverse Osmosis Systems

by

Aditya Sarvanand Bhujle

Submitted to the Department of Aeronautics and Astronautics
on January 29, 2013 in Partial Fulfillment of the
Requirements for the Degree of Master of Science in
Aeronautics and Astronautics

ABSTRACT

The supply of clean water in remote and off-grid areas has been a major global challenge for humanity. Over 780 million people lack access to clean water [1]. However, a significant fraction of these people have access to undrinkable surface, brackish or sea water. A promising solution to this problem is to use photovoltaic powered reverse osmosis (PVRO) systems to purify this unsafe water to produce clean drinking water. However, high initial capital costs and a lack of commercial viability have prohibited these systems for commercial and daily use.

For this approach to be feasible and reach large-scale commercial viability, PVRO systems need to be energy efficient and cost-competitive compared with reverse osmosis systems powered by conventional sources, such as diesel engines or electricity from the grid. The costs and energy consumption in a PVRO system can be significantly decreased by maximizing water production and minimizing the effects of membrane degradation to extend system life. The membrane degradation considered here is the fouling phenomenon in which suspended solids and dissolved substances collect on the surface and within the pores of the membrane thereby reducing its permeability

This thesis describes an innovative approach to autonomously controlling and optimizing community scale PVRO systems by controlling membrane degradation due to fouling, using a self-optimizing condition based maintenance algorithm. Additionally, by exploiting the energy compliance of PVRO elements and actively controlling the individual components of the system, water production can be maximized. The compliance in a PVRO system has been found to significantly affect PVRO performance by reducing system efficiency and resulting in long startup delays in producing clean water.

In this thesis, a controllable recovery ratio concept system has been presented. By actively controlling the PVRO system, an improvement of 47% over the existing performance of a fixed recovery ratio system has been shown in simulations. Use of condition based maintenance strategies show an improvement of over 10% in cumulative clean water production compared to scheduled quarterly maintenance and 58% over 1 year in cumulative clean water production compared to the case without any maintenance. This is interesting since typical community scale

and point of use systems can be and are operated without periodic maintenance [2]. Combining the optimal power control and condition-based maintenance strategies, an improvement in water production of 85 % is shown for a July day in Boston over the MIT PVRO system. Finally, a self-optimizing condition based maintenance algorithm is proposed as the optimal solution to control membrane degradation due to fouling.

Thesis supervisor: Richard M Wiesman
Title: Professor of the Practice of Mechanical Engineering

ACKNOWLEDGEMENTS

As life progresses and one moves from one peak to another, several people enter and exit our lives who make the journey worth travelling. I have been extremely fortunate to have had such people and institutions in my life who have not only made the journey thus far memorable but have inspired me for the journey that is about to begin. Unfortunately, I have never been able to thank them enough for this. Hence, I would like to take this opportunity to say a big thank you to one and all; my family, professors, teachers, close friends, and associates for their support, encouragement and guidance that has helped me achieve the things that matter to me.

I would like to thank Professor Steven Dubowsky and Professor Richard Wiesman for giving me the opportunity to work on the *Design and Manufacturing of Solar Power Systems and Devices for Challenging Environments* project in the Field and Space Robotics Laboratory at MIT. I sincerely appreciate the efforts of Professor Wiesman and Professor Dubowsky towards mentoring and advising me during my research and graduate studies.

I would like to thank the King Fahd University of Petroleum and Minerals in Dhahran, Saudi Arabia for sponsoring this research program through the Center for Clean Water and Clean Energy at MIT and KFUPM.

During my time here at MIT, I have had the great privilege of meeting and working with some fantastic people, specifically my colleagues in the FSRL. It has been great fun working with and learning from Jekan, Francesco, Dan, Amy, Leah, Beth, Roman, Jamie, Marco, Carolina, Huichao, Lifang, Li, Mei, Irina and Mai. An additional thank you goes out to Jekan Thangavelautham and Leah Kelley for reading and providing feedback on this thesis.

CONTENTS

LIST OF FIGURES

LIST OF TABLES

CHAPTER

1

INTRODUCTION

This thesis describes the work done towards better understanding the transient and steady state characteristics, and performance degradation of community scale photovoltaic reverse osmosis (PVRO) systems. This understanding is used to develop autonomous control and membrane maintenance optimization methods to improve the performance of PVRO systems, thereby making them more cost-effective. This work is part of ongoing research in the Field and Space Robotics Laboratory (FSRL) at MIT. Other contributions of this FSRL research project include the design and control of a thermal management system [3], the design of a controllable energy recovery device with experimental validation [4] and modular design architecture [5] for PVRO systems. The motivation for this research, the objective of this research and the organization of this thesis is presented in this chapter.

1.1 Motivation

Clean water and energy security are a major threat to the prosperity of humanity. Over 780 million people lack access to clean water and this presents a global crisis [1]. A majority of these people are scattered in rural and remote areas in the Middle East, Asia and Africa. Supplying these people with potable water is a complex and expensive mission. A majority of these people inhabit coastal areas or areas with substantial ground or surface water. The abundance of sea and ground water coupled with high solar insolation make solar powered desalination a natural solution. Photovoltaic reverse osmosis (PVRO) systems offer a viable solution to supply clean water to these remote communities.

Another application for this technology is mobile, on-site water production systems in war-torn and disaster areas. Providing access to clean water is critical to stabilizing these areas, particularly for peace keeping operations by armed forces [8]. Typically, transporting fossil fuels

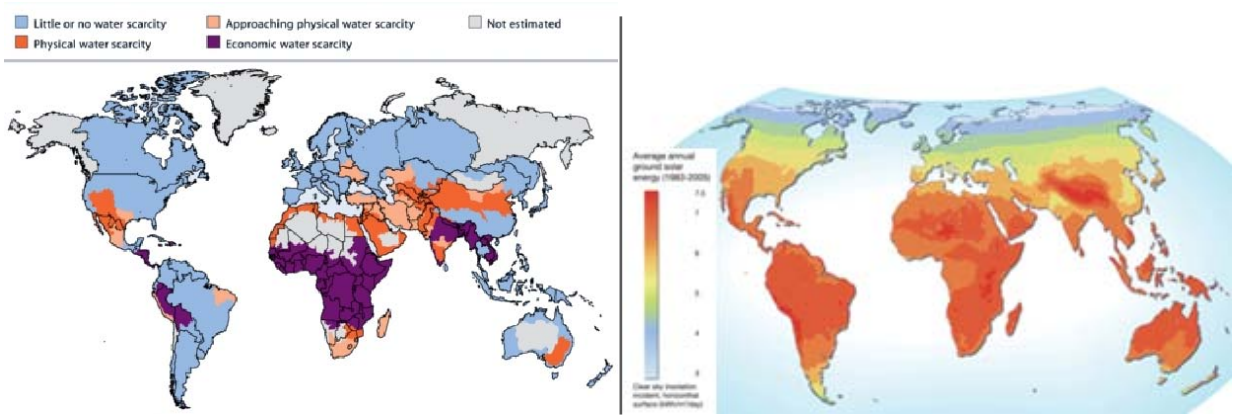

Figure 1-1: Areas of physical and economic water scarcity (left) [6] and average annual ground solar insolation (right) [7]. Credit: Hugo Ahlenius, UNEP/GRID-Arendal

to these areas is expensive and water supply infrastructures tend to be damaged or unusable for extended periods of time. One option is to use solar powered portable desalination systems that can produce potable water from sea, ground or surface water without drawing from non-renewable fossil fuels.

For solar powered desalination to be feasible, these systems must be energy efficient and cost-competitive with reverse osmosis systems powered by conventional sources, such as diesel engines. The costs and energy consumption of a solar-powered reverse osmosis system can be reduced by optimally controlling the system in real-time to maximize clean water production by increasing its efficiency.

1.1.1 Photovoltaic Reverse Osmosis Desalination is a Solution

The supply of clean water to remote areas has always been a great challenge. A solution to this problem is to use photovoltaic powered reverse osmosis (PVRO) systems. However, high initial capital costs and a lack of commercial viability have prohibited the use of these systems for commercial purposes and daily use. This research focuses on making community scale systems practical. Community scale systems are small scale systems that are capable of producing 500 to 10000 liters of clean water in one day.

Figure 1-2 shows the geographic areas where current state of the art PVRO technology is economically feasible when compared with diesel powered desalination systems at the

community scale [9]. The impact of a 25% improvement is seen by the increase in the geographical areas that become economical [9].

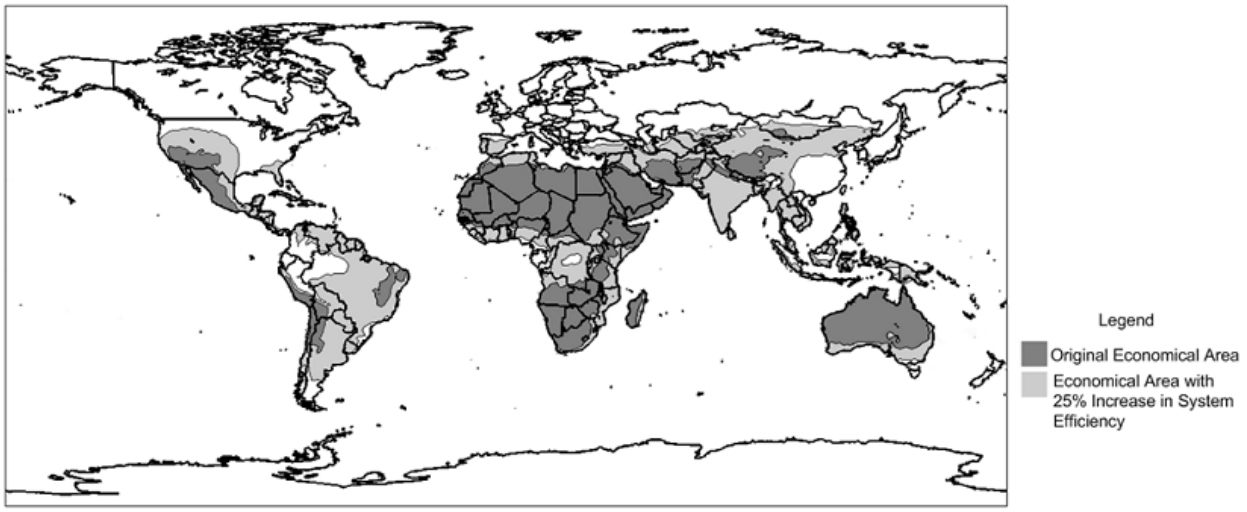

Figure 1-2: Economic feasibility of PVRO systems with state of the art technology and with a 25% improvement in system efficiency. Figure by Amy Bilton, used with permission [9]

1.1.2 Need for Controlling Degradation of Membranes

Over time, RO membranes degrade due to scaling and fouling. The International Union of Pure and Applied Chemistry (IUPAC) defines membrane fouling as a process resulting in loss of performance of a membrane due to the deposition of suspended solids, or dissolved substances on its external surfaces, at its pore openings or within its pores. Fouling and scaling need to be effectively controlled since they result in reduction of clean water flow through the membrane, reduction in effective membrane area, reduction in clean water quality and an increase in energy consumption. Additionally, membranes that get fouled or scaled need to be replaced more frequently, and this results in an increase in operational costs, rendering the actual costs of the permeate water much higher than expected.

There are several factors that affect the rate of fouling, which are discussed in detail in Chapter 4. An effective solution for small scale PVRO systems is to use preventive and condition based maintenance schedules that can keep the system running efficiently and in a cost effective manner.

1.1.3 Need for Power Modeling and Control

Reverse Osmosis is an energy intensive process. Unlike large scale sea water desalination plants, small scale PVRO plants are more energy intensive due to the lack of economies of scale [9]. Thus optimizing a small PVRO system to increase its efficiency can have significant implications and make it a clean, viable solution for large parts of the globe.

Figure 1-3 shows the breakdown of the energy consumption for the different stages in the sea water reverse osmosis process. The high pressure pumps that pressurize the feed water consume about 84% of the total energy in a sea water desalination plant. Thus, from a power optimization perspective, the high pressure pumping stage is the main area to focus our optimization efforts.

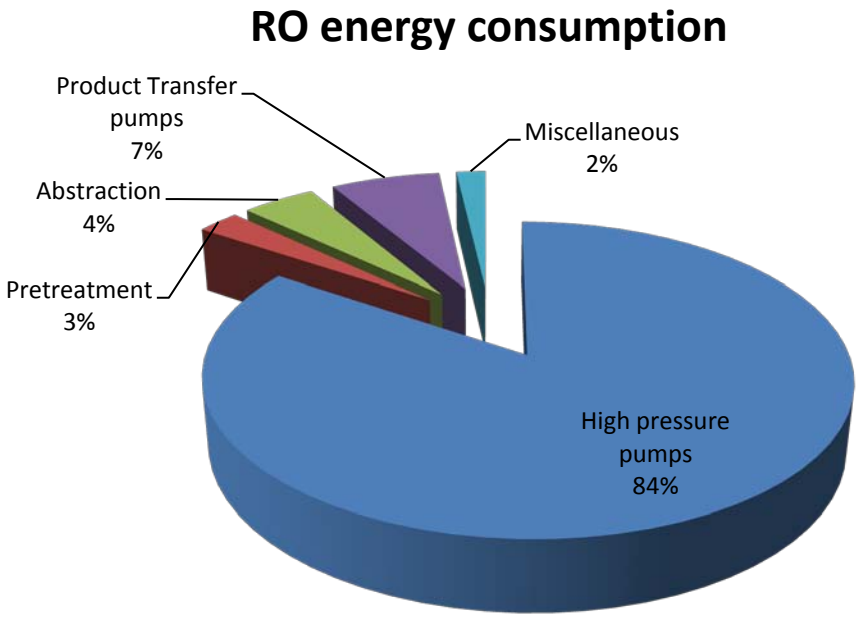

Figure 1-3: Energy consumption for different stages in sea water reverse osmosis desalination [10]

1.2 Research Objective

The objective of this research is to make photovoltaic reverse osmosis (PVRO) technology cost effective by maximizing water production. This requires improving system efficiency and

begins with modeling the system, followed by developing power and fouling control algorithms for PVRO systems to optimize their performance and thus decrease the final water cost. Avoiding full-time skilled operators for community-scale PVRO applications is critical to keep this approach cost-effective. Therefore autonomy is important and hence the control algorithms must control and optimize system output in real time in response to constantly changing conditions, such as varying water and air temperature, instantaneous solar radiation (insolation) and prevent conditions that would lead to membrane degradation and fouling. Eliminating the need for batteries that are used in conventional PVRO systems can reduce maintenance and substantially decrease the life-cycle cost. This study has developed transient and steady state models of PVRO systems, and control algorithms that optimize the maintenance schedules of the system and maximize the water produced by the system.

1.3 Thesis Organization

This thesis is comprised of 7 chapters. This chapter introduces the research topic and discusses the motivation for the research, and the objective of this work: improving the performance of a PVRO system by autonomous control and optimization of membrane maintenance scheduling. Chapter 2 gives an overview of PVRO technology and a literature review for the power modeling, fouling modeling, and control of reverse osmosis systems. Chapter 3 discusses the physics and working of PVRO systems and defines the fundamental relationships governing them. An energy compliance-based steady state system model is presented. Chapter 4 discusses the issues related to fouling control of PVRO systems, such as the feed and product water chemistry and standards, fouling causes, mechanisms, and prediction, pretreatments, types of membrane cleaning, and the influence of system operational parameters on the fouling of a system. Chapter 5 presents the total costs, capital costs and operation and maintenance costs of PVRO and large scale desalination systems. Chapter 6 covers the maintenance scheduling for autonomous PVRO systems. Simulations showing the effectiveness of frequency based and condition based maintenance schemes are presented. Finally, a case is made for real time self optimizing condition based maintenance algorithms. Chapter 7 presents a summary of the work and recommendations for future work. Appendix A presents the detailed power modeling and control feasibility of PVRO systems. Two models are introduced: a simplistic steady state model,

and an energy compliance based steady state system model. Significant work has been done on developing a set of physics based models to understand the transient, steady state and long-term degradation behaviors of a PVRO system. The compliance model was derived using empirical estimates and has been experimentally validated. Using these models, the feasibility of optimal control to maximize performance of a PVRO system is shown.

CHAPTER

2

BACKGROUND AND LITERATURE REVIEW

This chapter presents an overview of the PVRO technology. The MIT PVRO experimental system is described in detail. This chapter reviews state-of-the-art technical literature on the challenges and strategies for power modeling, fouling modeling and control of reverse osmosis systems.

2.1 PVRO System Technology

The basic structure of a typical community-scale PVRO system is assumed to consist of solar panels, high-pressure pumps, reverse osmosis membranes and energy recovery devices, as shown in Figure 2-1. The control system optimally adjusts the operating points of the individual components based on the key variables that affect water production, including solar panel temperature, electrical power from the solar panels and feed water characteristics. The complexity lies in the interdependencies throughout the system and the coupling between the components' operating characteristics.

Small scale PVRO systems have been developed and tested, and are now commercially available [11-17]. These systems are classified as brackish water or seawater systems. Brackish water PVRO systems operate at high recovery ratios and hence do not always use energy recovery systems. However, the Solarflow system developed and tested in Australia uses an energy recovery system [11]. Seawater PVRO systems typically have energy recovery devices, since the recovery ratios are lower than those for brackish systems and hence there is a lot of energy in the brine stream that can be recovered. These PVRO systems typically use batteries for energy storage, with exception of the system developed by Thomson et al. [12].

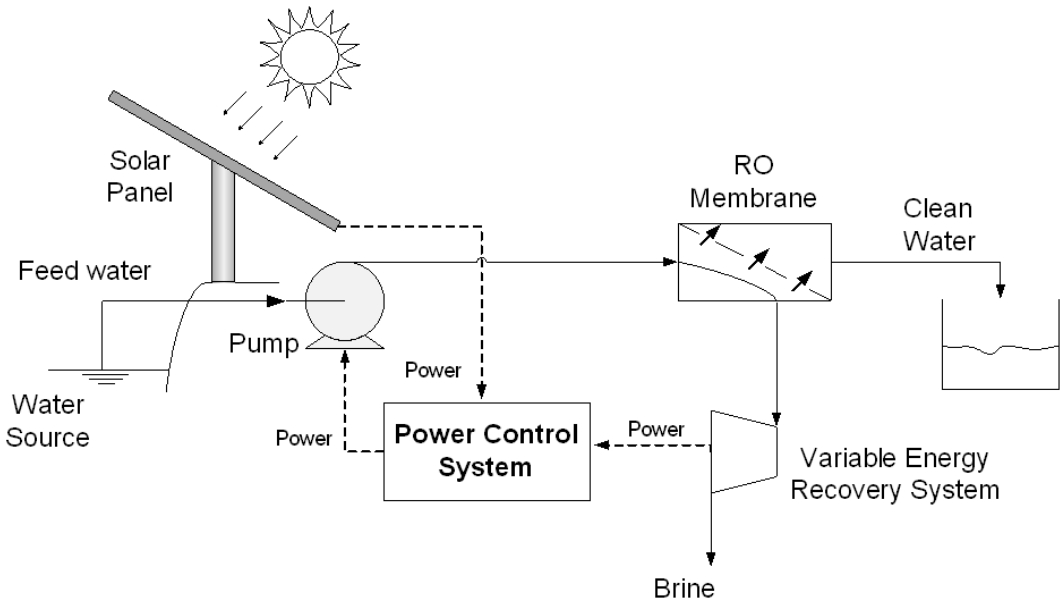

Figure 2-1: A typical photovoltaic reverse osmosis system, adapted from figure in [3] by Leah Kelley

2.1.1 Photovoltaics

Photovoltaic panels are used to generate electricity from incident solar radiation as per the photovoltaic effect. Photovoltaic panels are made up of solar cells which are made of materials that exhibit the photovoltaic effect. A solar cell is made by joining two separate layers of semiconducting materials. One layer forms the p-type (positive side) and the other layer forms the n-type (negative side) depending on the type of impurity added to the semi conductor's crystal lattice during the doping process. Pentavalent impurities (atoms with 5 valence electrons) produce n-type semiconductors by adding an extra electron while trivalent impurities (atoms with 3 valence electrons) produce the p-type semiconductor by creating an electron deficiency. When a photon hits the solar cell with an energy level higher than the threshold energy required to overcome the band gap, electrons jump from the valence band to the conduction band. The electron moves through the outer circuit and the hole moves through the semiconductor and combine at the on the other side this producing electricity [13].

The solar panels are classified on the basis of the material used. The major types of solar cells are monocrystalline silicon, polycrystalline silicon, amorphous silicon, dye-sensitized solar cells, organic solar cells, multi-junction photovoltaics, and thin film photovoltaics such as copper indium gallium selenide (CIGS), cadmium telluride and silicon thin film. The type of material

used affects the efficiency of light to electricity power conversion, since different materials behave differently when exposed to the various components of the light spectrum. The efficiency of a solar cell is defined as the ratio of the electrical power generated to the incident solar radiation. These efficiencies are calculated at 25 C and solar radiation of 1000 W/m^2 [14]. Under the AM1.5 spectrum (1000 W/m^2 ~ 1sun), crystalline silicon can achieve an efficiency of 25% while thin film gallium arsenide can achieve 28.8% [14]. Multi-Junction PV has the highest solar cell conversion efficiencies. Sharp's multijunction device has achieved 37.5% under 1 sun and 43.5% under 306 suns [14, 15].

The solar panels produce current and voltage as a function of the incoming solar radiation, panel temperature and load characteristics. Varying levels of sunlight due to atmospheric conditions such as cloud cover will affect the electric current produced.

2.1.2 Desalination and Reverse Osmosis

Water treatment technologies can be broadly classified into physical and chemical treatment technologies. Both types are used to treat water to remove suspended solids, dissolved solids and microorganisms. Physical treatment technologies include coagulation, settling/flotation, membrane filtration, multi-stage flash (MSF), multi-effect distillation (MED), vapor compression distillation, electro dialysis (ED), heat treatment, aeration/deaeration, UV radiation and acoustic techniques. Chemical treatment includes precipitation, ion exchange, demineralization, adsorption, acid/alkaline treatment, corrosion inhibitors, chlorination, halogen treatment, metallic treatment and oxidants [16].

The major desalination technologies are MSF, MED, VCD, and membrane technologies such as nanofiltration (NF) and reverse osmosis (RO). The choice of desalination technology depends on the site specific energy costs and feed water quality characterized by the total dissolved solids in the water. MSF produces the most desalinated water in the world. MSF is most feasible for high salinity water (>45000 ppm). However, for brackish water (1500 – 15000 ppm) and seawater (15000 – 45000 ppm), RO membrane technology is the most widely used and most economical method [17].

Osmosis is the process in which solvent particles move from a lower concentration solution across a semi-permeable membrane to a higher concentration solution until the concentrations are equal in both solutions. By applying a pressure higher than the osmotic pressure, this flow can be reversed and this process is known as reverse osmosis. RO can be used to produce clean potable water from saline water.

The four major types of desalination membranes are micro filtration (MF), ultra filtration (UF), nano filtration, and reverse osmosis. They differ in the pore sizes as shown in Figure 2-2. Higher pressure and more energy are required as the pore size decreases. Membranes with smaller pores can filter out more materials. Sand filtration and other media filtration are used to remove large particulate matter. For desalination and water treatment, MF and UF are used as pretreatment to remove large organic matter, colloids, viruses, bacteria and other larger molecules like proteins [17]. NF can remove smaller particles from water, such as the hardness causing divalent ions (Ca^{+2}, Mg^{+2}), and will reject molecules with a molecular weight greater than 200 g/mole [17]. RO is usually the final step and can remove particles such as the monovalent salt ions (Na^{+}, Cl^{-}), and other dissolved compounds such as arsenic, barium and nitrate. The pressure used in RO is between 5 bar and 80 bar depending on the feed water quality. In special cases, RO has been operated at pressures up to 200 bar. In NF, the operating pressure is between 5 bar to 60 bar, while for UF and MF, the operating pressure is below 10 bar [17].

The major RO membrane manufacturers, such as DOW Chemicals, Koch membrane systems, and Hydranautics, offer different types of RO membranes based on the end-user needs such as high pressure, lower energy, fouling resistant, and high operating temperature.

2.1.2.A RO module configuration:

Figure 2-3 shows the typical construction of a reverse osmosis membrane. Here a spirally wound RO membrane is placed inside the fiberglass pressure vessel. Inside the fiberglass vessel is a membrane shell that encases the RO membrane element.

The cross section of a typical RO element has the following layers: a feed channel comprising of the feed spacer, the polyamide or cellulose acetate RO membrane selective layer, the porous support layers for the selective layer, and the permeate spacer. The material used to make the selective layer of an RO membrane layer influences the performance and behavior of the entire

RO system. The most common types of commercially available RO membranes are cellulose acetate and polyamide. The second layer that supports the selective layer is made from polysulfone, which is mounted on a tertiary polymer layer [17].

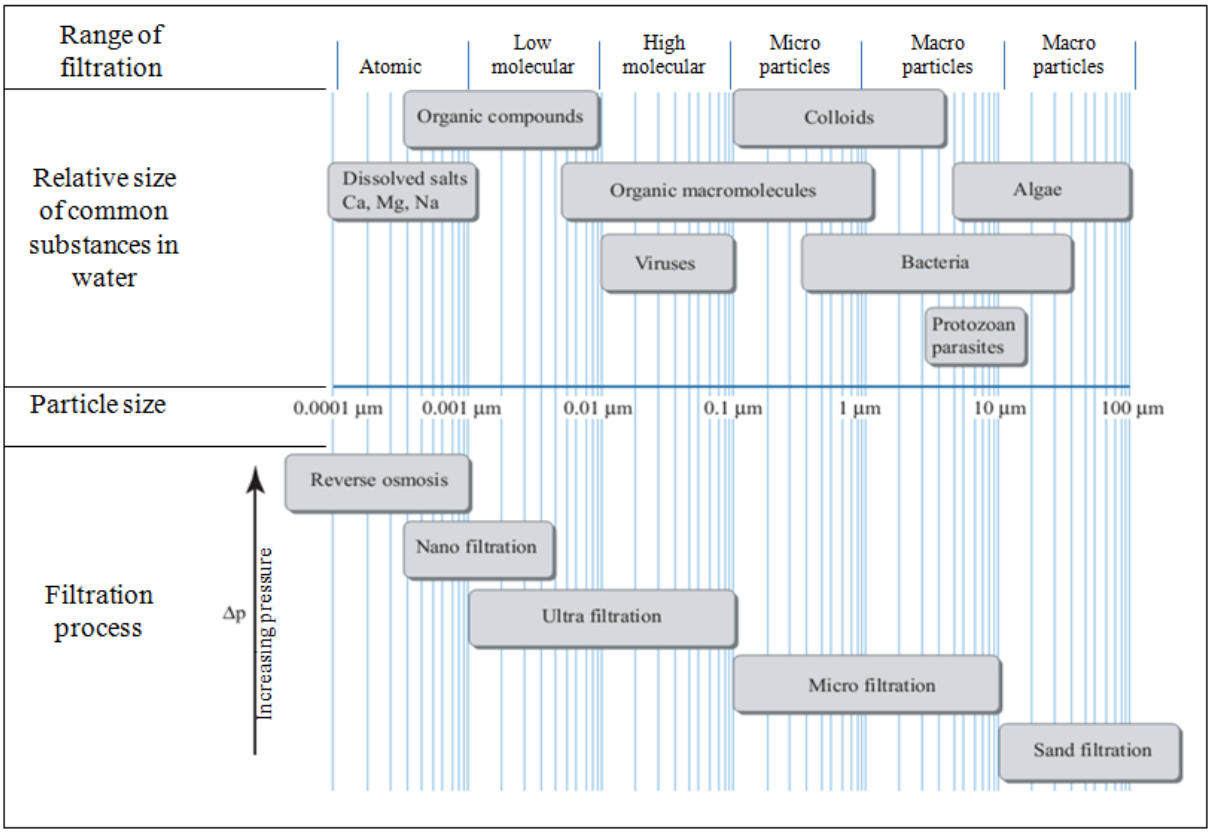

Figure 2-2: Comparison of membrane separation technologies. Figure adapted from MIT OpenCourseWare [19]

Feed water flows in from the feed side of the module as shown in Figure 2-3. Permeate water flows through the selective layer of the membrane and into the permeate spacer as per the cross flow filtration principle. Once in the permeate spacer, the permeate flows spirally inwards until it reaches the perforated permeate collection tube at the center.

RO modules are available in three major configurations: spiral wound, hollow fiber, and tubular. Today, spiral wound modules are the most widely used since they are cheap, easy to produce, have a high packing density of about 1,000 square meters of membrane area per m^3 and have high mass transfer rates. However, the spiral wound RO modules have the disadvantages of higher feed pressure loss, fouling problems and are harder to clean [17].

A lot of work is being done at the component level to improve RO membranes. Much of this work focuses on using nanotechnology and nano-engineering to change membrane characteristics. Several groups of researchers have used carbon nanotubes (CNT) to increase water flux. Such membranes are made of a dense layer of thin polymer films with carbon nanotube pores mounted on a porous support layer [20, 21]. These membranes are expected to have higher flux rates than conventional RO membranes, with high energy savings. However, mass producing such membranes is challenging. Nanoasis and Porifera are two companies working on creating CNT membranes.

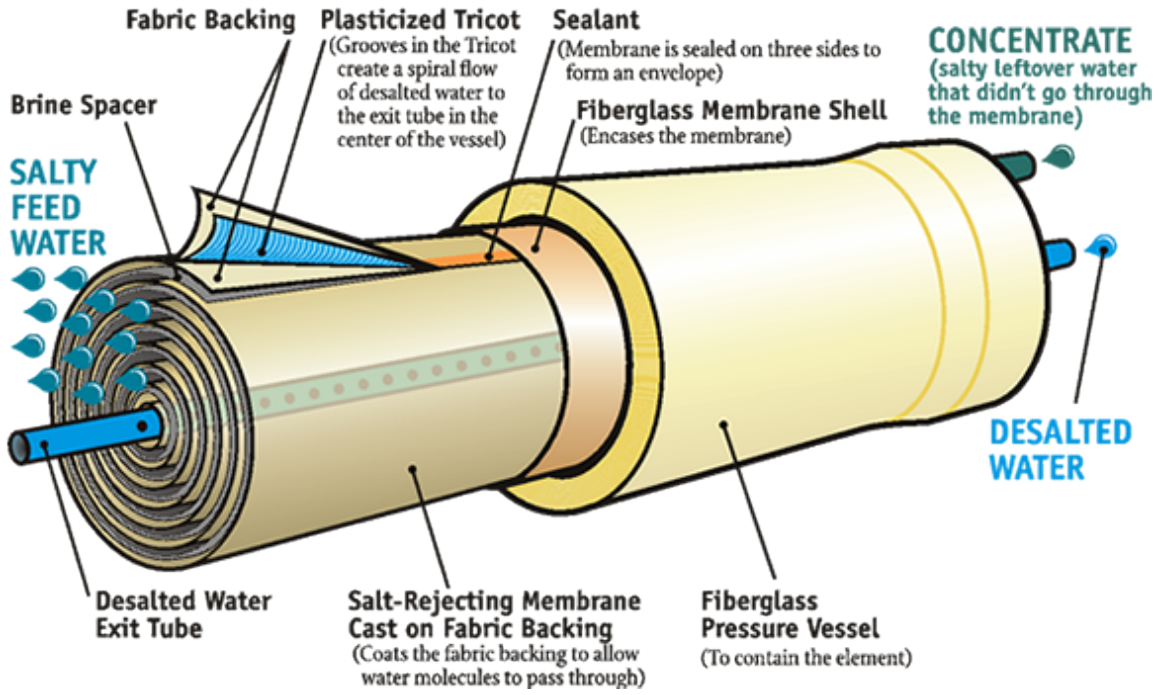

Figure 2-3: Reverse osmosis module construction. Figure Source: U.S. Department of the Interior, Bureau of Reclamation [18]

NanoH2O has an established technology and product that uses thin-film nanocomposites within traditional polymer architectures to increase the water permeability, thereby reducing the energy consumption [22].

Other research focuses on improving fouling and chlorine resistance of RO membranes. Clean Membranes is developing fouling resistant membranes using hydrophilic smart combs which act like brushes on the surface of the membrane to repel foulants [23, 24]. By reducing fouling, membrane productivity losses can be avoided. Chlorine tolerant, multilayer membranes are being

developed that can withstand chlorine in the feed water while maintaining high flux and high salt rejection [25].

2.2 MIT PVRO Experimental System Overview

The MIT PVRO experimental system is a small-scale, rooftop, 300 L/day PVRO system developed for validating PVRO system models and testing control algorithms. Figure 2-4 shows a block diagram of the MIT PVRO experimental system and the water flow diagram. The components of the MIT PVRO system include the coarse filter, fine filter, two motors, two boost pumps, a Clark pump energy recovery device and a reverse osmosis membrane housed inside a pressure vessel. The actual system installation and arrangement on the roof of MIT, Building 1, can be seen in Figure 2-5 [26].

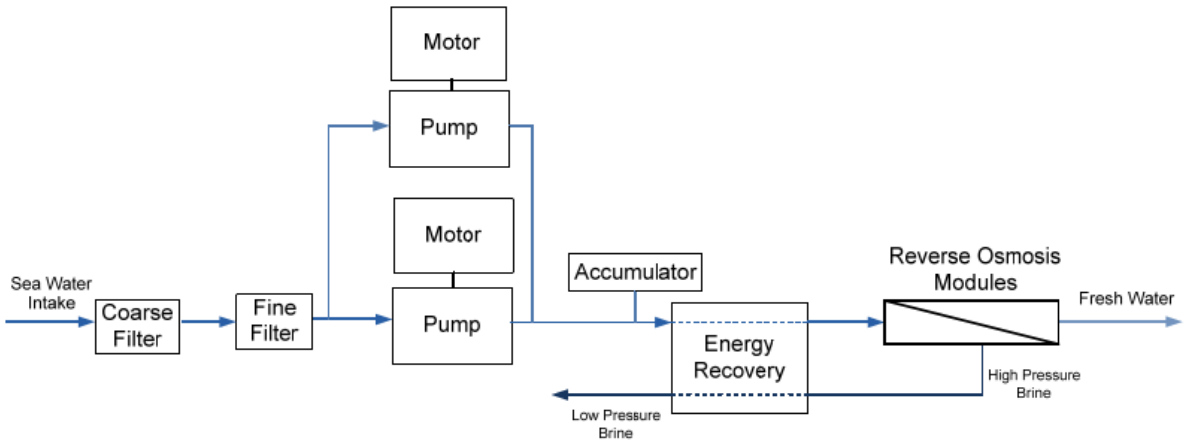

Figure 2-4: MIT PVRO system block diagram. Figure by Amy Bilton, used with permission [26]

The feed water must first pass through the filters to remove particulate matter and suspended solids that can otherwise clog the pumps and membrane, before the feed water is pressurized by the two boost pumps. The coarse filter is a stainless steel screen that removes larger particles while the second filter is a five micron pleated filter that removes finer particles. The two boost pumps, are positive displacement, powered by 1/8 horsepower, 24 V motors that pressurize the feed water to an intermediate pressure of about 12 bar. Included is a Spectra accumulator that

dampens vibrations and enables the Spectra Clark pump to operate smoothly and trouble-free. After the accumulator, the Spectra Clark pump raises the pressure of the feed water above its osmotic pressure so some of it will flow through the RO membrane and be desalinated. At full power, this pressure is approximately 60 bar. The Clark pump is a reciprocating pressure exchange device that extracts energy from the high pressure brine stream and raises the pressure of the incoming feed water. The recovery ratio of the PVRO system is determined by the ratio of areas of the inlet and outlet surface of the Clark pump pistons and thus remains fixed at 9 %. The overall efficiency of a Clark pump is around 95%. Finally, the highly pressurized feed water from the Clark pump is fed to the RO membrane, a spiral-wound DOW Filmtec SW30 2.5" X 40" polyamide membrane.

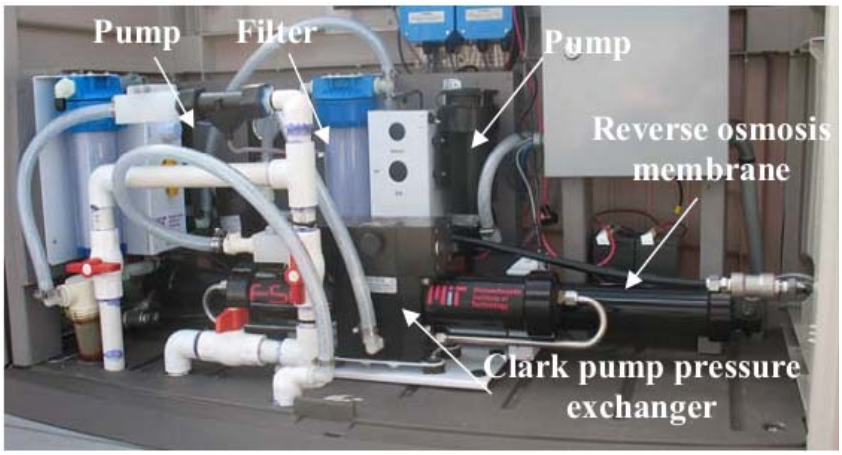

Figure 2-5: MIT PVRO system components. Figure by Amy Bilton, used with permission [26]

2.3 Literature Review

Control methods have been applied to PVRO systems. Alatiqi, et al., have presented an overview on process control in the water desalination industry through 1999 in which they discuss common and new control and instrumentation methods in RO plants [27]. The main objectives of process control in the desalination industry are to operate the systems at optimum conditions and maximize life of the systems to reduce costs. As pointed out by Alatiqi, et. al., in [27], various types of system models exist, varying from closed-form formulae to more detailed numerical

models. Alatiqi, et al., were the first to publish a paper on the closed loop control of RO desalination considering permeate flux and conductivity [28]. A dynamic model was experimentally established with pH and pressure as system inputs and permeate flux and conductivity as outputs. System identification was done using step experiments.

A tabulated summary of the literature survey on control configurations used for RO modules is presented in [29]. It shows the manipulated variables, the controlled variables, the type of model used, and the control algorithm used. The four major types of models used are the First Principle Model (FPM), which is the most widely used, the Transfer Function (TF) model, the Impulse Response Model (IRM) and the Time Domain (TD) model. The control algorithms used are Nonlinear Feed-forward/Feedback Control (NLFFFB), Fault Detection and Isolation and Fault-tolerant Control (FDIFTC), Model-Predictive Control (MPC), Dynamic Matrix Control (DMC) and Constrained Model-Predictive Control (CMPC), Proportional control, Proportional-Integral (PI) control and Proportional-Integral-Derivative (PID) control. The controlled variables, usually in pairs for any given model and control strategy, are brine velocity, permeate flux, conductivity, feed flow-rate, feed pressure, and bypass velocity (in the case where bypass configurations were used). The most frequently paired control variables are permeate flux and conductivity.

An alternate renewable energy source for powering RO is the use of wind turbines. A 2.2 kW wind turbine generator powering a variable-flow reverse osmosis (RO) desalination system model without batteries is presented by Miranda, et al. [30]. A model based control strategy to maximize the wind power generated and the clean permeate water subject to variations in wind speed has been proposed. The control is achieved by operating two variable speed medium and high-pressure pumps. The controller adjusts the speed of the pumps individually. Brine stream energy is recovered using a Clark pump. The operation of the two pumps were optimized to maximize wind power generated and clean water produced. The paper references a MATLAB-Simulink model developed by Thomson [12] and Miranda. However, this model does not account for the compliance energy storage within reverse osmosis systems. Thomson has demonstrated an experimental RO system driven by photovoltaics without batteries [12]. An example of this approach is the control of the Moineau pump that operates in parallel with a high pressure feed pump. Adding the Moineau pump to the PVRO system enables variable recovery ratio control using a Clark pump. In this system, the Moineau pump feeds the seawater to the

membrane in parallel with the Clark pump. However, this method of controlling the recovery ratio is not the most energy efficient.

Mcfall, et. al., worked on the control of an RO desalination process at high recovery ratios using feed-forward/feedback control techniques that use Lyapunov-based control laws while accounting for practical issues like sampled measurements, large time-varying characteristics and spatial variation in Total Dissolved Salts TDS and flow-rate inside the membrane [31]. The system model is derived from first principles based on a macroscopic kinetic energy balance of the system.

Bartman, et al., have worked on the design and implementation of a non-linear model-based control system for an experimental RO desalination system [32]. They are addressing large set-point changes and variations in feed water salinity. Their dynamic model is derived from first principles and is based on a mass balance of the entire system and an energy balance around the concentrate (brine) valve. The control system has two separate control loops: one that regulates the system pressure by adjusting the variable frequency drive speed that results in changing the feed flow rate, and a loop that uses a nonlinear model-based controller to determine the valve position based on the error between the actual concentrate velocity and its desired set-point.

Zhu, et al., optimize the energy consumption of reverse osmosis membrane desalination [33, 34]. Simple RO models are used to develop an optimization approach of product water recovery at pressures that approach the osmotic pressure of the exit brine stream [33]. The results suggest that higher recovery, multi-stage RO processes perform better from an energy consumption point of view. However, this has higher component costs and additional costs related to membrane fouling and scaling. Their work considers the effect of energy recovery devices, membrane permeability, process configuration, brine management cost, pump efficiency, and frictional pressure drop. Zhu, et al., studied how to optimize energy consumption of a RO desalination system under varying feed concentration, but with a constant clean water output [34]. A time-varying optimal operation strategy is found to have lower specific energy consumption compared to a time-invariant one. The results suggest using a higher overall recovery ratio, which will reduce brine disposal costs; however, this raises concerns related to membrane scaling and fouling.

In another work, Li minimizes the energy in RO water desalination [35]. In this approach, a set of dimensionless parameters is defined to characterize the RO desalination process and a non-linear optimization framework is used to minimize the specific energy conversion subject to certain constraints.

Constrained model-predictive control (CMPC) of RO systems has also been studied [36, 37]. Model predictive control is widely used in advanced process control. In particular, the dynamic matrix control algorithm has been employed and compared to the PI controller. The comparison shows that CMPC performs better than PI controllers [38, 39]. McFall, et al., implemented fault-tolerant control that combines fault detection and isolation (FDI) on RO desalination plants [40]. Different control configurations were identified and Lyapunov-based feedback control laws were used to determine closed-loop stability within a region. An FDI filter and a supervisory switching logic were developed to switch between control configurations. Gambier, et al., also worked on the dynamic modeling using lumped parameter models, model predictive control, and fault tolerant control of RO desalination plants [45-47].

More recently, Ali, et al., have modeled the transient behavior of an experimental reverse osmosis tubular membrane [41] and its robust model-based control [29]. The dynamic model for a tubular RO system derived from first principles is described by a set of differential equations where a unit is a series of single tubes and each tube is described by coupled ordinary differential equations. The tubes are modeled and solved sequentially such that the output of one tube is the input to the next. Using this model, an MPC algorithm was simulated by manipulating feed pressure and brine flow rate while the output variables were clean water flow rate and concentration.

Laborde, et al., present an optimization strategy for the design and operation of a small-scale, solar-powered desalination system [42]. This approach optimizes energy consumption based on input power. In their discussion, they note the importance of automatic pressure adjustment and control for the steady flow operation, so it can increase the lifetime of the membrane system. A systems analysis approach is taken without accounting for transient characteristics such as energy storage in a PVRO system.

Computation fluid dynamic (CFD) studies have been performed to model the detailed flow dynamics of RO processes [43, 44, 45]. These models are useful in understanding the dynamic

response of RO systems as a function of spatial location and time. Alexiadis, et al., used CFD models to calculate the response of high pressure RO membrane systems to pulse disturbances [45]. Using system identification techniques, transfer function models were determined which can be used to characterize the dynamics of the system. These approaches do a very detailed dynamic simulation of RO processes and components, but don't show overall implications for an entire system.

Operational control strategies have been presented by Schies, et al., with the aim of minimizing the specific energy consumption [46]. A specific configuration of three RO membranes is selected along with the typical high pressure pumps, energy recovery device and low pressure feed pumps. Control is done independently on the feed water conveying process involving the feed pump and then separately on the desalinating process. Depending on available solar power, the operating points of the pumps are adjusted and RO modules turned on or off to produce clean water.

The subject of fouling in RO systems by scaling, organic fouling and inorganic fouling has been an active area of research for several years [47]. Several studies and comprehensive literature reviews on the fouling and scaling issues in RO also exist [17, 48]. Notably, Goosen, et al., have presented a critical review of the literature on the fouling of RO membranes [49]. The review covers analytical methods of quantifying fouling, prevention of fouling and remedial actions for fouled membranes. The relevant literature in this area has been covered in greater detail in Chapter 4. The work in this field can be broadly classified into three major areas: prediction of fouling, modeling of fouling and the control of fouling.

2.3.1 Fouling Prediction

Scaling and fouling prediction for RO has largely depended on three indices: Langelier Saturation Index (LSI), Silt Density Index (SDI) and the Modified Fouling index (MFI). More recently, another method of scale prediction that is based on molar ratios has been presented by El-Manharawy and Hafez [50, 51]. Tay and Song have also demonstrated the use of a new fouling indicator based on the membrane resistance which can improve the fouling identification at the early stages and the effectiveness of membrane cleaning [52].

2.3.2 Modeling of Membrane Fouling

Concentration polarization (CP) is the buildup of excess amounts of salts around the surface of the membrane. The understanding of CP, its stages of development, modeling and prediction have been well documented. Cake filtration, boundary layer and film theory have been used to describe CP [53, 54].

Koltuniewicz predicted flux decline as a result of development of a CP layer using the surface renewal theory described by Danckwerts [55, 56]. A series resistance model was developed by Dal-Cin, et al., to model flux loss using a relative flux-loss ratio [57]. The objective of the model was to accurately quantify the individual contributions of the fouling mechanisms such as adsorption, pore blockage and CP. However, experimental and simulation data showed that the adsorptive fouling was underestimated while CP was overestimated.

While flux decline has been modeled for large scale RO desalination systems, the prediction of flux decline on account of fouling and scaling for RO membranes in community-scale PVRO systems is still not well defined.

2.3.3 Fouling Control

Fouling control can be achieved by preventive methods if the prediction is done accurately. However, if this fails, remedial steps such as membrane cleaning and regeneration need to be employed to remove the foulants. Several types of cleaning methods exist and they have been reviewed in the literature [58].

Zhu, et al., worked on optimizing the design and maintenance scheduling of flexible RO networks in industrial RO cases [59]. An iterative solution procedure has been proposed to implement the mathematical program where the design problem is formulated as a mixed-integer nonlinear programming (MINLP) problem [59]. The MINLP formulation was also used by Vince, et al., for the process optimization of the design of RO processes [60]. The simultaneous optimization of the RO process layout and operating conditions was solved using multi-objective optimization [60].

Model predictive control has also been used to address fouling and scaling issues by Bartman, et al., [61]. In this case, feed flow reversal is employed to prevent and/or reverse scaling. Feed-flow reversal must be done after reducing flow-rate from high flow operating points to prevent

membrane damage and water hammer. Using a dynamic, non-linear model and MPC, optimal transition from high flow operating point to low flow operating point has been identified.

Although much work has been done on fouling mitigation and control for large, industrial and conventionally powered desalination systems, there are no optimized autonomous maintenance scheduling and control systems for community scale PVRO systems.

CHAPTER

3

PHYSICS AND WORKING OF A PVRO SYSTEM

This chapter presents the physics and the fundamental relationships that govern the behavior of PVRO systems. It is necessary to understand the physics behind the different components of the PVRO system in order to accurately model and control them. The schematic of the MIT PVRO experimental system is shown in Figure 3-1. The system input is power from the photovoltaic panels. This is connected to power electronics, consisting of a variable DC-DC convertor that steps down the voltage for a pair of boost pumps. In this setup, a Clark pump is used as the energy recovery device.

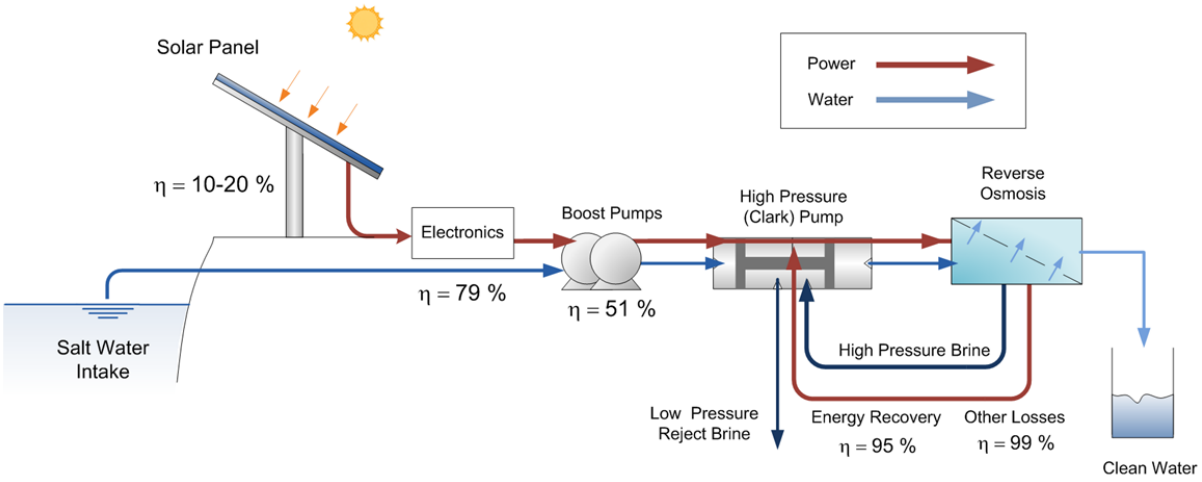

Figure 3-1: MIT PVRO experimental system schematic

An alternative setup consists of a conventional heavy duty pump as shown in Figure 3-2. The pump converts the electrical power into mechanical power. The water is pressurized and forced through an RO membrane. In the Clark pump setup, mechanical energy is recovered to pressurize the input stream. With a conventional pump, the pressurized brine stream is run through a controllable energy recovery device consisting of a Pelton-wheel generator.

First the models of the major components in the system are presented. This consists of the DC-DC convertor, pumps, RO membrane and energy recovery devices.

3.1 DC-DC Convertor Model

The conversion efficiency of the DC-DC convertor is assumed constant, which is accurate for a limited operating range of voltages relative to the input voltage.

$$\eta_{DC-DC} = \frac{P_{in}}{P_{out}} \quad \textbf{(1)}$$

In a typical scenario, $\eta_{DC\text{-}DC}$ is assumed to be 0.85. In a best case scenario, $\eta_{DC\text{-}DC}$ is assumed to be 0.95.

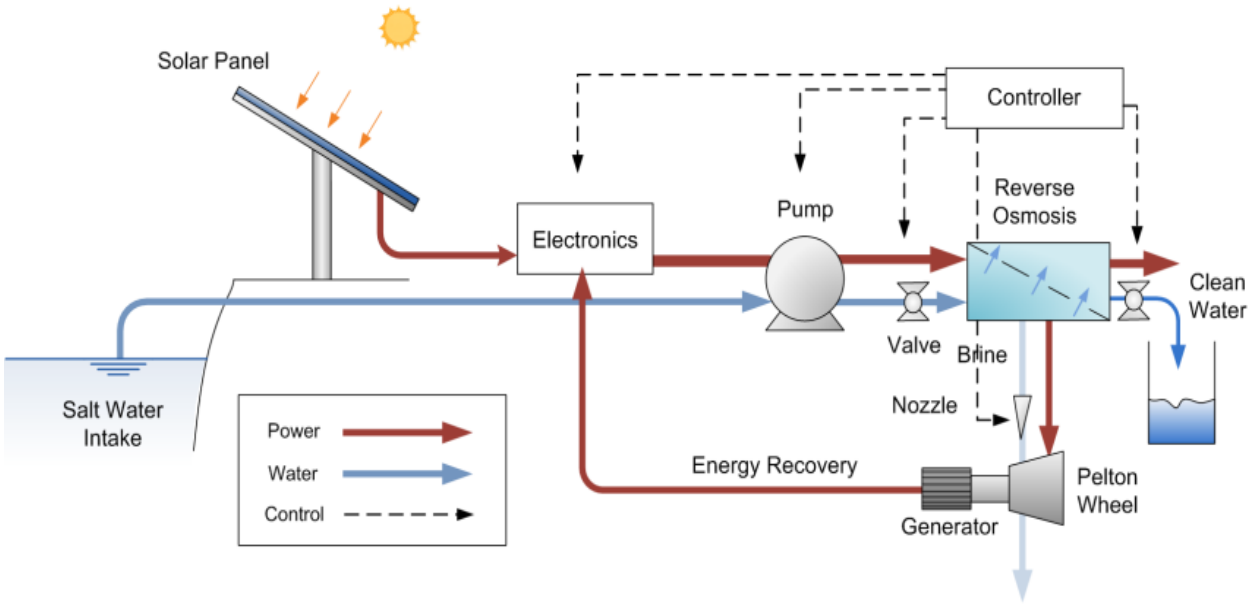

Figure 3-2: Concept system with controllable energy recovery schematic

3.2 Pump Model

The pump model includes both the pump and the motor driving it. The input voltage and input current of the motor are related as follows, where R_a is the armature resistance and V_b, the back emf voltage:

$$V_{in} = i_{in} R_a + V_b \tag{2}$$

The back-emf voltage, V_b is related to the angular velocity, ω of the motor as follows:

$$V_b = k_b \omega \tag{3}$$

where k_b is the motor constant.

The motor torque is related to the input current as follows:

$$\tau = k_a i_{in} \tag{4}$$

where k_a is the motor torque constant. The power output is given by:

$$P_{out} = \tau\omega = \frac{k_a i_{in} V_b}{k_b} = i_{in} V_b \tag{5}$$

The input power is given by:

$$P_{in} = i_{in} V_{in} = i_{in}^2 R_a + i_{in} V_b \tag{6}$$

The pump is considered next. For a typical vane pump [5],

$$\tau_{pump} = \frac{\Delta P D\left(1 + C_f\right)}{2\pi} + 2\pi C_d D\mu\omega + \tau_c \tag{7}$$

where ΔP is the difference between input and output pressure., D is the volume displacement of water, C_f is the friction coefficient, C_d is the viscous drag coefficient, τ_c is a constant, and ω is the angular velocity.

The flow through the pump is given by the following:

$$q_{pump} = 2\pi\omega D - \frac{C_s D \Delta P}{2\pi\mu} \tag{8}$$

The output power of the pump is given by the following:

$$P_{pump} = \left(\frac{\Delta P D k_p}{2\pi} + 2\pi C_d D\mu\omega + \tau_c \right)\left(2\pi\omega D - \frac{C_s D \Delta P}{2\pi\mu} \right) r \tag{9}$$

The efficiency of the pump is given by the following:

$$\eta_{pump} = \frac{P_{out}}{P_{in}} \tag{10}$$

$$\eta_{Pump} = \frac{\left(\frac{\Delta P D k_p}{2\pi} + 2\pi C_d D \mu \omega + \tau_c\right)\left(2\pi\omega D - \frac{C_s D \Delta P}{2\pi\mu}\right) r}{i_a^2 R_a + i_a k_b \omega} \tag{11}$$

This is the mechanical output of the pump divided by the input electrical power to the motor. The pump efficiency η_{pump} is assumed to be 0.85.

3.3 Reverse Osmosis Membrane Model

For the reverse osmosis membrane, the product flow, q_p is related to the feed pressure, P_f and P_{osm}, osmotic pressure [2]:

$$q_p = AS_E(TCF)(FF)(P_f - P_{osm}) \tag{12}$$

where A is the membrane permeability of water in liters per m^2-bar-sec, S_E is the membrane area in m^2, TCF is the temperature correction factor and FF is the fouling factor. This can be rewritten as [2]:

$$q_p = k(P_f - P_{osm}) \tag{13}$$

where k is the product of A, S_E, TCF and FF.

The osmotic pressure of the RO membrane is related to the recovery ratio, r, temperature, T and salinity C as follows:

$$P_{osm} = \frac{k_s TC}{2} \cdot e^{0.7r}\left(\frac{2-r}{1-r}\right) \tag{14}$$

The brine leaves the system at pressure, P_b and flow q_b.

The brine stream pressure is related to the feed stream pressure as follows:

$$P_b = P_f k_l \tag{15}$$

where k_l accounts for a pressure drop through the RO membrane. The brine flow, q_b is related to the product flow, q_p by the recovery ratio as follows:

$$q_b = \left(\frac{1-r}{r}\right) q_p \tag{16}$$

Using equations 2-16, the power in the brine stream is given by:

$$\mathrm{P}_b = \left(\frac{P_f}{r}\right)\left[P_f k_l k\left(1-r\right) - k_l k_s kTC \cdot e^{0.7r}\frac{\left(2-r\right)}{2}\right] \tag{17}$$

and the power used to produce clean water is given by:

$$\mathrm{P}_p = kP_f\left(P_f - \frac{k_s TC}{2}\cdot e^{0.7r}\left(\frac{2-r}{1-r}\right)\right) \tag{18}$$

3.4 Clark Pump Model

An empirical model of the Clark pump is utilized to determine its water output. The pressure losses in a Clark pump as presented by Thomson is [12]:

$$P_l = k_{cpf} q_f^2 + k_{cpp}\Delta P + P_{cpc} \tag{19}$$

where, k_{cpf} is the flow losses coefficient, k_{cpp} is the pressure losses coefficient and P_{cpc} is the pressure losses constant.

The flow losses in a Clark pump are:

$$q_l = k_{cpl} q_f P_H + q_c \tag{20}$$

where k_{cpl} is a flow losses coefficient and q_c flow losses constant.

The Clark pump efficiency is given by the following:

$$\eta_{cp} = 1 - \frac{P_l q_l}{P_{in} q_t} \tag{21}$$

where P_{in} is the pressure of the water into the Clark pump and q_t is the total flow into the Clark pump. For the operating range of the Clark-Pump, η_{cp} is assumed to be 0.95 as calculated from experimental data from the MIT PVRO experimental system.

3.5 Pelton Wheel Generator Model

The generator equation is given as follows:

$$i_a \mathrm{V}_{gen} + R_a {i_a}^2 + k_c \omega = \tau\omega = P_{wheel} \tag{22}$$

where ω is the angular velocity of generator, τ is the torque, k_c are the losses that remain constant for all loads, i_a is the armature current, R_a is the armature resistance and V_{gen} is the generator voltage. Substituting the torque in terms of current gives the following expression for the angular velocity:

$$\frac{i_a V_{gen} + R_a i_a^2}{\left(k_a i_a - k_c\right)} = \omega \tag{23}$$

The torque on the wheel as a result of the water jet that spurts from the nozzle is given by

$$k_a i_a = \tau = \rho q_b r \left(v_j - \omega r\right)(1+\cos\beta) \tag{24}$$

where ρ is the density of the fluid, q_b is the flow rate of the brine leaving the nozzle, r is the pitch circle radius of the wheel, v_j is the jet velocity and β is the angle of redirection. Rearranging equation 24 gives

$$\frac{v_j}{r} - \frac{k_a i_a}{k_d} = \omega \tag{25}$$

where

$$k_d = \rho q_b r^2 (1+\cos\beta) \tag{26}$$

Solving for current and angular velocity gives the following:

$$i_a = \frac{\left(k_d\left[k_a v_j - V_{gen} r\right] + r k_a k_c\right) \pm \sqrt{\left(k_d\left[V_{gen} r - k_a v_j\right] - r k_a k_c\right)^2 - 4r\left(k_c k_d v_j\right)\left(k_d R_a + k_a^2\right)}}{2r\left(k_d R_a + k_a^2\right)} \tag{27}$$

$$\omega = \frac{v_j}{r} - \frac{k_a}{k_d} \cdot \frac{\left(k_d\left[k_a v_j - V_{gen} r\right] + r k_a k_c\right) \pm \sqrt{\left(k_d\left[V_{gen} r - k_a v_j\right] - r k_a k_c\right)^2 - 4r\left(k_c k_d v_j\right)\left(k_d R_a + k_a^2\right)}}{2r\left(k_d R_a + k_a^2\right)} \tag{28}$$

The efficiency of the pelton wheel generator is given by:

$$\eta_{pwg} = \frac{i_a V_{gen}}{P_b q_b} \quad \textbf{(29)}$$

3.6 Compliance energy model

The complete PVRO system set up as described above exhibits unique transient and step response characteristics that have not been discussed in the literature. Passing clouds result in constantly varying amounts of power produced from the panels. This means that the feed pressure and hence the clean water flow also vary constantly. However, there are certain delays that are noticed once the cloud has passed and the system takes some time to reach the peak levels of water production. These delays can be attributed to compliance in the elements of the PVRO system. This has been discussed in further detail in Appendix A, section A.3.

The PVRO system compliance energy can be modeled based on the energy stored in a spring. The energy stored is proportional to the square of the internal pressure. This internal pressure is equal to the feed pressure that is measured on the feed side of the RO membrane. The feed pressure and consequently the compliance energy vary as a function of time and can be written as:

$$E(t) = \frac{1}{2} K P_f^2(t) \quad \textbf{(30)}$$

where $E(t)$ is the compliance energy stored in the system, K is the system compliance parameter, and $P_f(t)$ is the feed pressure. The system compliance parameter was empirically determined to be 1.34 and this is also discussed in further detail in Appendix A, section A.3.

In summary, this chapter has presented the fundamental physics and working of PVRO systems. The phenomenon of PVRO system compliance was discussed and a compliance energy model has been presented. The experimental validation of the model is included in Appendix A, section A.3.1. This model is interesting as it captures the transient characteristics of PVRO systems and can be used to effectively control and optimize the performance of PVRO systems as shown in Appendix A, section A.3.2.

CHAPTER

4

FOULING CONTROL OF A PVRO SYSTEM

As noted previously, the International Union of Pure and Applied Chemistry (IUPAC) defines membrane fouling as a process resulting in loss of performance of a membrane due to the deposition of suspended solids, or dissolved substances on its external surfaces, at its pore openings or within its pores. Due to the economic impacts, fouling needs to be avoided, mitigated or dealt with remedially.

This chapter covers the types of fouling in RO processes, the typical foulants and scalants in seawater and ground water, mechanisms of membrane fouling, potable water standards, water testing standards, RO water chemistry, scaling and fouling prediction, pretreatment, types of membrane cleaning and the influence of operational parameters on fouling.

4.1 Types of Fouling and Typical Fouling and Scaling Constituents in RO Feed Water

Figure 4-1 shows the typical foulants and scalants developed on membranes from around the world, as examined by Fazel, et al. [62]. The main foulants are organics, silica, iron oxide, aluminum oxide, calcium phosphate, calcium carbonate and calcium sulphate. The aluminum silicates are present as silt, clay, mullite, andalucite and Feldspar. The major types of fouling and scaling of RO membranes and the constituents in the feed water that cause them are as follows:

1. **Colloidal and particulate fouling:** Colloidal and particulate fouling is caused by the deposition and accumulation of particulate matter on the membrane surface. Aquatic colloids such as silt, suspended solids, colloidal silica, aluminum compounds, manganese, iron compounds, bacteria, clay, etc., are primarily responsible for colloidal fouling.

2. **Organic fouling:** Organic fouling is caused by the deposition and accumulation of proteins, humic, fulvic and other acids, oils, greases and other natural organic material on the membrane surface. Organic fouling is usually a precursor to biological fouling as the organic foulant layer can be consumed by microbes for growth and biofilm production.

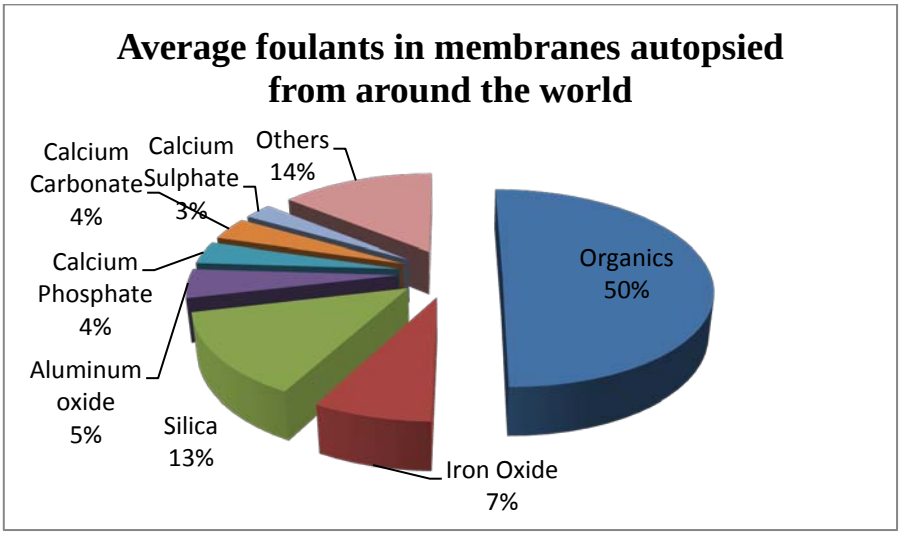

Figure 4-1: Typical foulants causing membrane fouling and scaling in 150 autopsied membranes from around the world [62]

3. **Biological fouling:** Biological fouling or Biofouling is caused by biological matter and microbes in feed water such as bacteria, fungi, algae and other microorganisms. Biofouling is characterized by the development of a biofilm on the membrane surface, composed of extra-cellular polysaccharides secreted by the microbes [63]. Organic or inorganic fouling can be a precursor to biofouling. The membrane autopsy studies by Fazel, et al., show that every membrane system has a biofilm [62]. Biofouling is most prevalent in surface brackish water. This is followed by sea water, tap water and finally well water [62]. Biofouling is measured in colony forming units per membrane surface area, cfu/cm^2, and is a concern when the bacterial count exceeds 10^5 cfu/cm^2.

4. **Scaling:** Scaling is defined as the precipitation of sparingly soluble salts and their deposition on membrane surfaces, pore openings or pore channels that result in a loss in performance. Some of the major scale-forming cations are calcium, magnesium, strontium and barium, and the anions are sulphates, carbonates, phosphates, fluorides and bicarbonates. The precipitation of these ions leads to the deposition of some of the common scale causing

constituents such as calcium carbonate ($CaCO_3$), calcium sulfate ($CaSO_4$), barium sulfate ($BaSO_4$), strontium sulfate ($SrSO_4$) and silica (SiO_2). Some of the less common scalants are calcium phosphate ($CaPO_4$) and calcium fluoride (CaF_2).

Table 4-1: Typical constituents of sea water

Constituent	**A (mg/kg)** [100]	**B (ppm)** [101, 102]	**C (mg/l)** [103]	**D (mg/l)** [2]
Sodium, Na^+	10781	10752	10900	10900
Magnesium, Mg^{++}	1284	1295	1310	1310
Calcium, Ca^{++}	412	416	410	410
Potassium, K^+	399	390	390	390
Strontium, Sr^{++}	13	13	13	13
Barium, Ba^{++}			0.05	0.05
Iron, Fe^{++}			<0.02	<0.02
Manganese, Mn^{++}			<0.01	<0.01
Chloride, Cl^-	19353	19345	19700	19700
Sulfate, SO_4^{-2}	2712	2701	2740	2740
Bicarbonate, HCO_3^-	126	145	152	152
Bromide, Br^-	67	66	65	65
Fluoride, F^-	1.3	1	1.4	1.4
Nitrate, NO_3^-			<0.7	<0.7
Silica, SiO_2	2		0.04~8	0.04~8
Boric Acid, $B(OH)_3$ or Borate, BO_3^-	26	27		4-5
Total dissolved solids, TDS	**35150.3**	**35124**	**35682.18**	**35682.18**

4.2 Potable Water Standards

The typical constituents of seawater are shown in Table 4-1. Multiple sources are used to show the consistency in what is regarded as seawater while designing a PVRO or any desalination plant. However, when designing an effective and efficient pretreatment and maintenance scheme, a complete inorganic and organic laboratory analysis of the feed water to be treated is required. A detailed composition of seawater with a total dissolved solids concentration of 35000 ppm is shown in Table B-1.

Organizations like the World Health Organization (WHO) and the Environmental Protection Agency (EPA) have established guidelines for drinking water quality and limits for the chemical constituents found in the water. The WHO specifies that the salinity of potable water must be less than 500 ppm [64]. The concentration limits for typical constituents in seawater and the reasons for the limits are shown in Table B-2.

4.3 RO Water Chemistry

Before deploying a PVRO system in the field, the incoming feed water must be analyzed to determine the pretreatment that may be required before the water is fed into the RO system. The American Society for Testing and Materials (ASTM) has specified the standards and testing guidelines for determining the constituents in the feed water. The relevant testing standards categories are:

- Inorganic constituents in water
- Methods for Analysis for Organic Substances in Water
- Methods of Radiochemical Analysis
- Water Microbiology

The AMTA suggests performing a water quality analysis that estimates the following constituents at a minimum: aluminum, ortho phosphate, ammonia, potassium, arsenic, selenium, bacteriological (coliform), bacteriological (total), silica soluble (as SiO_2), silica colloidal (as SiO_2), barium, silver, bicarbonates, sodium, cadmium, strontium, calcium sulfate, carbonate, total alkalinity (m value), carbonate alkalinity (p value), total dissolved solids (TDS), chloride, chlorine, total hardness, total iron, dissolved iron, chromium, total organic carbon (TOC), total phosphate, total suspended solids, turbidity (NTU), zinc, copper, color, conductivity, fluoride, free chlorine, lead, magnesium, manganese, nickel and nitrate. The AMTA also suggests on site monitoring of the ph, temperature, carbon dioxide and hydrogen sulfide [65].

Kucera has suggested estimates for compatible reverse osmosis feed stream and concentrate stream water quality [16]: the Silt Density Index (SDI) count should be less than 5 for colloids; the Nephelometric Turbidity Units (NTU) should be less than 1 for suspended solids; the Langelier Saturation Index (LSI) should be below 0 in the concentrate stream depending on the

pH and temperature to avoid calcium carbonate scaling, the LSI can go up to 2.5 with the use of appropriate antiscalants; the concentration of metals such as iron, manganese, aluminum, barium, and strontium should be below 0.05 ppm; hydrogen sulfide should be below 0.1 ppm, the colony forming units per milliliter (CFU/ml) should be below 1000 in the concentrate stream depending on the pH and temperature to prevent microbial issues, soluble silica can be present up to 140 to 200 ppm in the concentrate stream depending on the pH and temperature; the total organic carbon (TOC) should be less than 3 ppm; the color should be less than 3 APHA; the Chemical Oxygen Demand (COD) should be less than 10 ppm; for Cellulose acetate membranes, the pH should be between 4-6, the free chlorine should be less than 1 ppm and the temperature should be below 30 C while for polyamide membranes the pH should be between 2-12 depending on the membrane manufacturer, the free chlorine should be less than 0.02 ppm and the temperature should be less than 45 °C [16].

4.4 Mechanisms of Membrane Fouling

The main mechanisms of membrane fouling are adsorption, biofouling, blocking of pores, deposition and gel formation [48, 66]. Adsorption takes place due to the chemical interactions between the membrane material and the solutes. “Monolayers of particles and solutes can form even in the absence of permeation flux [48].” This increases the hydraulic resistance. Concentration polarization intensifies the adsorption process when the degree of adsorption is concentration dependent [48]. Concentration polarization is defined as the accumulation of solute and particles at the surface of the membrane. The effect of concentration polarization is essentially a reduction in the net driving pressure across the membrane and a reduction in permeate flux. This occurs because the effective osmotic pressure is higher than the osmotic pressure of the feed water, since the concentrated layer of solute and other particulate matter at the membrane surface is higher than that of the bulk feed water.

Biofouling is a major problem when bacteria are present in the feed water. The bacteria collect on the membrane surface and generate a biofilm with the extracellular polysaccharides that are secreted [63, 66]. The blocking of pores takes place when the membrane pores are obstructed, whether partially or completely, by the solute or other particulate matter. Deposition, also known as cake fouling, is the gradual deposition of layers of particles that effectively reduce the net

driving pressure across the membrane. Gel formation is a consequence of deposition and concentration polarization where gels are formed around the membrane surface, especially when proteins accumulate around the membrane.

4.5 Scaling and Fouling Prediction

In order to control fouling of a PVRO system, the fouling and scaling potential of the RO feed water must be predicted after conducting a thorough laboratory analysis of the water samples.

Scaling can be predicted by calculating the ionic concentrations of scale-forming anions and cations in the concentrate stream. This is done by measuring the ionic concentrations in the feed stream and using the recovery ratio to calculate the concentrations in the feed stream. Scaling occurs when the product of the molal concentration of the anion and the molal concentration of the cation of a scale-forming substance exceeds the solubility product of that substance. The solubility product is defined for specific temperatures and pH. The solubility product usually increases with temperature. In the case of calcium carbonate, the solubility decreases with increasing temperature. The scale forming tendency of a substance increases as the solubility product of that substance decreases. The units of solubility product are concentration raised to the power of the stoichiometric coefficients. For example, the solubility product of AgCl has units of M^2 or mol^2 per l^2 while that of $PbCl^2$ has units of M^3 or mol^3 per l^3[67].

The Langelier Saturation Index (LSI) or the Langelier Stability Index is used to predict calcium carbonate scaling. The LSI is equal to the difference in the actual pH of the feed water and the saturation pH. The LSI is widely regarded as an indicative tool that can predict a tendency to scale and is not a precise measure of the scale formation potential. The Stiff & Davis Stability Index (S&DSI) is another widely used index to predict calcium carbonate scale potential. The LSI is used mostly for brackish water when the TDS is below 4000 ppm. Above 4000 ppm and for higher salt content feed water such as sea water, the S&DSI is used [16].

The Silt Density Index (SDI) is used to predict the suspended solid and colloidal fouling potential of the feed water by measuring the time is takes for water to pass through a 0.45 micron membrane filter at 30 psi. This is done in 3 stages. First, the time required to collect the first 500 ml is measured. Then after 15 minutes in operation, the time required to measure the final 500 ml

is measured. From these measurements, a percentage flux decline per minute is calculated as described by the ASTM D4189-07 method for determining SDI. The SDI must be determined with the help of the SDI test apparatus just before the feed water enters the RO chamber and is usually done on site to calculate the index more accurately. The Modified fouling index (MFI) is an index that is derived from the SDI. It is measured using the same equipment. However, the MFI developed by Schippers & Verdouw also accounts for the cake filtration phenomena. Both SDI and MFI cannot estimate the fouling potential of particles smaller than 0.45 micron and are measured in dead-end filtration mode, whereas RO is a cross-flow filtration process. Turbidity is measured in Nephelometric Turbidity Units (NTU) to determine fine particulate matter in feed water.

There are several shortcomings of SDI and MFI, such as their inability to account for all possible foulants and their lack of correlation with the rate of fouling. Hence, there is a need for better fouling characterization parameters that can affect an RO membrane. These parameters should account for all possible foulants, have strong correlations between the fouling rate and development and should be measured in a cross flow mode instead of dead-end mode [68]. Tay and Song have demonstrated the use of a new fouling indicator based on the membrane resistance which can improve the fouling identification at the early stages and the effectiveness of membrane cleaning [52].

Another method of scale prediction that is based on molar ratios has been presented by El-Manharawy and Hafez [50][51]. In this method, there are four major classes of water: Class A: low chloride; Class B: medium chloride; Class C: high chloride; Class D: very high chloride. These four water classes are further divided into 10 water types depending on the chloride concentrations. It was observed that the solubility of carbonate and sulfate ions is largely dependent on the chloride ion concentration. After analyzing about 200 water samples, it was found that low chloride waters have low bicarbonate and sulfate scale problems. As the chloride content increases, the sulfate content also increases progressively. Bicarbonates are typically seen in low to medium chloride waters.

4.6 Pretreatment

Pretreatment for RO systems can be broadly classified into mechanical and chemical methods. In chemical pretreatment, coagulants are used to remove suspended solids and particulate matter from the feed water, scale inhibitors are used to prevent scale formation of low solubility compounds by either forming new compounds with better solubility or adsorbing to the surface of micro-crystals and preventing further crystallization, antifoulants are used to prevent iron fouling by preventing it from precipitating out, acids are used to lower the pH to reduce carbonate scaling and chlorination is used to deal with biological fouling. If chlorination is used, then bisulfites must be used to remove the chlorine before the feed water comes in contact with the RO membrane [65].

In mechanical pretreatment, prescreens, clarifiers and media filters are used to remove suspended solids and larger sized contaminants. Additionally, a cartridge filter is used as a coarse filter prior to the high pressure pumps. Activated carbon filters are used to remove organics and chlorine while greensand filters may be used to remove iron and manganese foulants. Ozone and UV treatment are used to mitigate biofouling. Microfiltration and ultrafiltration are used to remove bacteria, viruses and suspended solids. A typical pretreatment system designed to mitigate biofouling, particulate fouling and organic fouling will involve some form or coagulation/flocculation, sedimentation and media filtration [65].

4.7 Types of Membrane Cleaning

Membrane cleaning can be categorized as physical/mechanical cleaning, chemical cleaning and mechano-chemical cleaning methods.

4.7.1 Physical/Mechanical Cleaning

The physical cleaning methods use shear forces to remove the foulants from the membrane's surface. The major physical cleaning methods are sponge ball cleaning, air flushing, forward flushing, back flushing or reverse flushing, permeate backwashing and carbon dioxide back

permeation. These methods are well documented in the literature and are covered in detail in [66].

The efficiency of the mechanical and physical cleaning methods depends on the pressures on the permeate and feed side, the frequency of the cleaning cycles, the time between cleaning cycles, the flow rates, the time of cleaning and the amplitudes of pressure pulses applied.

4.7.2 Chemical Cleaning

Chemical cleaning is done using cleaning agents that remove foulants and scalants on the membrane by one or more of the following mechanisms [16, 69]:

- Actually removing the scale and fouling layer from the membrane surface
- Retarding the accumulation and build up of additional scale or fouling layers by altering the chemistry of the scale and foulant layers
- Retarding the accumulation and build up of additional scale or fouling layers by altering the structural properties of the scale and foulant layers.

A cleaning cycle is required when one of the following occur:

- A drop in the normalized permeate flow rate, usually when the normalized permeate flow rate drops by 10%-15% [16, 2]
- Normalized pressure drop (the difference between the feed pressure and the concentrate pressure) across the membrane increases, usually when the drop is10%-15% greater than the pressure drop recorded at the start up [16, 2]
- Normalized salt rejection drops by 5% - 10% from initial conditions [2].

The typical six stages of a cleaning reaction are [47, 70]: bulk reaction of detergents, transport of detergents to the fouled surface, transport into the fouled layer, cleaning reactions, transport of cleaning reaction products back to the interface and transport of products to the bulk solution. These stages may or may not all be present at the same time and can occur in a different order.

The following set of operations is typical of a cleaning cycle [47]: product water removal from the system, rinsing/flushing with clean water, cleaning in one or more steps, rinsing with clean

water and disinfection. However, these may differ depending on the degree of fouling, type of fouling or scaling, and membrane manufacturer's guidelines.

The major chemical cleaning methods are as follows:

4.7.2.A Off-site Membrane Cleaning or Clean Out of Place

Off-site cleaning is performed by removing RO membrane modules from the pressure vessels and sending them to a cleaning facility. Off-site membrane cleaning offers certain advantages and disadvantages. The major advantage of off-site membrane cleaning is a thorough diagnosis and analysis of fouling by qualified personnel [16]. This diagnosis can suggest necessary improvements in operational parameters that can help reduce the rate of fouling and cleaning, and provides better cleaning effectiveness on account of using customized solutions and methods. The major disadvantages of off-site cleaning are the high costs which can go up to $150 (as of 2010) for an 8-inch diameter RO module, and the need for an additional set of membranes to keep the system operational when the original membranes are sent to be cleaned [16].

4.7.2.B On-site Membrane Cleaning or Clean in Place (CIP)

Clean in place is a commonly employed method to clean smaller RO systems. Here, cleaning mechanisms are built into the system. The advantages of CIP are [16]: cleaning can be done without removing membrane modules from the pressure vessel, cleaning time is much less than off-site cleaning times, CIP can be automated to work on a frequency based or condition based maintenance schedule and CIP is much cheaper than off-site cleaning. An 8-inch diameter RO module can be cleaned in place for a cost ranging from $5 to $25 (as of 2010). The disadvantages of CIP are: the lack of expert analysis at the time of cleaning, lower membrane regeneration effectiveness, on site storage and handling of cleaning chemicals and additional cleaning system components.

Different membrane manufacturers have their own specifications for cleaning in place solutions and methods. It is imperative to consult with membrane manufacturers prior to designing a CIP system.

4.7.2.C Membrane Cleaning Efficiency and Effectiveness:

The type of membrane cleaning used depends on its cleaning efficiency and effectiveness. The major ways of measuring cleaning efficiency and effectiveness are as follows [16]:

- Comparing normalized permeate flow before and after chemical cleaning
- Evaluating flux recovery and fouling ratio: Liikanen, et al., defined flux recovery as the ratio of the flux after cleaning to the flux of the virgin membrane, and fouling ratio as the ratio of flux of a fouled membrane to the flux of a virgin membrane [71]. Madaeni, et al., define flux recovery in a slightly different way, as the ratio of the difference between the flux after cleaning and the flux after washing the membrane with distilled water to the difference between the flux after washing the membrane and the initial water flux [72].
- Resistance removal: Madaeni, et al., define resistance removal as the ratio of the difference between the membrane resistance after fouling and the membrane resistance measured after rinsing with water to the membrane resistance after fouling [72].

The existing cleaning methods are not ideal and have several disadvantages. Cleaning chemicals pose some logistical issues, especially when PVRO systems are deployed in remote locations. Disposal of chemicals, membrane damage and system down time are other concerns. Hence, the development of new and better cleaning methods is an area of active research. Some unconventional cleaning methods are osmotic backwashing with hyper saline solution, magnetic fields, electric fields, electrochemical methods and ultrasonic fields [16].

4.7.3 Industrial practices to mitigate fouling and scaling

A questionnaire was created with the purpose of understanding the operational methodologies and state of the art in the RO industry with regards to fouling control and pretreatment of PVRO systems. After personal communication with representatives of leading RO chemical manufacturers such as GE Water, Avista Tech and PWT chemicals, it appears that most manufacturers use sophisticated models and tools to predict desired performance characteristics and fouling control methods, while a lot of unscientific and heuristic methods still seem to be used to deal with fouling control. The concept of optimizing back flushing frequency or chemical

cleaning with the objective of maximizing permeate water production or even minimizing specific volume costs of water production do not seem evident in their approaches or guidelines.

The questionnaire focused on three major areas of RO chemical treatment: antiscalants, coagulants and flocculants, all of which are membrane cleaning chemicals. The objectives were to understand the following:

- Water analysis requried to determine the use of antiscalants, coagulants and flocculants and membrane cleaning chemicals
- The impact of these chemicals on the permeate water production
- The impact of the chemicals on membrane life
- Cost functions and trade offs for the chemicals used

It was emphasized that water analysis should reveal at the very least, the turbidity, TDS, and SDI, silica, phosphates, sulfates and metals such as barium, calcium, magnesium, iron and copper. A full scale lab analysis is regarded as the best way to analyse feed water in a particular location when designing pretreatment systems. Additionally, it is necesssary to have a good understanding of the opertating conditions such as tempertaure, recovery ratio, pressure, flow rates, etc. On-site water testing can be done using water test kits; however, the accuracy is a concern. Pretreatment using media filters such as sand and anthracite, and membrane systems such as ultrafiltration and nanofiltration, are needed to remove turbidity, suspended solids and algal blooms from red tide events. Such filters would have a physical foot print of about one square meter for a 500-1000 liter/day system. Higher recovery systems need to use appropriate dosage of antiscalants especially when saturation indices predict scaling. The calcium carbonate precipitation potential is considered to be a more accurate way of predicting scaling. The use of anitscalants increases the life of the membranes as scale formation on the membranes is reduced, thereby decreasing the frequency of membrane cleaning. Membrane cleaning chemicals negatively impact the life of the membrane. The use of antiscalants also enables RO systems to operate at higher recovery ratios without running into scaling issues. A question of interest was the cost benefit of using physical pretreatment as opposed to chemical pretreatment and vice versa. The answer is that this is highly subjective and varies depending on the set up. Low SDI

waters can run without any physical pretreatment, but this increases the frequency of chemical cleaning.

With regard to coagulants and flocculants, the NTU, organic level, colloidal level, biological contents and major fouling elements such as iron, silica, aluminum, phosphates, etc., determine their need and use. Coagulants and flocculants need to be used before any media filter to bring the NTU below 0.2, or 100 particles per ml. The use of coagulants and flocculants also increases the lives of the membranes by reducing the frequency of chemical cleaning and, more importantly, the irreversible fouling of the membrane surface.

GE recommends backflushing daily for about 10 minutes, whether chemical cleaning agents are used or not. PWT Chemicals and DOW both recommend backflushing once a day or multiple times a day if chemicals are not used to clean membranes. AvistaTech recommends frequent permeate flushing either before shut down every day or on alternate days. For idle periods, it is better to leave the system flushed and soaked with permeate water than with feed water. Chemical cleaning is recommened when the normalized permeate flow has decreased by 10% to 15%, or as per membrane manufacturer's specifications. The cleaning chemicals should be circulated for about an hour.

For systems susceptible to biofouling, chlorine is added to mitigate biofouling. However, polyamide membranes have a chlorine tolerance of about 1000 ppm-hours. Hence, sodium metabisulfite (SMBS) must be used to dechlorinate the water prior to feeding the water to the RO chamber. Recently, Kathon biocides have been gaining popularity since they are non-oxidizing biocides. DBNPA, or 2,2-dibromo-3-nitrilopropionamide, is another commonly used light oxidizer.

For small scale single element systems that are used to produce potable water from seawater or tap water, DOW suggests that preventive membrane cleaning is sufficient for controlling scaling and fouling [2]. These systems typically operate at lower recovery ratios (25% and below) without pretreatment, and with membrane lifetimes of 1-2 years. This cleaning can be done by a simple forward flush at low pressures by opening the concentrate valve or with cleaning chemicals [73].

4.8 INFLUENCE OF SYSTEM OPERATIONAL PARAMETERS

Several factors affect the fouling and cleaning frequency of small scale PVRO systems. They are:

- **Pressure:** Higher pressures increase the fouling of membranes for two reasons: 1) higher pressures compact the fouling layers, reducing porosity and increasing membrane fouling, and 2), since RO filtration is cross flow filtration, foulants will be forced to accumulate on the membrane surface [74].
- **Pretreatment:** Inadequate pretreatment is a major cause of membrane fouling and the resultant need for membrane cleaning. The compatibility of pretreatment chemicals with the membrane influences the degradation of the membrane [75].
- **Membrane characteristics:** Some membranes are more fouling resistant than others. A membrane's hydrophilicity and adsorptive potential for organic matter determines how rapidly it can be fouled by organic matter [75]. Hydrophobic membranes are more susceptible to organic fouling than hydrophilic membranes [74]. Thus, the rate of fouling is severely impacted by the membrane's characteristics and its fouling potential.
- **Temperature:** The operating temperature of the RO system affects the rate of biofouling and also affects the solubility of scale forming compounds. Generally, a decrease in temperature leads to an increase in fouling [75].
- **Flow rates:** Higher flow through and across the membrane lead to an increase in fouling as more foulants interact with the membrane.
- **Recovery ratio:** Higher recovery ratios are a major reason of scaling as the ionic concentration of scale-forming ions increase and begin to precipitate out of the solution. Similarly, other foulants tend to accumulate more rapidly with increase in recovery ratios.
- **Cleaning agents:** The type of cleaning agent plays a huge role in the cleaning effectiveness of membranes, which determines how fast a membrane gets fouled after cleaning and the time before the next cleaning cycle. If permeate water is being used to back flush, the quality of the permeate water plays a significant role in cleaning effectiveness and fouling rate.

- **Effect of Spacers:** The thickness of spacers plays an important role in the performance of the membrane, as shown by Sablani, et al. [76]. Reducing the thickness of the feed spacer below a certain optimum design value reduces the flux as the flow in the feed channel becomes laminar. The lack of turbulence aggravates concentration polarization and this decreases the flux [76]. Additionally, the spacers most likely have a thin mesh built in to increase the turbulence, thus reducing fouling. However, the trade off is the reduction in driving pressure downstream and the possibility of the spacers entrapping foulants.

Some of the factors affecting chemical cleaning performance and efficiency are [16]:

- **Type of chemical used:** The right type of chemical must be used for any foulant after consulting with the membrane manufacturer. Otherwise, the cleaning may not be effective and could possibly damage the membrane.
- **Membrane characteristics:** Fouling-resistant membranes are easier to clean as the foulants can be removed more readily, sometimes with just a permeate water back flush.
- **Amount of chemical used:** Usually the cleaning efficiency increases with the amount of chemicals used. However, excess chemicals can damage the membrane. After a point, the cost of chemicals exceeds the value of increasing the water production.
- **Temperature:** Higher temperatures are usually preferred for membrane cleaning.
- **pH:** Cleaning is usually done with acids first, followed by a caustic cleaning agent. The high-low pH cleaning performs better than a steady pH cleaning. High pH cleaners are used to clean a membrane that is fouled with biofilms, silica, sulphate scale, organic foulants and colloidal material. Low pH cleaners are used to deal with calcium carbonate scale and iron oxide deposition. Neutral pH cleaners such as DBNPZ (dibro monitriloproprionamide) are used to deal with some microbes.
- **Flow rate while cleaning:** Higher flow rates are better at scouring membrane surfaces and removing foulants.

- **Exposure time:** Cleaning cycle time affects membrane cleaning. Soak times, chemical exposure times and scouring times are proportional to amount of foulants removed from the surface of fouled membranes.

In summary, this chapter has presented the major types of fouling that affect small scale PVRO systems and the mechanisms by which the fouling takes place. Typical sea water constituents and the potable water standards were discussed. Acceptable standards for RO feed water as outlined by membrane manufacturers and the AMTA are outlined. Scaling and fouling prediction methods were discussed and commonly used pretreatment options were covered.

An overview of membrane cleaning methods was presented with an emphasis on chemical cleaning methods. Interview excerpts from RO membrane and RO chemical manufacturers were presented to understand the operational methodologies and state of the art in the industry with regards to fouling remediation and pretreatment of PVRO systems. The influence of system operational parameters that affect the rate of fouling and consequently the frequency of cleaning were discussed. These factors include the operating pressure, pretreatment, membrane-specific characteristics, water temperature, flow rates, recovery ratio, cleaning agents and feed and permeate spacers. Finally, the factors affecting the effectiveness of a maintenance operation were presented. These include the type of chemical used, the membrane-specific characteristics, amount of chemical used, temperature of cleaning solution, pH of cleaner, flow rates while cleaning and the exposure time.

CHAPTER

5

REVERSE OSMOSIS COSTS AND ECONOMICS

This chapter discusses the costs and economics of PVRO systems that determine the feasibility of such systems in the desired locations and ambient conditions. These also influence the cost optimization function, described in the following sections, used to determine the optimum operation and maintenance routine. Such costs vary drastically for different locations, feed water conditions and local environmental, social and political conditions.

Some of the major factors affecting autonomous PVRO desalination costs are as follows [77]:

- **Size of the system:** As the size of the PVRO system increases, the unit product costs decrease.
- **Feed water quality and salinity:** Better quality feed water lowers the unit product costs as fewer anti-scalants and anti-foulants are required. The rate of deterioration of the membrane is also lower. Likewise, as the salinity of the feed water decreases, the unit product costs drop as higher amounts of feed water can be recovered.
- **Location:** The location of PVRO systems in relation to the feed water source and point of end-use strongly affects the costs associated with the procurement of feed water and the distribution of the product clean water. Feed water quality can vary drastically from location to location. The amount of solar power produced by the PV panel also varies considerably with location.

  Additionally, logistical costs related to transporting the system to the point of use, transporting consumables such as the chemicals and membranes and bringing in service personnel are significantly affected by the location of the PVRO system.
- **System component life:** The lives of the components used in small scale PVRO systems affect the costs of the clean product water. Rapid degradation and frequent replacement

of components such as RO membranes, pumps, and pretreatments increase the costs of clean water drastically.

- **Maintenance and servicing:** Frequent maintenance and servicing of PVRO systems may be required due to inadequate pretreatment, bad feed water quality or faulty system design. This can drive up costs drastically, especially if adequately skilled technicians are not locally available.

5.1 Typical Costs for Autonomous Community Scale PVRO Systems

5.1.1 Total Costs

The total cost of a PVRO system is equal to the sum of the capital costs, and the operating and maintenance (O&M) costs. Most capital costs are incurred at the start of a PVRO installation and several O&M costs are incurred in the following years throughout the life of the system. Additionally, some capital costs are incurred as and when the components wear out. However, water is produced on a daily basis assuming there is sufficient sunlight and feed water. Hence, for accurate costing of water produced by PVRO units, annualized costs are considered.

The total equivalent annualized cost for PVRO systems can be expressed as [9]:

$$A_{Total} = A_{CC} + A_{O\&M} \tag{31}$$

where A_{cc} is the annualized capital cost of the PVRO systems, $A_{O\&M}$ is the sum of the annual O&M costs for the PVRO system.

Using A_{Total}, the specific cost of water produced ($/m^3) is given by [9]:

$$SC_w = \frac{A_{Total}}{365nuV_{day}} \tag{32}$$

where n is the life of the system in years, u is the PVRO system availability and V_{day} is the amount of water produced daily in m^3/day.

Table 5-1 shows the water costs for Albuquerque, Boston, Brisbane, Cape Haiten and Limassol for PVRO systems that are designed to produce 1 m^3 of clean water in a day. These systems have

been optimized using computer-based modular design methods by Bilton [78]. This method can enable non-experts to configure PVRO systems from a given inventory of modular components.

Table 5-1: Water costs for 1 m^3 per day PVRO systems using modular design optimization methods (as of 2012) [78]

Location	Feed water salinity (ppm)	Average annual solar insolation ($kWh/m^2/day$)	Water cost ($/m^3$)
Albuquerque, New Mexico	3000 (brackish)	5.79	1.08
Boston, Massachusetts	32664	4.21	1.65
Brisbane, Australia	35438	5.31	1.32
Cape Haiten, Haiti	36275	6.05	1.28
Limassol, Cyprus	39182	6.25	1.24

As seen in Table 5-1, the cost of the product water varies from location to location. Thus for the purposes of this thesis, an average water cost of \$1.37 per m^3 is used by averaging the water costs produced from sea water from the table.

5.1.2 Capital Costs

The equipment costs represent most of the capital costs and are known as direct capital costs. The indirect capital costs include costs such as freight, insurance, installation, etc. The direct capital costs includes the costs for the solar panels, the pumps, the RO membranes, the pressure vessels, energy recovery devices, sea water intake, pretreatment and post treatment.

The costs of a PVRO system are determined by its size, location and feed water conditions. The costs of PVRO system reduce as the size of the system increases [79]. Hafez and El-Manharawy studied small scale RO desalination systems that were connected to the grid and noted that product water costs decline as the plant size increased. It varied from 2.23 $/m^3$ for a 250 m^3/day system to 1.14 $/m^3$ for a 4800 m^3/day system (as of 2002) [80].

The capital costs of the PV system include the costs of the power control electronics, electrical connections and installations. The costs of the PV system are given by:

$$C_{PV} = SC_{PV}W \quad \textbf{(33)}$$

where SC_{PV} is the costs per watt of the photovoltaics used and W is the peak power rating of the PV array in watts.

The total cost of the RO system including sea-water intake, pretreatment, post-treatment and installation is given by [9]:

$$C_{RO} = 24 Q_p SC_{RO} \quad \textbf{(34)}$$

where SC_{RO} is the specific cost of the reverse osmosis system in \$/m^3/day and Q_p is the daily water production of the designed system in m^3/day.

5.1.3 Operating and Maintenance (O&M) Costs

The total annual O&M cost for the PVRO system is given by [9]:

$$A_{O\&M} = A_L + A_{chem} + A_{r,RO} + A_{r,PV} \quad \textbf{(35)}$$

where A_L is the annual cost of labor, A_{chem} is the annual cost of chemicals, $A_{r,RO}$ is the annual cost of RO component replacement and $A_{r,PV}$ is the annual operating cost of the PV system in \$.

The annual cost of labor is given by [9]:

$$A_l = 365 \gamma u V_{day} \quad \textbf{(36)}$$

where γ is the specific operating labor cost in \$/m^3-day, u is the plant availability factor and V_{day} is the amount of water produced daily in m^3/day. The specific operating labor cost can range from 3 \$/m^3-day as indicated in [81], while Ettouney, et al., specify it as \$0.05/m^3 (as of 2002) in [82].

Helal, et al., analyzed remotely located PVRO plants of the size of 20 m^3/day [81]. An annual labor cost of \$18,000 was assumed, which is 2.47 \$/m^3 (as of 2008) for this system. In contrast, conventional RO plants have a labor cost of 0.03 \$/m^3.

The costs of the chemicals are influenced by the type of feed water used and the temperature of the feed water, and these vary considerably with location. The total annual cost of pre-treatment chemicals is given by [9]:

$$A_{chem} = 365 k u V_{day} \quad \textbf{(37)}$$

where *k* is the average cost of chemicals in $/m3. The cost of cleaning chemicals can be assumed to be the about the same as the cost of pretreatment chemicals.

Estimated chemical costs, dosing rates, annual quantity of chemicals to be stored and annual costs are shown in Table 5-2, below, on a per unit volume of clean product water basis. The unit cost, dosing rate, and specific costs were obtained from Ettouney, et al. [82]. These estimates are averages of commonly encountered cases. They can vary drastically depending on feed water conditions, locations of PVRO systems in relation to the point of manufacture of the chemicals and climate and operating temperatures.

Table 5-2: Chemical costs, dosing rates, annual quantity, annual costs (as of 2002)

Chemical[79]	**Unit cost, $/kg**[82]	**Dosing rate, kg/m^3 water**[82]	**Specific cost, $/m^3 water**[82]	**Annual qty. (kg) (1m^3/day system)**	**Annual costs ($) (1m^3/day system)**
Sulfuric Acid	0.504	0.0242	0.0122	5.11	3.577
Caustic soda	0.701	0.014	0.0098	1.825	3.4675
Antiscalant	1.9	0.005	0.0095	1.46	0.70445
Chlorine	0.482	0.004	0.00193	0	0
TOTAL	3.587	0.0472	0.03343	8.395	7.74895

The unit chemical costs decrease as the size of the system goes up, as shown in [82].

Kucera suggests that Clean-in-place (CIP) on-site membrane cleaning is cheaper than off-site membrane cleaning procedures [16]. This is reasonable given the transportation and labor costs involved with off-site cleaning procedures, over and above the cost of an extra replacement set of membranes. Off-site cleaning costs can be between $5 and $25 (as of 2010) per cleaning cycle for an 8-inch diameter RO module, depending on the type of chemicals used. For smaller 4-inch diameter RO modules, the cleaning costs can be conservatively estimated to be about half of that, i.e. $2.5 to $12.5 (as of 2010).

The other major operating costs are due to degradation of the reverse osmosis membrane, the pump, the motor and the energy recovery device. Over time, these wear out and need to be replaced. The lives of these components are affected by the varying power, feed water and climate conditions. For the purpose of calculating annualized costs, the system components are assigned an annual replacement rate as follows [9, 80, 81]:

- Membranes cost about 40% of reverse osmosis components and have a 40% annual replacement rate
- Pumps, motors and energy recovery devices cost 15% of reverse osmosis components, each and have an annual replacement rate of 10%.
- The reverse osmosis components amount to 25% of system capital costs

Using the information above, the annual cost for component replacement can be written in a form similar to the one written in [9]:

$$A_{r,RO} = RR_{mem}C_{mem} + RR_{motor}C_{motor} + RR_{pump}C_{pump} + RR_{erd}C_{erd} \quad \textbf{(38)}$$

where C represents the component costs and RR is the component replacement rate.

The PV panel has an expected life of 25 years. Hence, it does not contribute any annual maintenance costs if the life-cycle analysis spans 25 years. The annual O&M costs for the PV system are the costs associated with the replacement of the power electronics. The annual replacement rate for electronics is 10% and the cost is given by [9, 83]:

$$C_{PV,E} = 0.71W \quad \textbf{(39)}$$

where W is the peak power rating of the PV array in Watts. Therefore, the annual operating costs of the PV system are given by:

$$A_{r,PV} = C_{PV,E}RR_{PV,E} \quad \textbf{(40)}$$

where $RR_{PV,E}$ is the annual replacement rate of the PV system, assumed to be 10%.

This chapter discussed the costs associated with PVRO systems. In summary, the major factors affecting the community scale PVRO systems are the size of the system, location, components' lifetimes, maintenance and servicing. Next, the total costs associated with these PVRO systems were discussed. These costs are broken down in to capital costs and operating costs. Simple formulas from the literature were presented that can be used to estimate costs. The major capital costs are for the RO system and the PV system. The operating costs are broken down into labor costs, chemical costs, and the component replacement costs.

CHAPTER

6

MAINTENANCE SCHEDULING AND OPTIMIZATION

Figure 6-1 shows a schematic of an RO system with conventionally scheduled back flushing and chemical cleaning. As discussed in section 4.7.3, small scale reverse osmosis systems can be operated without pretreatment, simply using preventive and remedial membrane cleaning. The membrane cleaning methods include a permeate water back flush and a chemical cleaning procedure. For autonomous PVRO systems to work well, the cleaning-related maintenance scheduling must be optimized and automated. This chapter investigates the simulation of flux degradation over time, the optimization of membrane cleaning using back flushing and chemical cleaning, and maintenance scheduling using schedule based maintenance and condition based maintenance. Finally, a cost function and self-optimizing condition-based maintenance algorithm are presented.

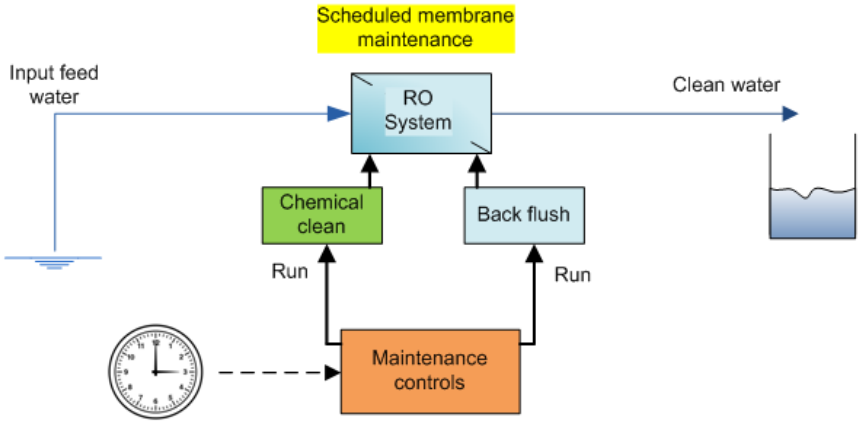

Figure 6-1: RO system schematic with conventional scheduled back flushing and chemical cleaning

6.1 Membrane Flux Degradation Model

Modeling of membrane flux decline has been an active area of research for a few decades. The most accurate way of modeling membrane flux decline is to observe the normalized permeate flow for a given system over a long period of time and empirically deduce a flux decline model. One such study was reported by Zhu, et al., [59], using data from [84] and [85]. A DuPont B-10 hollow fiber RO module was used to desalinate sea water at 35000 ppm. Fouling and scaling causes the water permeability to decline. After about one year of operation, the permeability went down from 3.0 X 10^{-10} kg/sN to 1.0 X 10^{-10} kg/sN. An exponential decay model was used to describe this water permeability decline as follows [59]:

$$Q = Q_0 e^{-t/T} \tag{41}$$

where Q_0 is 3.0 X 10^{-10} kg/sN and T is 328 days.

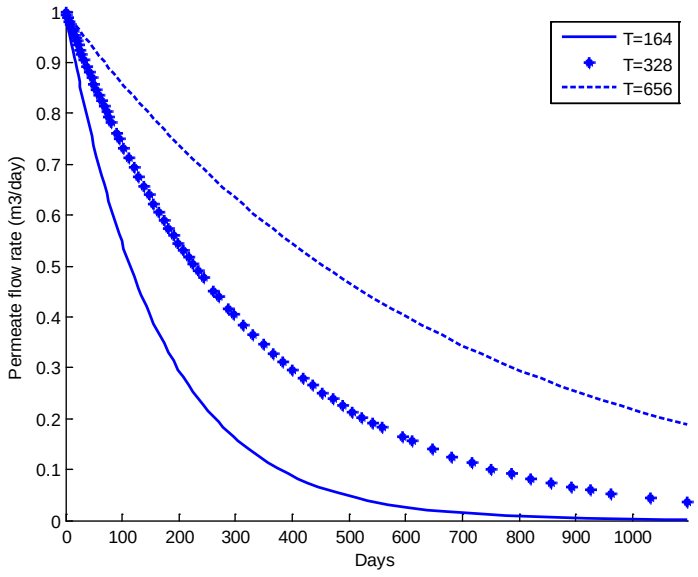

Figure 6-2: Permeate production decline caused by fouling and scaling without regenerating membranes for a 1 m^3 per day PVRO system. The expected decline in permeate production for three decay constants of 164, 328 and 656 days are shown

Spiral wound RO membranes also show similar exponential flux degradations due to fouling of the membranes. This model can be scaled to smaller scale PVRO systems. Using this time constant of 328 days, the permeate production of a 1000 liter (1 m^3) per day PVRO system can be predicted using the exponential decay model. The water permeability for a membrane is a

factor which, when multiplied by the net driving pressure, the area of the membrane, the temperature correction factor and the fouling factor, gives the permeate flow rate. Hence, the permeate flow rate would have the same time constant and exponential behavior as the permeability. Figure 6-2 shows the predicted decline in permeate production caused by fouling and scaling without regenerating membranes for a 1 m^3 per day PVRO system. The expected decline in permeate production for three decay constants of 164 days, 328 days and 656 days are shown. Time constants of 164 days and 656 days were picked to show a range of possible decay rates depending on the feed water quality.

Sections 6.2 and 6.3 analyze the performance of two schedule-based maintenance strategies and two condition-based maintenance strategies for the three cases.

6.2 Schedule-Based Maintenance

In this section, the performances of two schedule based maintenance strategies are analyzed over a one-year period. The strategies are 1) daily back flushing with monthly chemical cleaning, and 2) weekly back flushing with weekly chemical cleaning.

Assumptions and definitions:

- In a **back flush** (BF), some of the clean permeate water, w_1, runs through the membrane from the brine side to the feed side, opposite the feed flow direction.
- Back flushing generally does not restore water production to 100%. Hence, chemical cleaning (cleaning-in-place) may be required.
- In a **chemical cleaning (CC) cycle,** a mixture of clean permeate water, w_2, and cleaning chemicals runs through the membrane either along or opposite the feed flow direction.
- Back flushing recovers the water production drop by an average r_b %.
- Chemical cleaning recovers the water production drop by an average r_c %.
- During permeate back flush and chemical cleaning, all power generated is used to back flush or chemically clean, as there is no power storage in this PVRO system.
- *s*: average specific energy consumption (SEC) of PVRO unit in kWh/m^3. The MIT PVRO experimental system has achieved SEC of 2.5-4 kWh/m^3. Thus, a value of 3 kWh/m^3 was selected for *s* in this analysis.

- w_1: water required for a single back flush in m^3.
- w_2: water required for a single chemical cleaning cycle in m^3.
- e_1: energy required for a single back flush in kWh. It is assumed that

$$e_1 = s \times w_1 \quad \textbf{(42)}$$

- e_2: energy required for a single chemical cleaning cycle in kWh. It is assumed that

$$e_2 = s \times w_2 \quad \textbf{(43)}$$

- b_1: number of back flushes
- c_1: number of chemical cleaning cycles
- T: decay constant in days

Figure 6-3, Figure 6-4, Figure 6-5 and Figure 6-6 illustrate the performance of the weekly back flushing and weekly chemical cleaning maintenance schedule for a decay constant of 328 days for a 1000 liter per day system, while Figure 6-7, Figure 6-8, Figure 6-9 and Figure 6-10 illustrate the performance with a daily back flushing and monthly chemical cleaning maintenance schedule. For the analysis that follows, only the performance of the empirical time constant of 328 days is illustrated in the figures. The system performance for the cases with the two other time constants that are used to show ranges of feed water quality are included in Table 6-1.

Figure 6-3 and Figure 6-7 show drastic improvement in permeate flow rate and production over a year's time when scheduled maintenance is used, as opposed to no maintenance. The no maintenance case was selected as a basis for comparison as typical community scale point of use systems can and are operated without any maintenance [2]. This does result in higher membrane replacement rates. In large desalination plants, out of place cleaning is usually done three to four times a year while the frequency of back flushing is determined by the type of feed water and stoppages [16].

Figure 6-4 and Figure 6-5 show the net water produced in a day during the first 90 days and one year, respectively, after accounting for the water used to back flush and chemically clean once per week. These figures are important as they show the minimum daily product water production levels that can be produced given that the amount of sunlight required to produce that minimum is available. In the absence of large storage reservoirs, meeting minimum daily water needs is critical and directly influences system design, sizing and effective cost of water produced. The

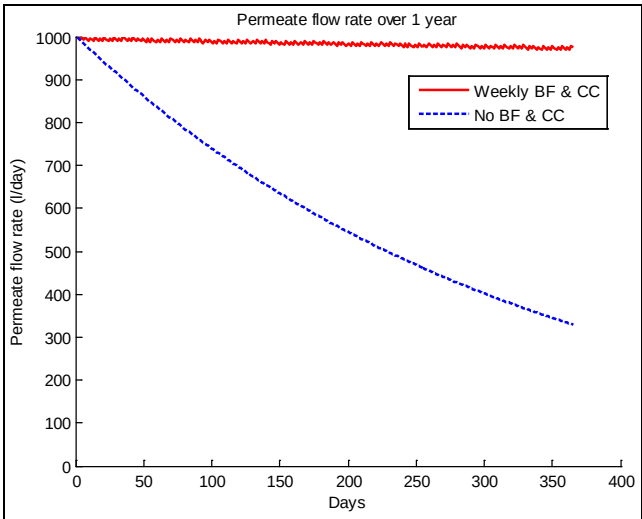

Figure 6-3: Daily permeate flow rate over one year with weekly back flushing and weekly chemical cleaning maintenance schedule (T=328)

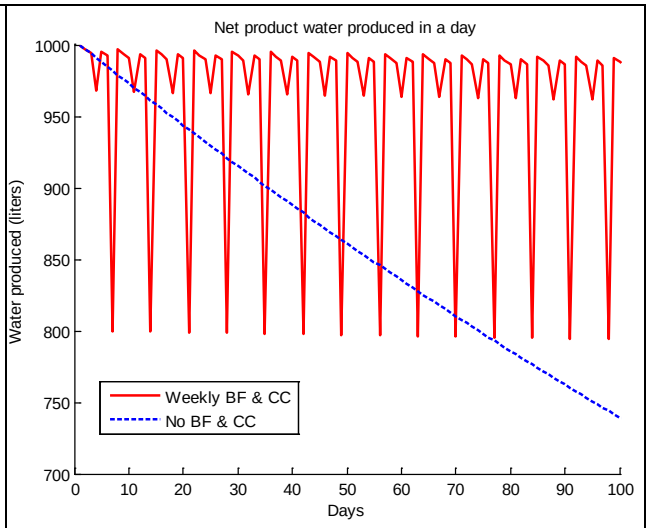

Figure 6-4: Net water produced in a day during first 90 days after accounting for water used in the weekly back flush and weekly chemical cleaning

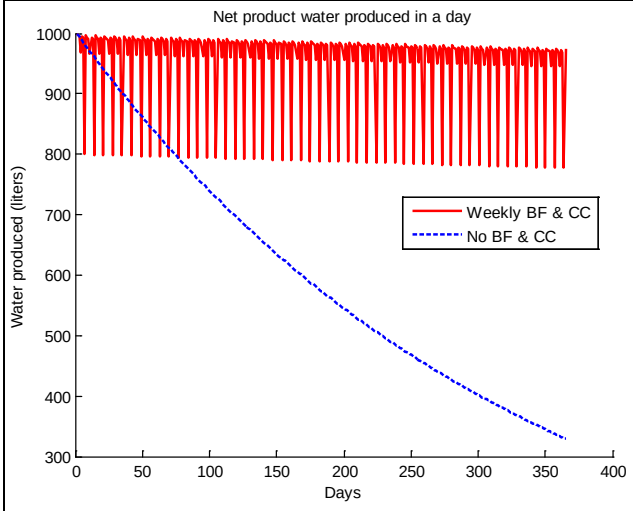

Figure 6-5: Net water produced per day during first year, after accounting for water used in weekly back flushing and weekly chemical cleaning

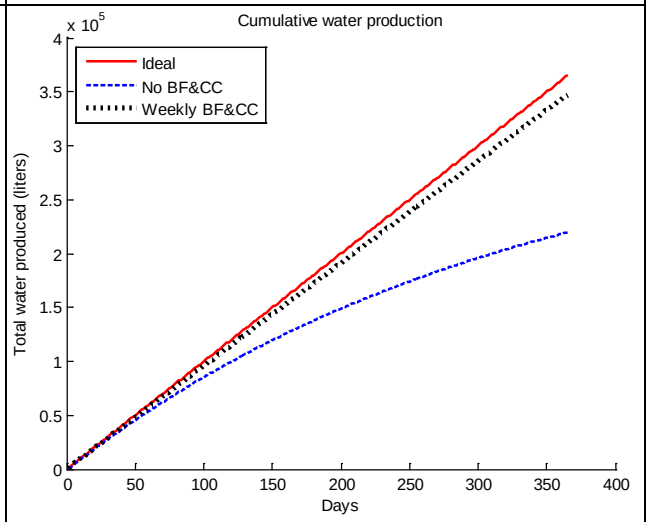

Figure 6-6: Cumulative water produced over a year with weekly back flushing and weekly chemical cleaning

lowest amount of water is produced when a chemical cleaning cycle is completed as a chemical cleaning cycle uses a significant amount of water. Similarly, Figure 6-8 and Figure 6-9 show the net water produced in a day during the first 90 days and one year, respectively, after accounting for the water used for the daily back flushing and monthly chemical cleaning.

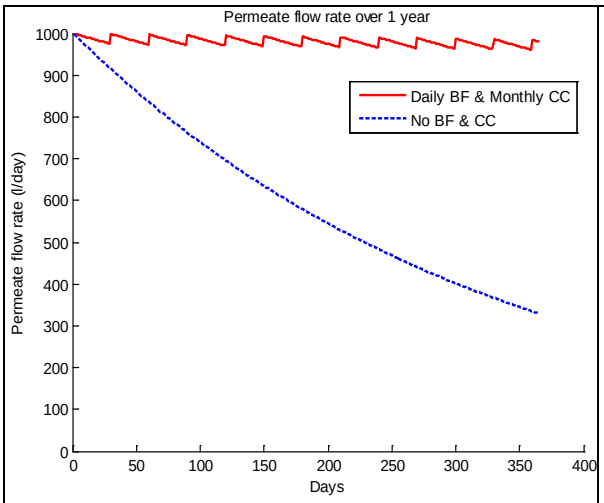

Figure 6-7: Daily permeate flow rate over one year with daily back flushing and monthly chemical cleaning

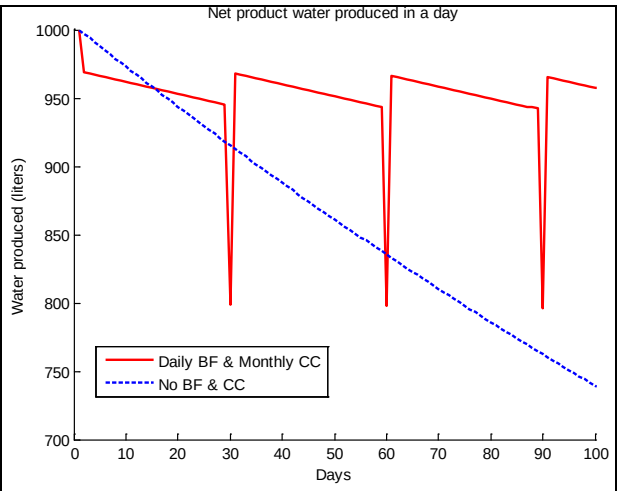

Figure 6-8: Net water produced in a day during first 90 days after accounting for water used in daily back flushing and monthly chemical cleaning

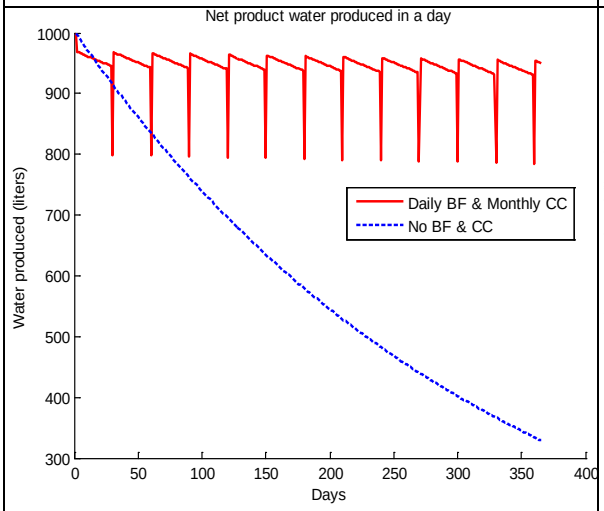

Figure 6-9: Net water produced in a day during first year after accounting for water used for daily back flushing and monthly chemical cleaning

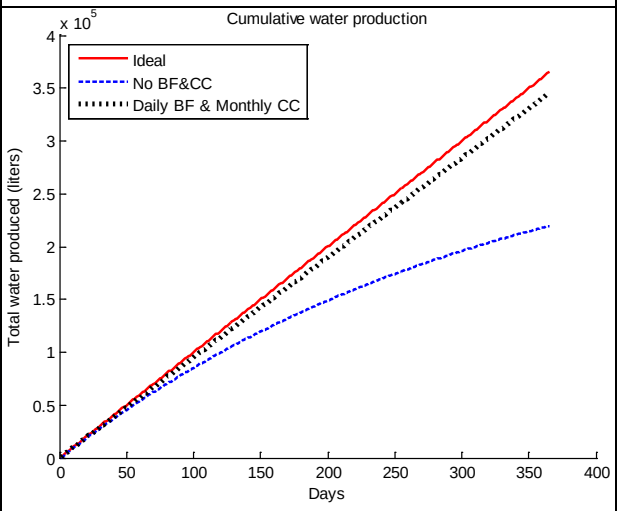

Figure 6-10: Cumulative water produced over a year with daily back flushing and monthly chemical cleaning

Figure 6-6 and Figure 6-10 show the cumulative water production over a year for the weekly BF and weekly CC maintenance schedule and daily BF, monthly CC maintenance schedule, respectively. The “ideal” curve shows the water produced over a year by a system that does not undergo any flux decline. The black dotted lines show the actual amount of water produced by implementing the maintenance schedules and the improvement over the case without any maintenance.

Table 6-1 summarizes the key maintenance parameters and compares the performance of the two schedule-based maintenance strategies. Both maintenance schedules show comparable improvements in total water produced, despite the difference in the frequencies of chemical cleaning and back flushing between the cases. The number of chemical cleanings performed increases the total cost of maintenance, and is further discussed in section 6.4.2. Section 6.4.1 compares the performance of several schedule-based maintenance strategies. More importantly, as feed water quality worsens, as implied by shorter flux decay constants (T), the improvement in water produced is much higher when the maintenance schedules are used, as opposed to performing no maintenance. This is demonstrated by both of the schedule-based maintenance strategies. This demonstrates the importance of doing some sort of maintenance when the feed water quality is in need of significant treatment to make it potable.

Table 6-1: Performance comparison of two schedule-based maintenance strategies over a one year period

	1000 L/day system with 3 kWh per day energy production							
Daily BF, monthly CC - Over 1 year					Weekly BF, weekly CC - Over 1 year			
r_b	70.0%	70.0%	70.0%		r_b	70.0%	70.0%	70.0%
r_c	95%	95%	95%		r_c	95%	95%	95%
s (kWh/m^3)	3	3	3		s (kWh/m^3)	3	3	3
w_1 (m^3)	0.02	0.02	0.02		w_1 (m^3)	0.02	0.02	0.02
w_2 (m^3)	0.1	0.1	0.1		w_2 (m^3)	0.1	0.1	0.1
e_1 (kWh)	0.06	0.06	0.06		e_1 (kWh)	0.06	0.06	0.06
e_2 (kWh)	0.3	0.3	0.3		e_2 (kWh)	0.3	0.3	0.3
T (days)	656	328	164		T (days)	656	328	164
b_1	352	352	352		b_1	52	52	52
c_1	12	12	12		c_1	52	52	52
Total water produced over a year								
Ideal (m^3)	365	365	365		Ideal (m^3)	365	365	365
With BF & CC (m^3)	348.382	344.704	338.258		With BF & CC (m^3)	350.071	346.589	341.400
Without BF & CC (m^3)	280.150	220.543	146.734		Without BF & CC (m^3)	280.150	220.543	146.734
% increase	**24.356**	**56.298**	**130.524**		**% increase**	**24.958**	**57.152**	**132.666**

6.3 Condition-Based Maintenance

In this section, the performance of two condition-based maintenance strategies is analyzed over a one-year period. The condition-based maintenance strategies are; 1) back flushing at 5% drop in normalized permeate flow (NPF) and chemical cleaning at 10% drop in NPF, and 2) back flushing at 7.5% drop in NPF and chemical cleaning at 15% drop in NPF.

The key assumptions and definitions remain the same. The major difference here is the condition at which back flushing and chemical cleaning is triggered.

- Back flushing is triggered when the normalized permeate flow rate (NPF) drops by d_b %, when condition-based maintenance is used. This is the percentage drop from the previous back flush operation.
- Chemical cleaning is triggered when the normalized permeate flow rate (NPF) drops by d_c % in the case of condition based maintenance. This is the percentage drop from the previous chemical cleaning operation.

Figure 6-11, Figure 6-12, Figure 6-13 and Figure 6-14 illustrate the performance of the Back flushing at 5% drop in NPF and chemical cleaning at 10% drop in NPF maintenance schedule for a decay constant, T of 328 for a 1000 liter per day system while Figure 6-15, Figure 6-16, Figure 6-17 and Figure 6-18 illustrate the performance of the PVRO system with a back flush at 7.5% drop in NPF and chemical clean at 15% drop in NPF maintenance schedule.

In this analysis, only the performance of the empirical time constant of 328 days has been illustrated in the figures. The performance for the cases with the two other decay constants are included in Table 6-2.

Figure 6-11 and Figure 6-15 show significant improvements in permeate flow rate and permeate production over one year, when compared with the performance of a system that is not maintained. Figure 6-12 and Figure 6-13 show the net water produced in a day during the first 90 days and one year, respectively, after accounting for the water used in back flushing at 5% drop in NPF and chemical cleaning at 10% drop in NPF maintenance schedule. The minimum water produced in a day is comparable to that of the schedule based maintenance strategies. Similarly, Figure 6-16 and Figure 6-17 show the net water produced in a day during the first 90 days and

one year, respectively, after accounting for the water used in back flush at 7.5% drop in NPF and chemical clean at 15% drop in NPF maintenance schedule.

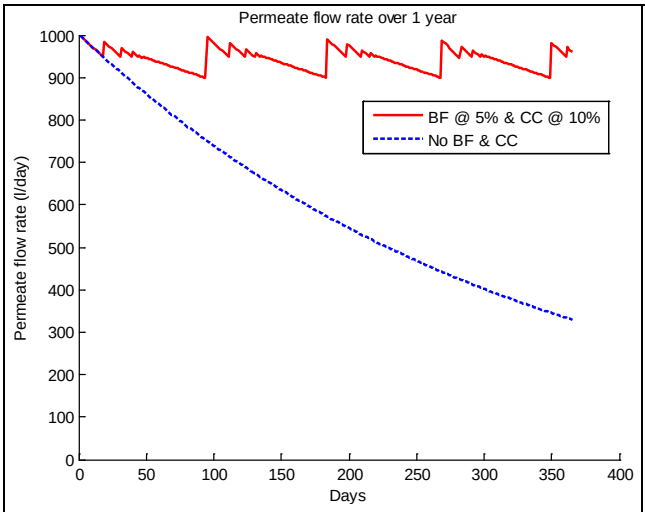

Figure 6-11: Daily permeate flow rate over one year with back flushing after a 5% drop in NPF and chemical cleaning after a 10% drop in NPF

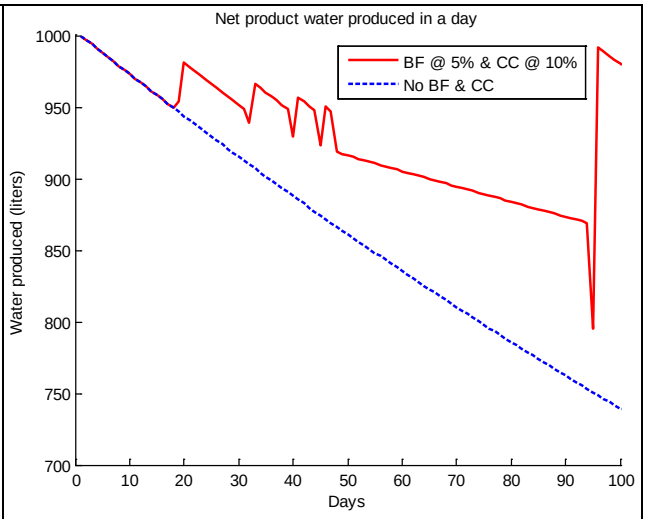

Figure 6-12: Net water produced in a day during first 90 days after accounting for water used with back flushing at 5% drop in NPF and chemical cleaning at 10% drop in NPF

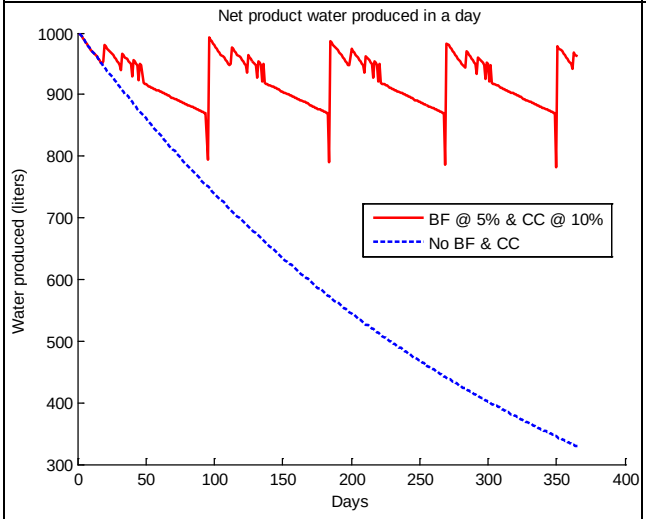

Figure 6-13: Net water produced in a day during first year after accounting for water used with back flushing at 5% drop in NPF and chemical cleaning at 10% drop in NPF

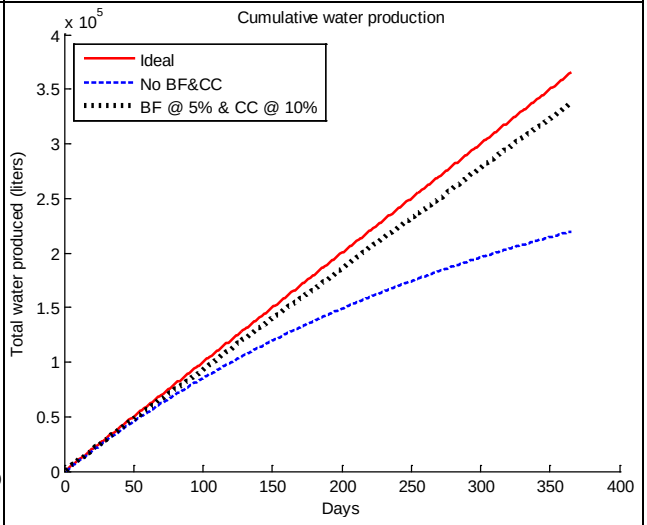

Figure 6-14: Cumulative water produced over a year with back flushing at 5% drop in NPF and chemical cleaning at 10% drop in NPF

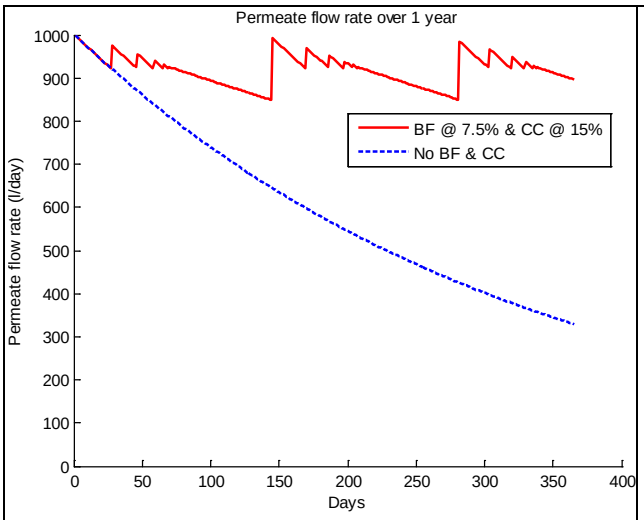

Figure 6-15: Daily permeate flow rate over one year with back flushing at 7.5% drop in NPF and chemical cleaning at 15% drop in NPF

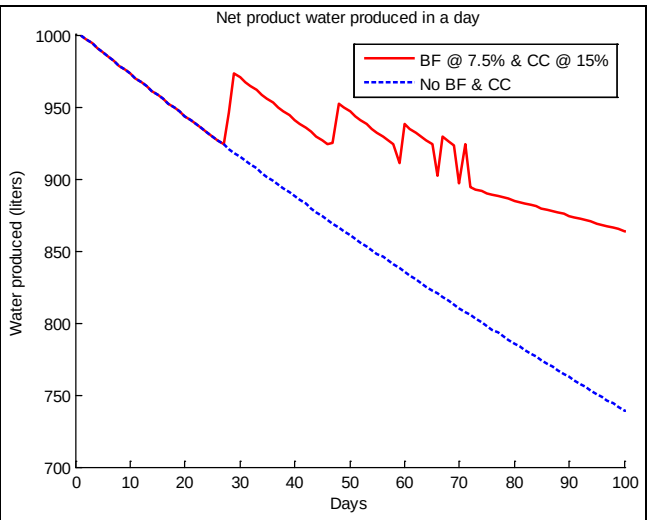

Figure 6-16: Net water produced in a day during first 90 days after accounting for water used with back flushing at 7.5% drop in NPF and chemical cleaning at 15% drop in NPF maintenance schedule

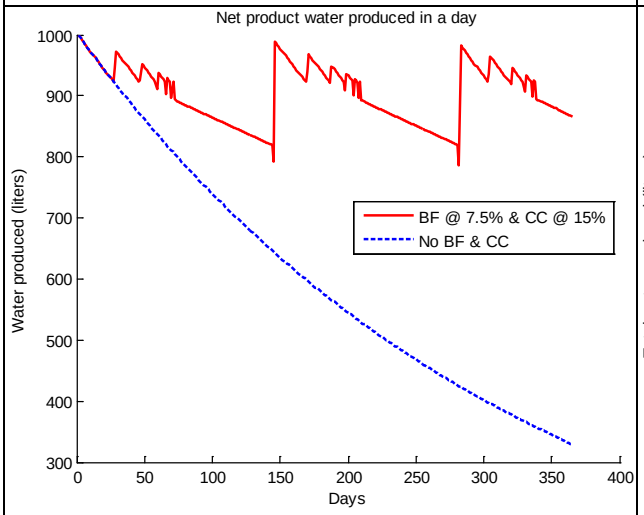

Figure 6-17: Net water produced in a day during first year after accounting for water used with back flushing at 7.5% drop in NPF and chemical cleaning at 15% drop in NPF

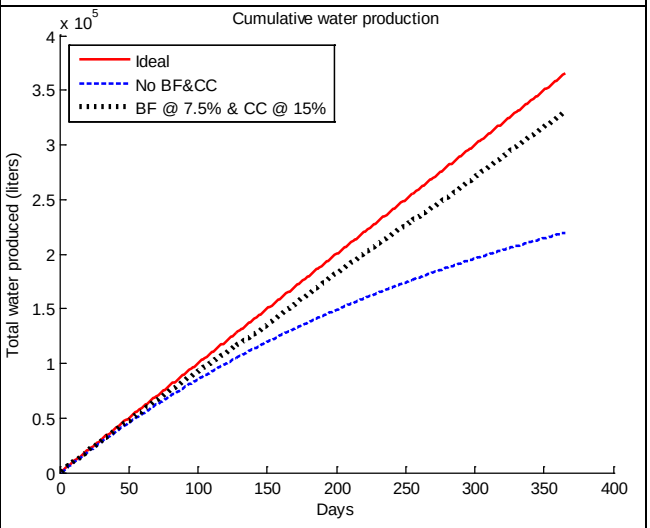

Figure 6-18: Cumulative water produced over a year with back flushing at 7.5% drop in NPF and chemical cleaning at 15% drop in NPF

Figure 6-14 and Figure 6-18 show the cumulative water production over a year for the two condition-based maintenance schedules respectively. The “ideal” curve shows the water produced over a year by a system that does not undergo any flux decline. The black dotted lines

show the actual amount of water produced by implementing the maintenance schedules and the improvement over the case without any maintenance.

Table 6-2 summarizes the key maintenance parameters and compares the performance of the two condition-based maintenance strategies. The BF at 5%, and CC at 10% maintenance strategy shows a higher yield in total water produced over a year for all three decay constants. This scheme requires more chemical cleanings than the other condition-based maintenance scheme, which will affect the system lifetime costs. This is discussed in section 6.5.2. Section 6.5.1 compares the performance of several condition-based maintenance strategies.

It is known that insufficient membrane cleaning and delaying maintenance until after some fouling has occurred can result in permanent fouling [16]. It is also known that frequent cleaning with chemicals has adverse effects on the membrane, thereby shortening its ability to reject salt and its life. Hence, using condition-based maintenance is better than using schedule-based maintenance, since the timing of maintenance cannot be predicted accurately due to seasonal and stochastic changes in feed water quality and operating conditions. When these fluctuations are frequent and membrane fouling cannot be analytically predicted, schedule-based maintenance will certainly not work as well as condition-based maintenance.

Table 6-2: Performance comparison of two condition based maintenance schedules over a one-year period

1000 l/day system -- 3 kWh per day energy production								
5% BF, 10% CC - Over 1 year					7.5% BF, 15% CC - Over 1 year			
d_b	5%	5%	5%		d_b	7.5	7.5	7.5
d_c	10%	10%	10%		d_c	15	15	15
T	656	328	164		T	656	328	164
b_1	197	205	236		b_1	153	186	217
c_1	2	4	9		c_1	1	2	5
Total water produced over a year								
Ideal (m^3)	365	365	365		Ideal (m^3)	365	365	365
With BF & CC (m^3)	338.422	338.467	333.655		With BF & CC (m^3)	332.927	327.848	325.742
Without BF & CC (m^3)	280.150	220.543	146.734		Without BF & CC (m^3)	280.150	220.543	146.734
% increase	**20.800**	**53.470**	**127.387**		**% increase**	**18.839**	**48.655**	**121.994**

6.4 Optimal Schedule-Based Maintenance Strategies

6.4.1 Maximum Water Production Schedule

Figure 6-19 shows the percentage improvement in annual water production for a range of schedule-based maintenance strategies when compared with the water production of a system without any maintenance. Here, the optimal schedule-based maintenance strategy under the conditions and assumptions outlined previously is monthly chemical cleaning and semi-weekly back flushing. This strategy gives a 59 % increase in water production over a system without any maintenance. When monthly chemical cleaning is used, the alternate day back flushing and weekly back flushing schedules also show comparable improvements. As the frequency of chemical cleaning decreases, back flushing has a greater effect on increasing the annual water production. Alternatively said, when the use of chemicals decreases, back flushing needs to be done more frequently. The case without any chemical cleaning shows that an increase of about 40% can be achieved. While this is considerably lower than the optimal case, it shows that back flushing can be effective in mitigating fouling if the system runs out of cleaning chemicals. Alternatively, for places where the use, storage, replenishment and disposal of chemicals are difficult or expensive, using a back-flushing schedule may be better than not performing any maintenance.

6.4.2 Most Cost-Effective Schedule

As mentioned in section 4.7.2, the cleaning costs for 4-inch diameter membranes can be anywhere from \$2.50 to \$12.50 for each chemical cleaning cycle. Using an average price of \$7.50 for the cost of a chemical cleaning cycle, the tradeoff between the cost of chemically cleaning the membrane and the increase in water production can be calculated. Figure 6-20 shows the net value of water produced in one year after accounting for the cost of cleaning chemicals, i.e. the total amount of water produced multiplied by the average cost of water and then subtracting the total annual cost of chemicals. The quarterly chemical cleaning cycles are the most cost-effective. When paired with semi-weekly and weekly back flushing, the net value of water produced in a year is about \$441. Without any maintenance, the total amount of clean water produced in a year is 220.543 m^3. At an average water cost of \$1.37 per m^3, this is an

annual value of $302.14. Thus, the most cost effective maintenance schedule increases the value of water produced per year by 46%.

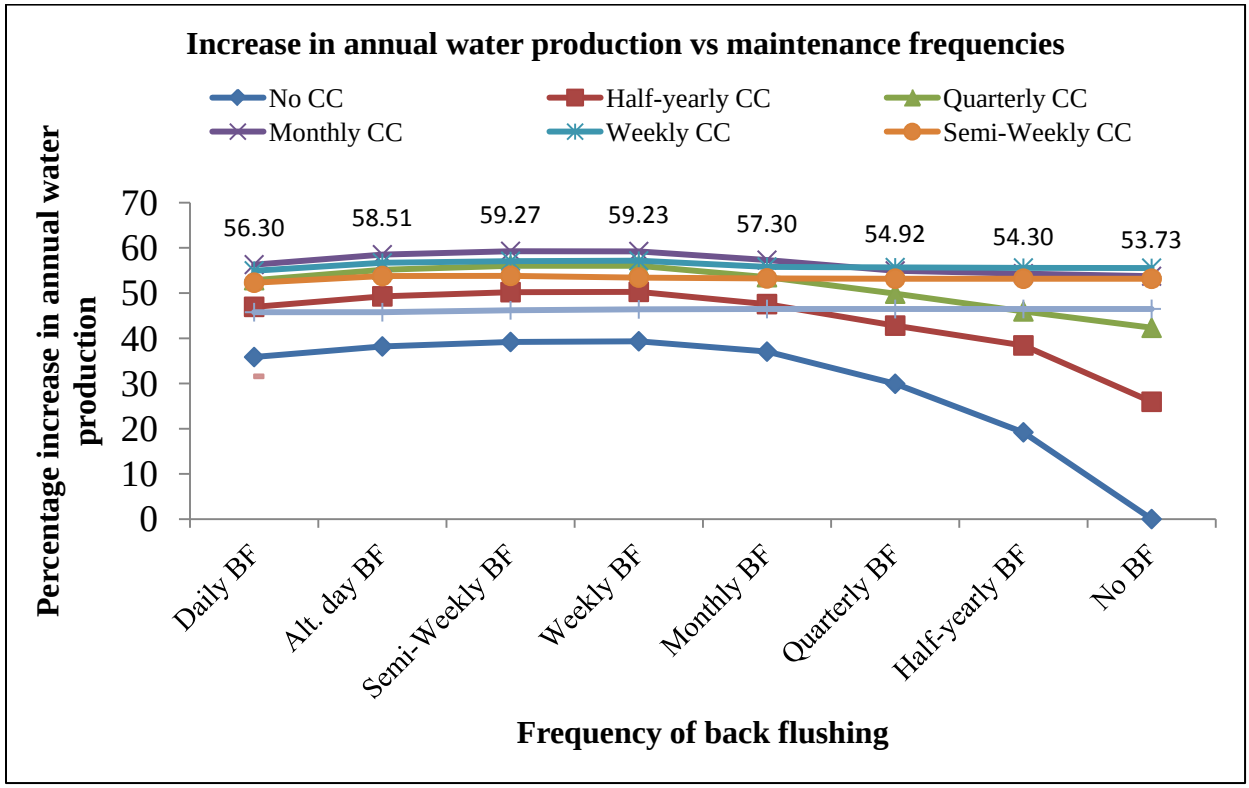

Figure 6-19: Improvement in annual water production for a range of schedule-based maintenance strategies

In cases where the water production increases are comparable, it may be better to back flush more frequently, since this removes the foulant layer at an earlier stage. This will have an effect on the regeneration efficiency of the maintenance cycles. The results show that the no chemical cleaning, half yearly, quarterly and monthly chemical cleaning schemes result in similar performance compared to an unmaintained system from a net cost perspective. As the frequency of chemical cleaning increases, the cost of water increases and so the net value goes down. In cases where multiple chemical cleaning schedules show similar performance, the choice of chemical cleaning frequency will depend on the cost of chemicals, the amount of chemical available on-site, the ease of replenishing the chemical tank and, most importantly, the effect of the chemicals on the life of the membrane. Frequent chemical cleaning has an adverse effect on the RO membranes as mentioned previously.

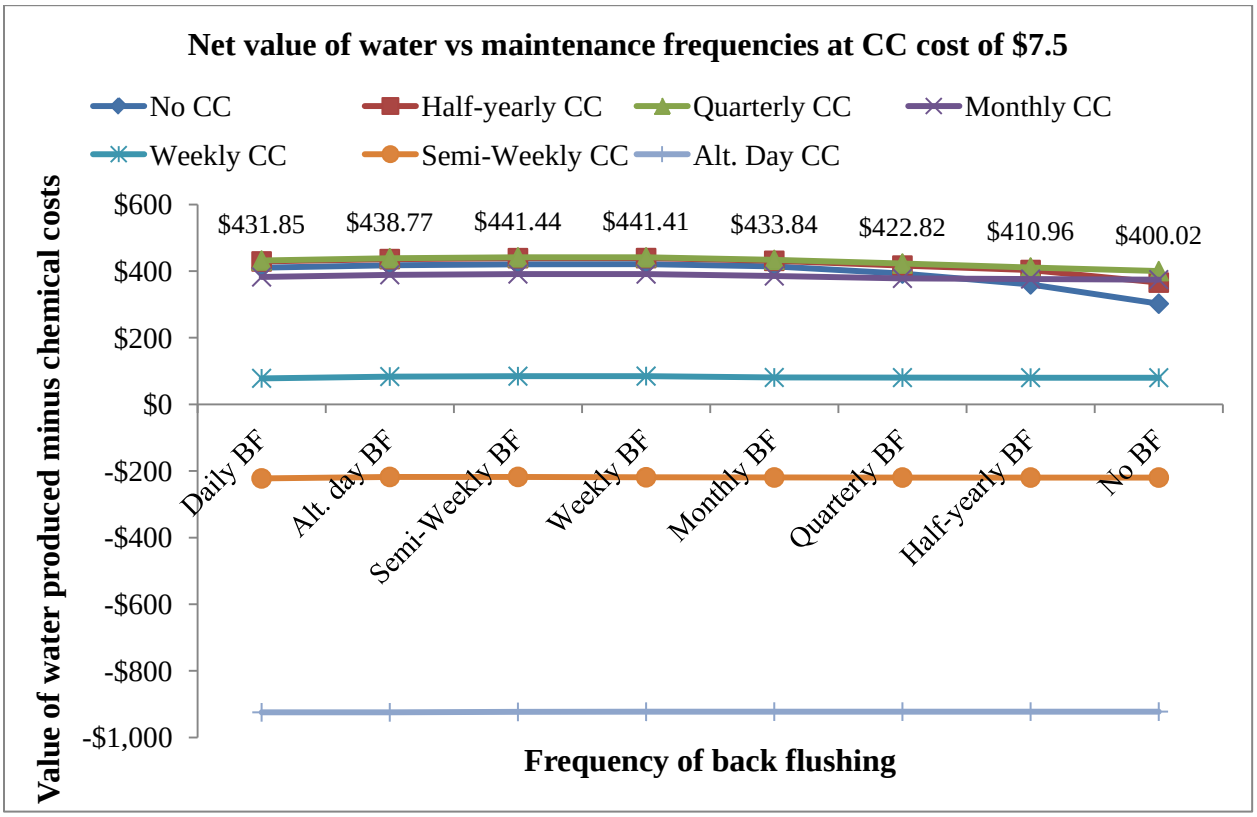

Figure 6-20: Net value of water produced in 1 year after accounting for cleaning chemicals used in a range of schedule based maintenance strategies

6.5 Optimal Condition-Based Maintenance

6.5.1 Maximum Water Production Strategy

Figure 6-21 shows the percent improvement in annual water production for a range of condition-based maintenance schemes, compared to the water production of a system without any maintenance. This shows that the optimal condition-based maintenance scheme under the conditions and assumptions outlined previously triggers a chemical clean at a 5% drop in normalized permeate flow (NPF) and a back flush at a 2.5% drop in NPF. Using these trigger points results in over 10% increase in cumulative annual water production compared to scheduled quarterly maintenance cycle and a 58% increase in water production. For most scheduled maintenance systems, quarterly maintenance is the most commonly used. The quarterly maintenance performance is shown in Figure 6-19.

The scheme with the least amount of chemical cleaning is the one that triggers a CC at an NPF drop of 15%. A 15% drop was selected as the maximum permissible drop before a CC is initiated based on membrane manufacturers' recommendations. Using the 15% trigger for chemical cleaning and varying the point at which back-flushing is triggered results in 48% to 50% increases in water production.

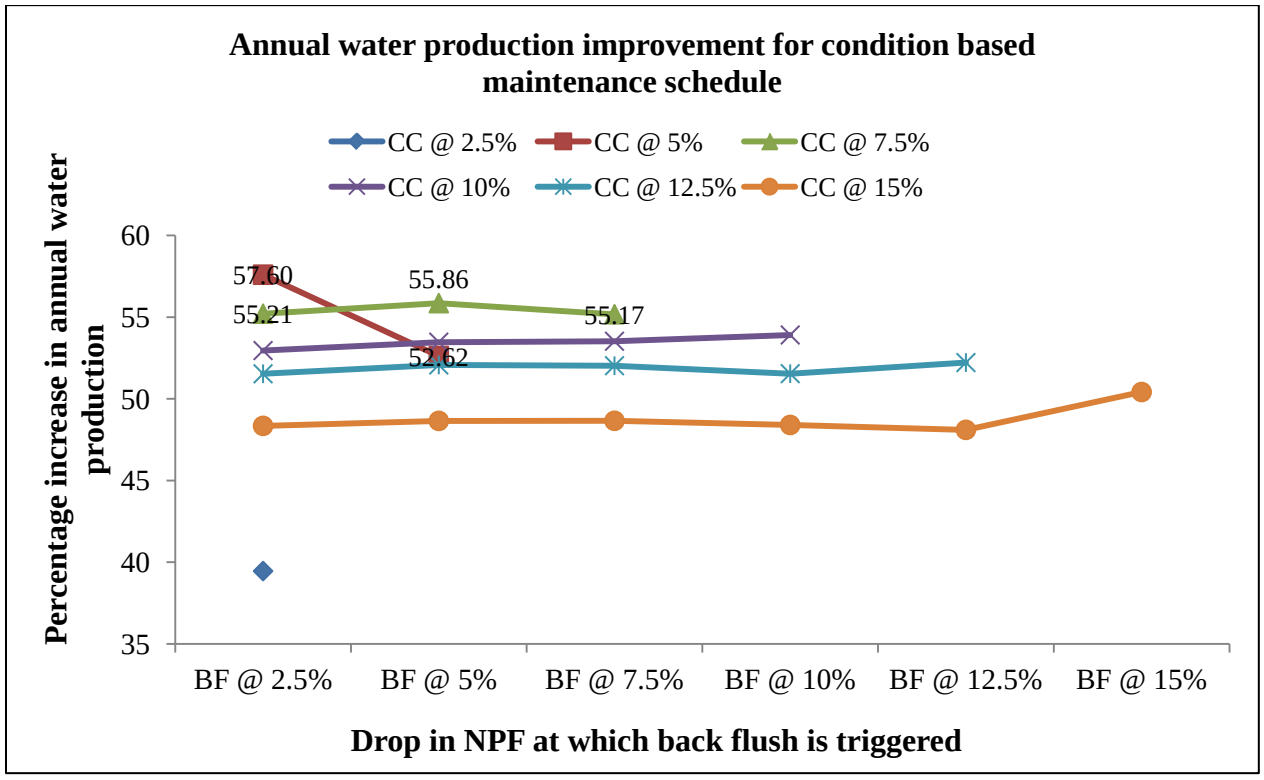

Figure 6-21: Improvement in annual water production for a range of condition-based maintenance strategies

The performance of the best schedule-based maintenance strategy and the best condition-based maintenance strategies are very similar; 59 % and 58 % respectively for the assumptions stated. This shows that it is possible to achieve the same performance with either strategy as long as the operating conditions and the long term behavior of the system remain constant. However, in reality this is not the case and the operating parameters change throughout the day. Consequently, membrane fouling cannot be predicted accurately. In community scale PVRO systems, these changes are more pronounced as the point of use can vary considerably. As a result schedule-based maintenance could result in running the system without maintenance even

after the membrane has degraded sufficiently and requires cleaning. Waiting too long can result in irreversible fouling and loss of water production. Cleaning before maintenance is required can result in excess use of chemicals, wasted water and damage to the membranes due to cleaning. Hence, condition-based maintenance is always better than schedule-based maintenance as it ensures maintenance is carried at the exact instant it is required.

6.5.2 Most Cost-Effective Condition-Based Maintenance Strategy

Once again, using an average of $7.50 for the cost of one chemical cleaning cycle, the tradeoff between the cost of chemically cleaning and the increase in water production can be calculated. Figure 6-22 shows the net value of water produced in one year after accounting for the cost of cleaning chemicals for a range of condition-based maintenance schemes. Note that in cases where the chemical cleaning and the back flush are triggered by the same NPF, the chemical cleaning overrides the back flush cycle. This explains why the case with back flushing and chemical cleaning triggered at a 5% drop in NPF shows such poor performance. Here, the chemical cleaning cycle is triggered too frequently, resulting in high chemical and water costs per cleaning cycle. The most cost-effective condition-based cleaning schemes are those with CC at a 12.5% drop in NPF and BF at a 5% or a 7.5% drop in NPF. Both result in a net value of water produced of $444 in a year. This is an improvement of about 47% over the value of water produced by a system with no maintenance: $302/year.

In cases showing similar increase in water value, it may be better to back flush at lower percentages of pressure or flow drops, since this removes the foulant layer at an earlier stage and is likely to have an effect on the regeneration efficiency of the maintenance cycles. If back flushing is done more often, the regeneration efficiency is better and this will extend membrane life as well as the productivity of the membrane. The results show that condition-based maintenance schemes perform similar to each other from a net annual value perspective. In cases where multiple chemical cleaning schemes show a similar performance, the choice of chemical cleaning trigger point will depend on the amount of chemical available on-site, the ease of replenishing the chemical tank, and, most importantly, the effect of the chemicals on the life of the membrane.

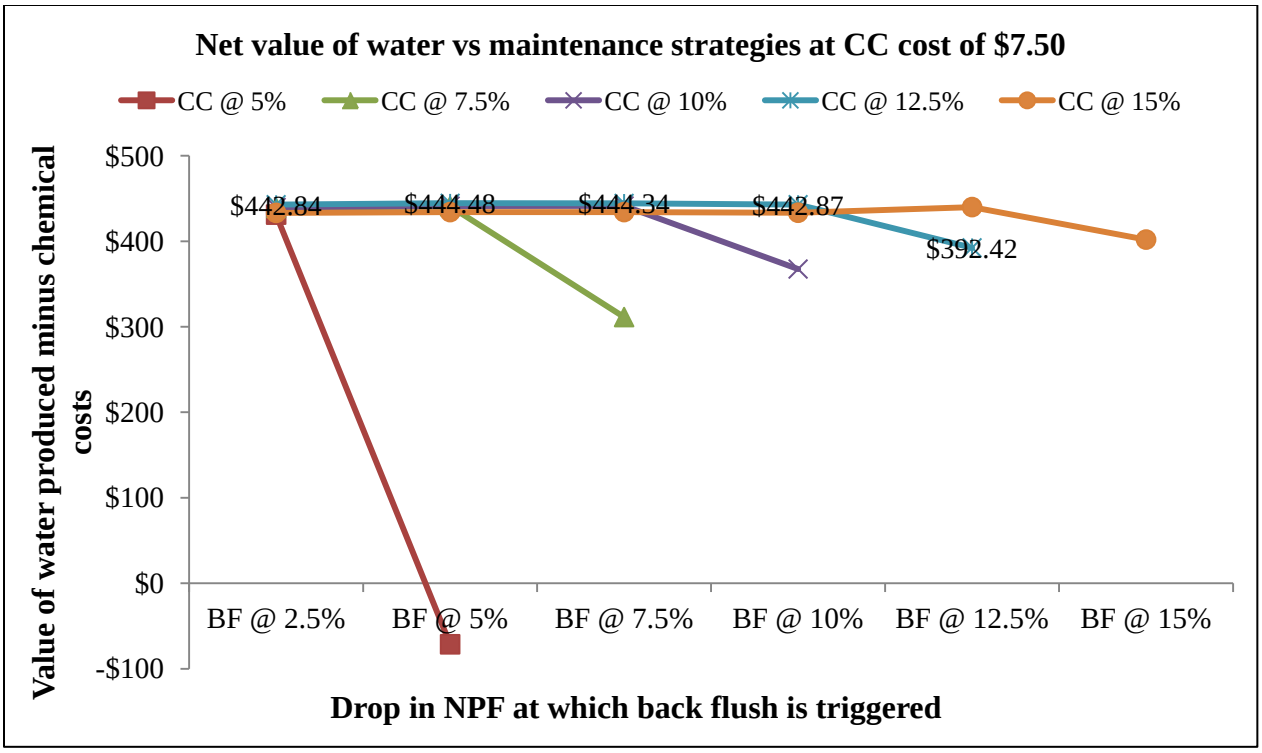

Figure 6-22: Net value of water produced in one year after accounting for cleaning chemicals used in a range of condition-based maintenance schemes

6.6 Sensitivity of Net Value of Water Produced to the Price of Chemical Cleaning

This section analyses the price sensitivity of net value of water produced to the cost of the cleaning chemicals. Figure 6-23 and Figure 6-24 show the net value of water for schedule-based maintenance strategies at a CC cycle cost of $2.50 and $12.50. When the cost of a CC is $2.50, the half yearly, quarterly and monthly chemical cleaning schedules show similar performance. When the cost of a CC is $12.50, the half yearly, quarterly and no chemical cleaning schedules show similar cost. As the cost of the cleaning chemicals increases, the cleaning schedules with higher chemical cleaning frequency get more expensive and thus have a lower net value over a one-year period.

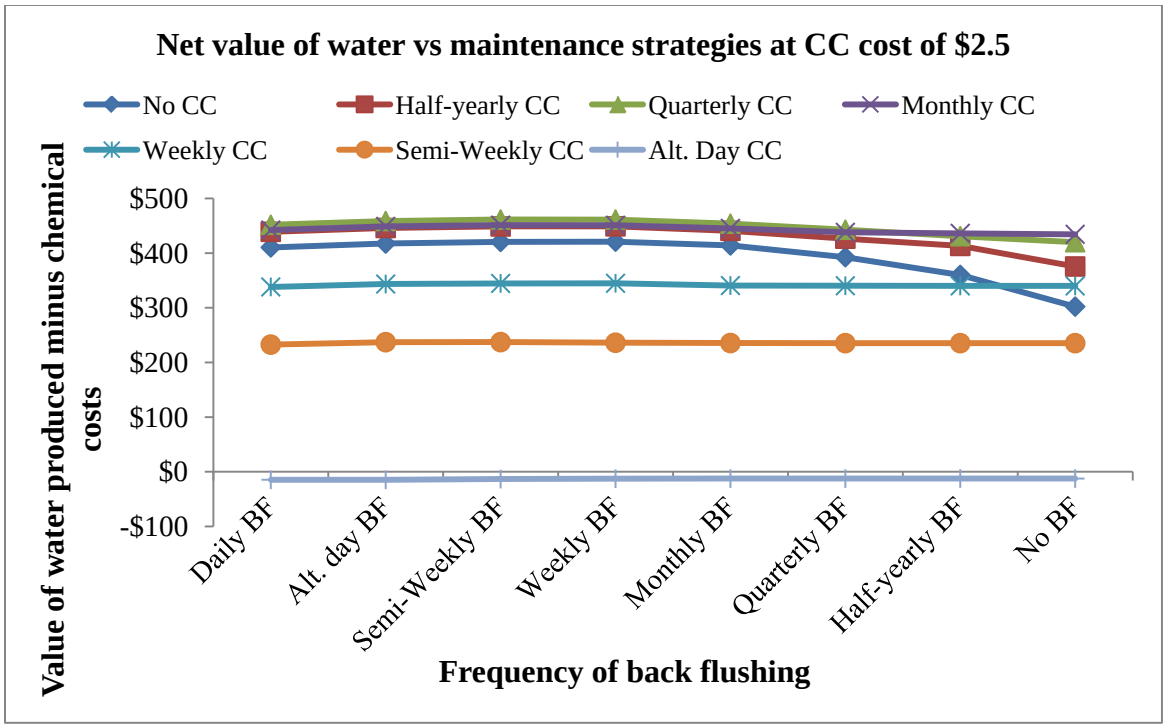

Figure 6-23: Net value of water produced in one year after accounting for cleaning chemicals used in a range of schedule-based maintenance strategies with a CC cost of $2.50

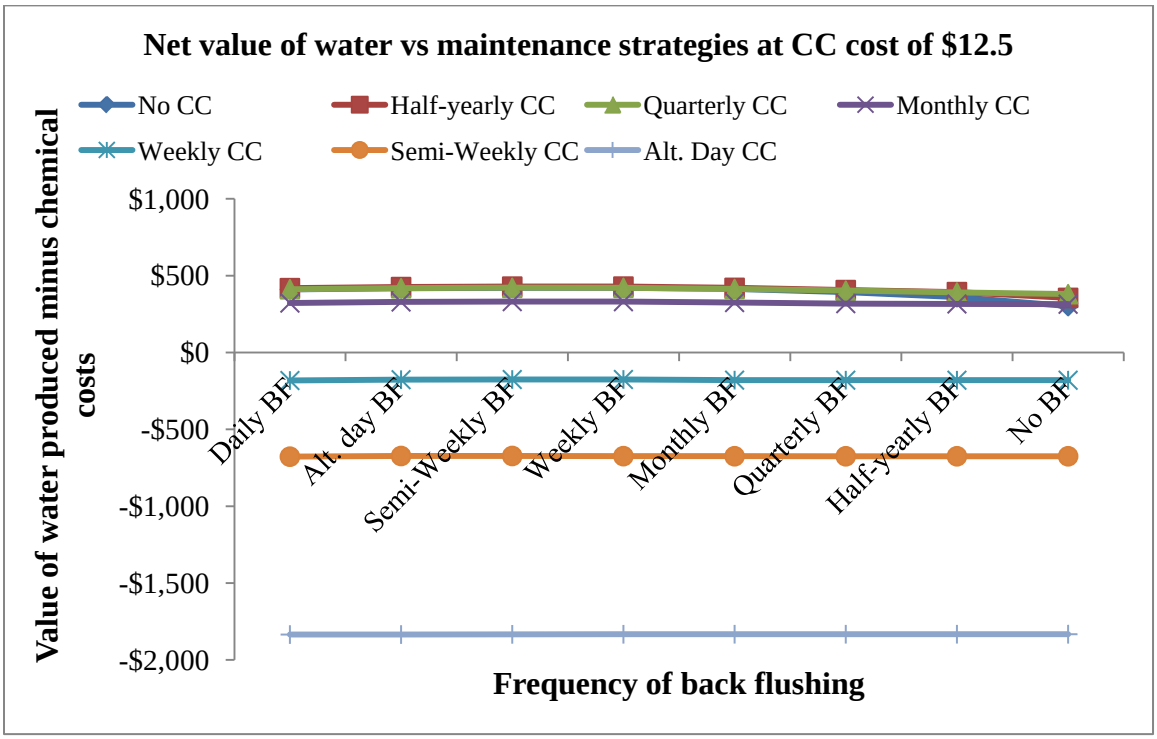

Figure 6-24: Net value of water produced in one year after accounting for cleaning chemicals used in a range of schedule-based maintenance strategies with a CC cost of $12.50

Figure 6-25 and Figure 6-26 show the net value of water for condition-based maintenance strategies at a CC cycle cost of $2.50 and $12.50, respectively. Overall the condition-based maintenance strategies do not show a significant variation for a given cost of chemical cleaning. When the cost of a CC is $2.50, the strategy that triggers back flushing at 2.5% and chemical cleaning at 5% shows the highest annual net value of water produced: about $461/year. When the cost of a CC is $12.50, the strategy triggering back flushing at 5% and chemical cleaning at 12.5% shows the highest net annual value of water produced: about $435. As the cost of the cleaning chemicals increase, strategies which trigger chemical cleaning at lower percentages of normalized pressure drops become more expensive, resulting in lower net values of water produced over one year. When the net annual values are relatively similar, it is better to use strategies that trigger the chemical cleaning and back flushes at lower normalized drops, as this will likely prevent the irreversible fouling of membranes. This advantage needs to be balanced by the membrane damage done by the cleaning chemicals.

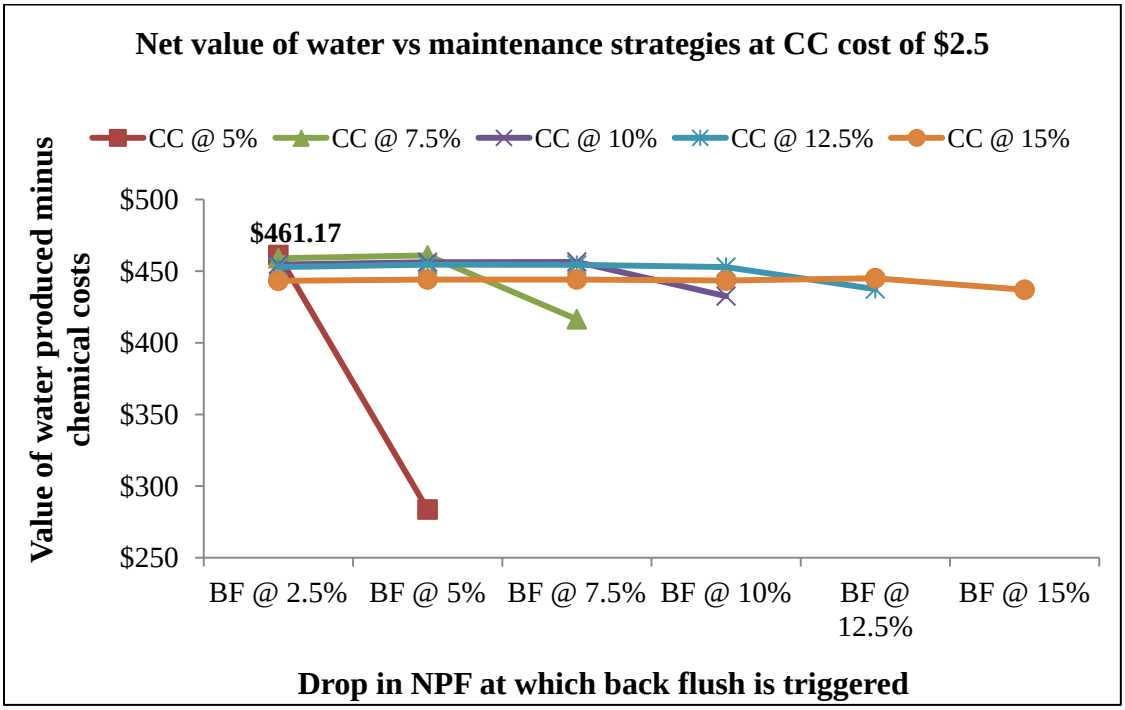

Figure 6-25: Net value of water produced in one year after accounting for cleaning chemicals used in a range of condition-based maintenance schedules with a CC cost of $2.50

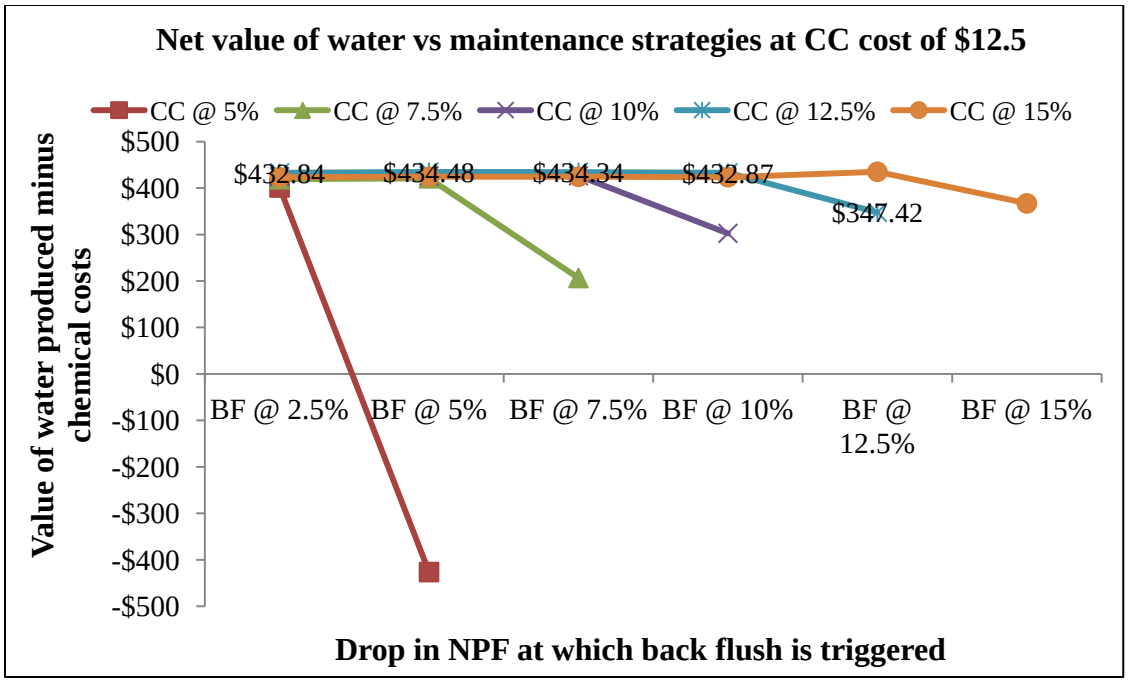

Figure 6-26: Net value of water produced in one year after accounting for cleaning chemicals used in a range of condition-based maintenance strategies with a CC cost of $12.50

6.7 Effect of Simultaneous Power and Fouling Control

Using the energy compliance model discussed in Chapter 3 and Appendix A, the concept PVRO system with the variable recovery ratio, pelton wheel generator energy recovery device can be optimally controlled to produce the maximum clean water. The details of the control methodology and the control feasibility simulations are discussed in Appendix A, section A.3.2. The simulations show that the controllable recovery system can achieve an improvement of 47 % over the 318 liters of water produced by the fixed recovery MIT PVRO system for a July day in Boston.

Using the optimal condition-based maintenance strategy of chemical cleaning at a 5 % drop in normalized permeate flow (NPF) and back flushing at a 2.5 % drop in NPF, the combined effect of power and fouling control is shown. The fouling factor for the membrane on any given day

can be obtained from the condition-based maintenance simulations. The power control simulations were rerun using this fouling factor in the permeate flow rate equation for the membrane. The daily water production for the controllable energy recovery concept system for a July day in Boston was compared to the performance of the MIT PVRO experimental system for cases with and without power and fouling control.

The MIT PVRO experimental system produced 318 liters. This is without any power control. If the same system was operated continuously for one year without any maintenance, and assuming the flux declines as predicted by the exponential model used in the simulations, this system would produce only 246 liters at the end of one year for the same climate and feed water conditions. If the optimal condition-based maintenance strategy was used to control the membrane fouling, then the system would produce 317 liters in a July day after one year of continuous operation. This is a difference of about 29 %.

As shown in the Appendix A, if a controllable energy recovery system was used instead of the fixed recovery MIT PVRO system, the same amount of sunlight can be used to produce about 470 liters of water in a July day. If the controllable energy recovery system's flux also declined as per the exponential model, then after one year of continuous operation, the system would be able to produce only 315 liters on the same July day. However, if the optimal condition-based maintenance strategy was used, the controllable energy recovery system would produce 455 liters. This is a difference of 44.4 %.

Assuming flux degradation as predicted by the exponential decay model, the productivity of the MIT PVRO system and the controllable energy recovery system drop significantly. However, condition-based maintenance can improve the productivity of the systems after one continuous year of operation by 29 % and 44.4 % respectively as compared to running the systems without any maintenance. The best case performance after one year of continuous operation is that of the controllable energy recovery system at 455 liters. The worst case performance is the one without any fouling control for the MIT PVRO system which is about 246 liters. When compared with the uncontrolled, unmaintained MIT PVRO system performance, the controllable energy recovery system with the optimal condition-based maintenance and control strategy shows an improvement of 85 %. Thus, the effect of condition based maintenance can be tremendous on both the MIT PVRO system and the controllable energy recovery system.

6.8 Cost Function

The net gain in permeate water after using a maintenance schedule can be expressed using closed form expressions.

The water production gained due to back flushing and cleaning, $w_{G,}$ is calculated using:

$$w_G(t_i - t_{i-1}) = \int_{t_{i-1}}^{t_i} \frac{x(b,t)}{s(t)} P(t)dt \qquad \text{in m}^3 \qquad \textbf{(44)}$$

where *x(b,t)* is the average percentage drop in water production at time *t*. This is the drop from the water production level at the same pressure at *t = 0*. For the sake of simplicity, the average percentage drop between a BF or CC window represents the water gained due to BF and/or CC that would have been lost otherwise.

P(t) is the power production at time *t* in kW

s(t) is the instantaneous specific energy consumption at time *t* in kWh/m^3

b_{ti} is the total number of back flushes in elapsed time $(t_i - t_{i-1})$

c_{ti} is the total number of chemical cleaning cycles in elapsed time $(t_i - t_{i-1})$

The water lost due to back flushing and cleaning w_L is the sum of the water required for back flushing and cleaning as well as the water not produced with the energy required for cleaning, and is calculated using:

$$w_L(\mathrm{t_i} - \mathrm{t_{i-1}}) = w_1 b_{ti} + \frac{e_1 b_{ti}}{s} + w_2 c_{ti} + \frac{e_2 c_{ti}}{s} \qquad \text{in m}^3 \qquad \textbf{(45)}$$

where

b_{ti} is the total number of back flushes in elapsed time $(t_i - t_{i-1})$

c_{ti} is the total number of chemical cleaning cycles in elapsed time $(t_i - t_{i-1})$

s is the average specific energy consumption (SEC) of PVRO unit in kWh/m^3. As noted previously, a value of 3 kWh/m^3 was selected for this analysis.

w_1 is the water required for one back flush in m^3.

w_2 is the water required for one chemical cleaning cycle in m3.

e_1 is the energy required for one back flush in kWh. This is assumed to be equal to s*w1.

e_2 is the energy required for one chemical cleaning cycle in kWh. This is assumed to be equal to s multiplied by w_2.

Hence, the net gain in water production is given by:

$$Net\ gain = w_G - w_L \quad \textbf{(46)}$$

A cost function is required for optimizing back flushing and chemical cleaning routines. It is used to determine the optimal maintenance schedules once the key parameters of flux recovery, triggering point for maintenance cycles, duration of cycles and amount of cleaning are determined empirically. The same cost function can be used with the self-optimizing algorithm presented in the following section. The cost function is as follows:

$$C = A_{cc}c_{cc} + \Delta RR_{mem}c_{mem} + \frac{\delta}{\rho}\left(W_d - C_{sys}S_{sys}\eta_{sys}\right) + C_L M_E + C_{trans} - \left(w_G - w_L\right)c_w \quad \textbf{(47)}$$

where:

c_w is the life-cycle amortized specific cost of clean permeate water in \$/m^3. This cost is the initial cost calculated at the time of designing an optimal system for the specified requirements. An average water cost of \$1.37 per m^3 is used by averaging the water costs produced from sea water from Table 5-1.

A_{CC} is the amount of cleaning chemicals used

C_{CC} is the cost of cleaning chemicals in \$/m^3

ΔRR_{mem} is the change in the membrane replacement rate

c_{mem} is the membrane replacement cost

δ is the factor that scales the demand – supply mismatch for a known reserve ratio. This factor can be linear or non-linear. For example, the demand factor can be very high for desert regions but low for semi-urban regions as the cost of finding alternate sources of water will be lower in semi-urban areas than desert areas.

ρ is the reserve ratio, defined as the ratio of the volume of clean water present in the reservoir tank to the size of the reservoir tank. A reserve ratio of one means that the tank is full. However, reserve ratios of less than one mean that the reserve water levels are fast depleting.

W_d is the desired flow rate

C_{sys} is the specific cost of the system expressed in \$/m^3/day.

S_{sys} is the rated capacity of the system to produce clean water, expressed in m^3/day.

η_{sys} the percentage of flow rate as compared to the rated flow rate. This gives the actual amount of water the system can produce.

C_L is the labor cost that will vary from location to location and can comprise up to 5% of the capital costs [9], [86]. Thus, the labor costs per service work out to 5% of the equipment and consumables repaired, replaced or refilled during that service.

M_E are the costs of any extra maintenance services required.

C_{trans} are costs associated with shipping and usually amount to 5 % of the total direct costs in large scale desalination plants [81]. In the case of small scale PVRO systems, this cost is much higher as the locations can be remote and difficult to access. Hence, a transportation cost of about 25% of the total direct costs is assumed.

6.9 Parameter Estimation and Condition Based Maintenance Learning Algorithm

The fundamental behavior and function of reverse osmosis membrane desalination systems is well understood and modeled. However, fouling characterization and fouling parameter estimation is still an area of active research. More importantly, maintenance scheduling is strongly determined by the cleaning efficiency and effectiveness. As discussed in section 4.7.2, there are several factors that affect the cleaning effectiveness, such as the time of exposure, the type of chemicals used, the condition at which the membrane was cleaned and so on. Thus, an autonomous PVRO system must continuously evaluate the cleaning effectiveness to determine

an accurate condition-based maintenance strategy that maximizes cumulative water production or optimizes the system-specific cost function. Simultaneously, the condition-based maintenance also affects the cleaning effectiveness and thus continuous parameter estimation and system learning is required.

There are two unknown parameters in the algorithm: 1) the flux recovered after a back flush (r_b) and 2) the flux recovered after a chemical cleaning cycle (r_c). The two set points that need to be determined are the normalized percentage drops in permeate water production at which back flushing (d_b) and chemical cleaning (d_c) are triggered. It is also necessary to empirically determine the optimal duration of the maintenance cycles and the corresponding amount of cleaning chemicals that should be used. The cost function presented in the previous section will be used to determine these empirical values.

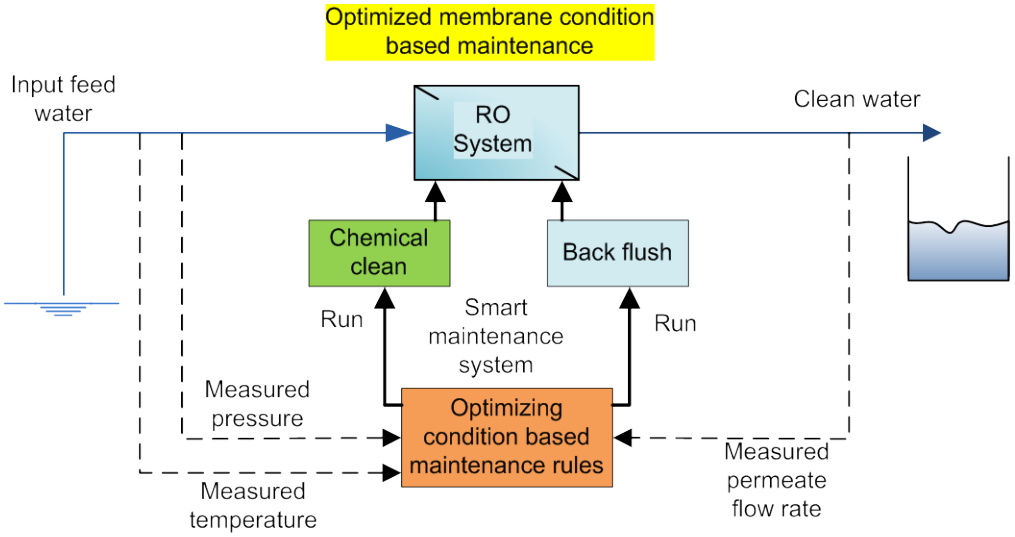

Figure 6-27: Schematic of an optimized condition based maintenance system for community scale PVRO systems

An empirical value or estimate is used to initialize r_c, r_b, d_c and d_b. Once initialized, the condition-based maintenance algorithm is executed by the onboard computer and the maintenance system starts self-optimizing to determine optimal maintenance strategy. A schematic of such an optimized condition-based maintenance system in operation is shown in Figure 6-27. The key parameters that need to be estimated in real time will change as the system ages and degrades. Hence, the maintenance-optimizing algorithm will have to run continuously

to account for degradation. A flow chart showing the logic of the self-optimizing algorithm is shown in Figure 6-28.

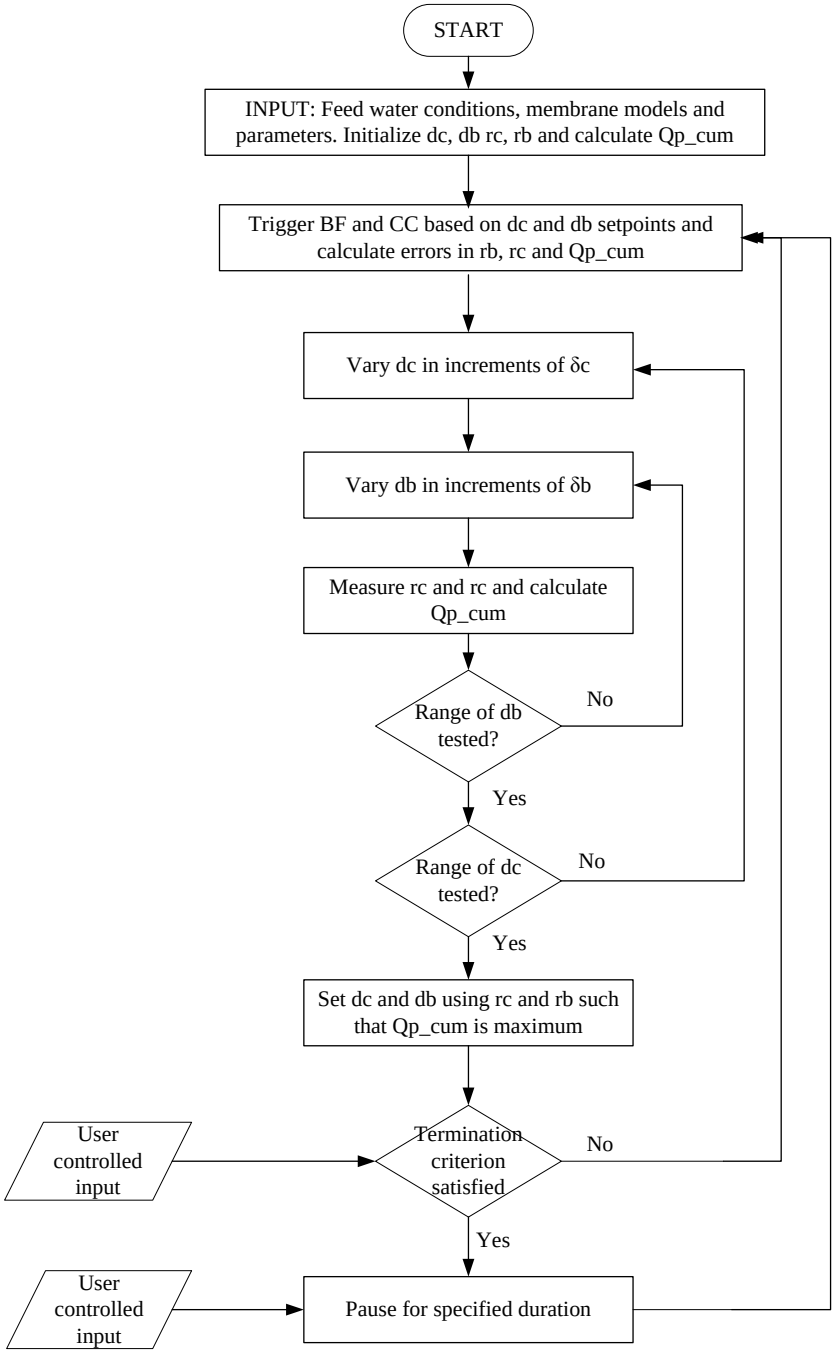

Figure 6-28: Self optimizing condition-based maintenance algorithm

To summarize the work reported in this chapter, a flux degradation model from the literature is used to simulate the performance drop of PVRO systems on account of fouling and scaling. Next, membrane maintenance using back flushing and chemical cleaning was simulated using schedule based maintenance and condition based maintenance. From a range of cases, the optimal schedule based maintenance and condition based maintenance strategies were identified from an increase in annual water production perspective and from an increase in the net value of water produced after accounting for the maintenance costs. The sensitivity of the maintenance strategies to the cleaning chemical costs was studied to understand the impact of the cost of chemical cleaning. Additionally, the sensitivity of the maintenance strategy to the feed water quality was studied. This showed that the feed water quality significantly affects the degradation of the membrane performance and the maintenance strategy used to control fouling, thus influencing the economics of the PVRO system.

As discussed earlier, it may be possible to find schedule-based maintenance strategies that work. However, this is highly impractical for community scale PVRO systems where the operating conditions are constantly varying and maintenance cannot be timed accurately. Hence, condition-based maintenance is the most accurate way of maintaining PVRO systems. However, due to certain unquantifiable parameters, a self optimizing condition-based maintenance algorithm is required and has been proposed.

For the assumptions stated, the optimal condition-based maintenance strategy from a cost perspective is the one with CC at a 12.5% drop in NPF and BF at a 5% drop in NPF showing an improvement of 47% in water production over one year. From a productivity perspective, the best strategy is the one with CC at a 5% drop in NPF and BF at a 2.5% drop in NPF showing an improvement of 58 % in annual water production for the assumed conditions. Using this strategy and the optimal power control strategy for a controllable recovery PVRO system as discussed in Appendix A, an improvement of 85% in water production for a July day in Boston after one year of continuous operation was shown to be feasible.

CHAPTER

7

SUMMARY AND CONCLUSIONS

7.1 Summary

This thesis describes an autonomous controls approach to optimizing community scale PVRO systems; first, by controlling membrane fouling using self-optimizing condition-based maintenance algorithms and strategies and second, by exploiting the energy compliance characteristics of PVRO elements and actively controlling the individual components of the system. By optimizing the performance of community scale PVRO systems for a system-specific cost function, a variety of objectives can be met, such as minimizing the life-cycle cost of water produced by the system, prolonging the life of the components within the system, reducing operation and maintenance costs and simplifying the operation of these systems.

Chapter 1 introduces the research project and presents the motivations for and objectives of this research. Clean drinking water is a global challenge and PVRO systems are a possible solution. However, PVRO systems tend to be expensive, energy intensive and easily susceptible to membrane degradation. By optimizing the energy consumption of these systems and controlling the membrane degradation, the life cycle cost of water can be greatly reduced and these systems can become economically feasible in more geographic locations.

Chapter 2 presents an overview of the technology used in PVRO systems, the relevant work done in the power modeling, fouling modeling and control of PVRO systems. There is no work that captures the compliance energy characteristics of PVRO systems and consequently none that discuss the control of PVRO systems by exploiting the system compliance. Additionally, fouling control of community scale PVRO systems using autonomous maintenance strategies has not been developed.

Chapter 3 describes the physical behavior of PVRO systems and presents physics-based models. These models are used to understand the transient and steady state characteristics of the system, thus enabling the control of PVRO systems. The phenomenon of energy storage in the compliance of the system elements has been identified and presented.

Chapter 4 presents the major types of fouling in PVRO systems and the mechanisms by which they occur. The acceptable standards for potable water and RO feed water are discussed. Scaling and fouling prediction, pretreatment methods and various membrane cleaning methods are discussed. Finally, the factors affecting fouling, maintenance frequency and maintenance effectiveness are reviewed.

Chapter 5 presents the major costs of a PVRO system, broken down in to capital costs and operating costs.

Chapter 6 presents the simulation of schedule-based and condition-based maintenance strategies to control membrane degradation. The strategies are evaluated from a productivity perspective and cost perspective. The optimal condition-based maintenance strategy showed an annual performance improvement of 58 % compared to unmaintained systems while an annual net value improvement of 47 % after accounting for the cost of cleaning was shown. Condition-based maintenance is most appropriate as operating conditions are constantly varying. Due to certain system specific parameters that cannot be determined analytically, a self-optimizing condition-based maintenance algorithm has been proposed.

Appendix A presents a simplistic RO system steady state model, and a complete PVRO system steady state compliance energy model. The energy compliance phenomenon in PVRO systems is identified, modeled and experimentally validated. A compliance model was derived using empirical estimates and was experimentally validated. Using a novel control technique for controllable recovery PVRO systems that exploit the system compliance phenomenon, a 47 % improvement in water produced over a fixed recovery PVRO system for a July day in Boston is shown to be feasible.

The performance of a controllable energy recovery PVRO system using a combined optimal condition-based maintenance and power control strategy was compared to the performance of a fixed recovery, unmaintained MIT PVRO system. Assuming exponential membrane degradation after one continuous year of operation, simulations show that the controllable system can

produce 85 % more water than the MIT PVRO system in July using the optimal power and fouling control strategies.

7.2 Suggestions for Future Work

Technologies presented in this thesis suggest a significant improvement of up to 85 % in water production for a system simulated in Boston weather conditions. Such improvements will make PVRO technology feasible in many areas of North America, South America, Africa, the Middle East, India and China. Hence the experimental validation of the power control and condition-based maintenance strategy to control fouling is necessary.

In the area of fouling control, the empirical estimation of parameters used in the fouling control models and simulations for varieties of feed water types should be carried out. The sensitivity of the condition-based maintenance algorithms to these parameters need to be understood. An important next step in this area of research is the design and implementation of a self-optimizing condition-based maintenance algorithm for community scale PVRO systems. The performance of the algorithm needs to be evaluated under a variety of feed water conditions, system configurations and applications with varying cost function parameters.

As noted in Appendix A, the power control of PVRO systems is still an active area of research at the FSRL at MIT. Additional work needs to be done to understand the dynamics of the energy recovery loop and its interactions with the power electronics and high pressure pump. The detailed design and selection of appropriate actuators, sensors and controller is necessary to experimentally validate the control approach shown in this feasibility study. The impact of component degradation and the integrity of different system configurations with the energy compliance model also need to be understood.

Finally, practical considerations such as the strain rate sensitivity of the different components in the PVRO system to intermittent operations as governed by the autonomous control systems need to be studied.

BIBLIOGRAPHY

[1] UNICEF and World Health Organization, "Progress on Drinking Water and Sanitation: 2012 Update," New York, 2012.

[2] DOW Water & Process Solutions, "DOW FILMTEC Reverse Osmosis Membranes - Technical Manual," [Online]. Available: http://www.dowwaterandprocess.com/support_training/literature_manuals/prod_manuals.htm. [Accessed 6 November 2012].

[3] L. C. Kelley, "The Design and Control of a Thermal Management System for a Photovoltaic Reverse Osmosis System, MS Thesis," Massachusetts Institute of Technology, Cambridge, MA., 2011.

[4] E. A. Reed, "The Design of a Controllable Energy Recovery Devicefor Solar Powered Reverse Osmosis Desalination with Experimental Validation," Massachusetts Institute of Technology, Cambridge, MA., 2012.

[5] A. M. Bilton, "A Modular Design Architecture for Application to Community-Scale Photovoltaic Reverse Osmosis Systems," Massachusetts Institute of Technology, Cambridge, MA., 2012.

[6] UNEP/GRID-Arendal, "Areas of physical and economic water scarcity - http://www.grida.no/graphicslib/detail/areas-of-physical-and-economic-water-scarcity_1570," 2008.

[7] Hugo Ahlenius, UNEP/GRID-Arendal, "Natural resource - solar power (potential) - http://www.grida.no/graphicslib/detail/natural-resource-solar-power-potential_b1d5," UNEP/GRID-Arendal, 2008.

[8] Personal correspondence with Major General Rick Lynch, Cambridge, MA., 2011.

[9] A. M. Bilton, R. Wiesman, A. Arif, S. M. Zubair and S. Dubowsky, "On the feasibility of community-scale photovoltaic-powered reverse osmosis desalination systems for remote locations," *Renewable Energy*, no. 36, pp. 3246-3256, 2011.

[10] M. Wilf, "Fundamentals of RO–NF technology," in *International Conference on Desalination Costing*, Limassol, 2004.

[11] S. Dallas, N. Sumiyoshi, J. Kirk, J. Mathew and N. Wilmot, "Efficiency analysis of the Solarflow – An innovative solar-powered desalination unit for treating brackish water," *Renewable Energy*, vol. 34, pp. 397-400, 2009.

[12] M. Thomson, "Reverse-Osmosis Desalination of Seawater Powered by Photovoltaics Without Batteries, PhD Thesis," Loughborough University, 2004.

[13] M. Green, Solar Cells: Operating Principles, Technology, and System Applications, Prentice-Hall, 1981.

[14] M. A. Green, K. Emery, Y. Hishikawa, W. Warta and E. Dunlop, "Solar cell efficiency tables (version 40)," *Progress in Photovoltaics: Research and Applications*, vol. 20, no. 5, pp. 606-614, 2012.

[15] Sharp Corporation, "Sharp Develops Concentrator Solar Cell with World's Highest Conversion Efficiency of 43.5% | Press Releases | Sharp Global," 31 May 2012. [Online]. Available: http://sharp-world.com/corporate/news/120531.html. [Accessed 15 December 2012].

[16] J. Kucera, Reverse Osmosis, Scrivener Publishing LLC., 2010.

[17] C. Fritzmann, J. Lowenberg, T. Wintgens and T. Melin, "State-of-the-art of reverse osmosis

desalination," *Desalination,* vol. 216, pp. 1-76, 2007.

[18] U.S. Department of the Interior, Bureau of Reclamantion, Lower Colorado Region, "Bureau of Reclamation: Lower Colorado Region," 27 July 2012. [Online]. Available: http://www.usbr.gov/lc/yuma/facilities/ydp/yao_ydp_operations_ro.html. [Accessed 24 December 2012].

[19] J. H. Lienhard, "2.500 - Desalination and Water Purification, Spring 2009. (Massachusetts Institute of Technology: MIT OpenCourseWare)," [Online]. Available: http://ocw.mit.edu/courses/mechanical-engineering/2-500-desalination-and-water-purification-spring-2009/readings/MIT2_500s09_lec01.pdf. [Accessed 24 December 2012].

[20] J. Holt, H. G. Park, Y. Wang, M. Stadermann, A. Artyukhin, C. Grigoropoulos, A. Noy and O. Bakajin, "Fast Mass Transport Through Sub-2-Nanometer Carbon Nanotubes," *Science,* vol. 312, no. 5776, pp. 1034-1037 , 2006.

[21] D. Sholl and J. Johnson, "Making High-Flux Membranes with Carbon Nanotubes," *Science,* vol. 312, no. 5776, pp. 1003-1004, 2006.

[22] C. Kurth, R. Burk and J. Green, "Utilizing nanotechnology to enhance RO membrane performance for seawater desalination," in *IDA World Congress,* Perth, 2011.

[23] A. Asatekin, E. Olivetti and A. Mayes, "Fouling resistant, high flux nanofiltration membranes from polyacrylonitrile-graft-poly(ethylene oxide)," *Journal of Membrane Science,* vol. 332, no. 1-2, pp. 6-12, 2009.

[24] "Ultrafiltration Membranes Incorporating Amphiphilic Comb Copolymer Additives Prevent Irreversible Adhesion of Bacteria," *Environmental Science and Technology,* vol. 44, no. 7, pp. 2406-2411, 2010.

[25] H. Colquhoun, D. Chappell, A. Lewis, D. Lewis, G. Finlan and P. Williams, "Chlorine tolerant, multilayer reverse-osmosis membranes with high permeate flux and high salt rejection," *Journal of Materials Chemistry,* vol. 20, no. 22, pp. 4629-4634, 2010.

[26] A. Bilton, R. Geykhman, D. D. Pozzo and J. Thangavelautham, "MIT Lavare PV/RO Experimental System, FSRL Technical Report FSRL-CWCE-005," Cambridge, 2010.

[27] I. Alatiqi, H. Ettouney and H. El-Dessouky, "Process control in water desalination industry: an overview," *Desalination,* vol. 126, pp. 15-32, 1999.

[28] I. Alatiqi, A. Ghabris and S. Ebrahim, "System identification and control of reverse osmosis desalination," *Desalination,* vol. 75, pp. 119-140, 1989.

[29] M. Al-haj Ali, A. Ajbar, E. Ali and K. Alhumaizi, "Robust model-based control of a tubular reverse-osmosis desalination unit," *Desalination,* vol. 255, pp. 129-136, 2010.

[30] M. S. Miranda and D. Infield, "A wind-powered seawater reverse-osmosis system without batteries," *Desalination,* no. 153S, pp. 9-16, 2002.

[31] C. W. McFall, A. Bartman, P. D. Christofides and Y. Cohen, "Control of a reverse osmosis desalination process at high recovery," in *American Control Conference*, Seattle, Washington, USA, 2008.

[32] A. R. Bartman, P. D. Christofides and Y. Cohen, "Nonlinear Model-Based Control of an Experimental Reverse-Osmosis Water," *Industrial and Engineering Chemistry Research,* vol. 48, no. 13, pp. 6126-6136, 2009.

[33] A. Zhu, P. D. Christofides and Y. Cohen, "Effect of Thermodynamic Restriction on Energy Cost Optimization of RO Membrane Water Desalination," *Industrial & Engineering Chemistry Research,* vol. 48, no. 13, pp. 6010-6021, 2009.

[34] A. Zhu, P. D. Christofides and Y. Cohen, "Energy Consumption Optimization of Reverse Osmosis Membrane Water Desalination Subject to Feed Salinity Fluctuation," *Industrial & Engineering*

Chemistry Research, vol. 48, no. 21, pp. 9581-9589, 2009.

[35] M. Li, "Minimization of Energy in Reverse Osmosis Water Desalination Using Constrained Nonlinear Optimization," *Industrial & Engineering Chemistry Research,* no. 49, pp. 1822-1831, 2010.

[36] J. Assef, J. Waters, P. Deshpande and I. Alatiqi, "Advanced control of a reverse osmosis desalination unit," *Journal of Process Control,* pp. 283-289, 1997.

[37] A. Burden, P. Deshpande and J. Waters, "Advanced process control of a B-9 Permasep permeator desalination plant," *Desalination,* no. 133, pp. 271-283, 2001.

[38] M. Robertson, J. Waters, P. Deshpande, J. Assef and I. Alatiqi, "Model based control of reverse osmosis desalination processes," *Desalination,* no. 104, pp. 59-68, 1996.

[39] A. Abbas, "Model predictive control of a reverse osmosis desalination unit," *Desalination,* vol. 194, pp. 262-280, 2006.

[40] C. W. McFall, P. D. Christofides, Y. Cohen and J. F. Davis, "Fault-Tolerant Control of a Reverse Osmosis Desalination Process," in *8th International IFAC Symposium on Dynamics and Control of Process Systems,* Cancún, Mexico, 2007.

[41] M. Al-haj Ali, A. Ajbar, E. Ali and K. Alhumaizi, "Modelling the transient behvior of an experimental reverse osmosis tubular membrane," *Desalination,* vol. 245, no. 1-3, pp. 194-204, 2009.

[42] H. Laborde, K. Franca, H. Neff and A. Lima, "Optimization strategy for a small-scale reverse osmosis water desalination system based on solar energy," *Desalination,* vol. 133, pp. 1-12, 2001.

[43] D. Wiley and D. Fletcher, " Computational fluid dynamics modelling of flow and permeation for pressure-driven membrane processes," *Desalination,* vol. 145, pp. 183-186, 2002.

[44] D. Fletcher and D. Wiley, "A computational fluid dynamics study of buoyancy effects in reverse osmosis," *Journal of Membrane Sciences,* vol. 245, pp. 175-181, 2004.

[45] A. Alexiadis, J. Bao, D. Fletcher, D. Wiley and D. Clements, "Dynamic response of a high-pressure reverse osmosis membrane simulation to time-dependent disturbances," *Desalination,* vol. 191, pp. 397-403, 2006.

[46] A. Schies, J. Went, C. Heidtmann, M. Eisele, F. Kroemke, H. Schmoch and M. Vetter, "Operating Control Strategies and Dimensioning of Photovoltaic-Powered Reverse-Osmosis Desalination Plants without Batteri," *Desalinaiton and Water Treatment,* vol. 21, pp. 131-137, 2010.

[47] G. Tragardh, "Membrane Cleaning," *Desalination,* vol. 71, pp. 325-335, 1989.

[48] R. Field, "Fundamentals of fouling," in *Membranes for Water Treatment: Volume 4,* Weinheim, WILEY-VCH Verlag GmbH & Co. KGaA, 2010, pp. 1-23.

[49] M. Goosen, S. Sablani, H. Al-Jinai, S. Al-Obeidani, R. Al-Belushi and D. Jackson, "Fouling of Reverse Osmosis and Ultrafiltration Membranes: A Critical Review," *Separation Science and Technology* , vol. 39, no. 10, pp. 2261-2297, 2005.

[50] S. El-Manharawy and A. Hafez, "Molar ratios as a useful tool for prediction of scaling potential inside RO systems," *Desalination,* vol. 136, pp. 243-254, 2001.

[51] S. El-Manharawy and A. Hafez, "Watertype and guidelines for RO system design," *Desalination,* vol. 139, pp. 97-113, 2001.

[52] "A more effective method for fouling characterization in a full-scale reverse osmosis process," *Desalination,* vol. 177, pp. 95-107, 2005.

[53] E. Hoek and M. Elimelech, "Cake-Enhanced Concentration Polarization: A New Fouling Mechanism for Salt-Rejecting Membranes," *Environ. Sci. Technol.*, vol. 37, no. 24, pp. 5581-5588, 2003.

[54] S. Kim and E. Hoek, "Modeling concentration polarization in reverse osmosis processes,"

Desalination, vol. 186, no. 1-3, pp. 111-128, 2005.

[55] A. Koltuniewicz and A. Noworyta, "Dynamic Properties of Ultrafiltration Systems in Light of the Surface Renewal Theory," *Ind. Eng. Chem. Res.*, vol. 33, no. 7, pp. 1771-1779, 1994.

[56] P. Danckwerts, "Significance of Liquid-Film Coefficients in Gas Absorption," *Industrial & Engineering Chemistry,* vol. 43, no. 6, pp. 1460-1467, 1951.

[57] M. M. Dal-Cin, F. McLellan, C. N. Striez, C. M. Tam, T. A. Tweddle and A. Kumar, "Membrane performance with a pulp mill effluent: relative contributions of fouling mechanisms," *Journal of Membrane Science,* vol. 120, no. 2, pp. 273-285, 1996.

[58] J. M. Arnal, B. García-Fayos and M. Sancho, "Membrane cleaning," in *Expanding Issues in Desalination*, InTech, 2011.

[59] M. Zhu, M. M. El-Halwagi and M. Al-Hamad, "Optimal design and scheduling of flexible reverse osmosis networks," *Journal of Membrane Scienece,* vol. 129, pp. 161-174, 1997.

[60] V. François, M. François, A. Emmanuelle and B. Philippe, "Multi-objective optimization of RO desalination plants," *Desalination,* vol. 222, no. 1-3, pp. 96-118, 2008.

[61] A. R. Bartman, C. W. McFall, P. D. Christofides and Y. Cohen, "Model-predictive control of feed flow reversal in a reverse osmosis desalintion process," *Journal of Process Control,* vol. 19, no. 3, pp. 433-442, 2008.

[62] M. Fazel and E. D. Darton, "A Statistical Review of 150 Membrane Autopsies," in *The International Water Conference,* Pittsburgh, PA, 2001.

[63] J. Baker and L. Dudley, "Biofouling in membrane systems - A review," *Desalination,* vol. 118, no. 1-3, pp. 81-90, 1998.

[64] World Health Organization, *Guidelines for Drinking-water Quality - Fourth Edition*, World Health Organization, 2011.

[65] American Membrane Technology Association (AMTA), "Membrane Technology Fact Sheets - Pretreatment for membrane processes," February 2007. [Online]. Available: http://www.amtaorg.com/publications-communications/membrane-technology-fact-sheets/. [Accessed 1 November 2012].

[66] J. M. Arnal, B. García-Fayos and M. Sancho, "Membrane cleaning," in *Expanding Issues in Desalination*, InTech, 2011.

[67] "www.chemicool.com," [Online]. Available: http://www.chemicool.com/definition/solubility_product_ksp.html. [Accessed March 2012].

[68] L. Song and K. G. Tay, "Advanced Membrane Fouling Characterization in Full-Scale Reverse Osmosis Processes," in *Handbook of Environmental Engineering, Volume 13: Membrane and Desalination Technologies*, Humana Press, 2008, pp. 101-134.

[69] Q. Li and M. Elimelech, "Organic Fouling and Chemical Cleaning of Nanofiltration Membranes: Measurements and Mechanisms," *Environmental Science and Technology,* vol. 38, no. 17, pp. 4683-4693, 2004.

[70] E. Plett, "Cleaning of fouled surfaces," in *Fouling and Cleaning in food processing by D Lund, E Plett and C SAndu (Eds)*, Madison, University of Wisconsin, Madison, WI, Extension Duplicating, 1985, p. 286.

[71] R. Liikanen, J. Yli-Kuivila and R. Laukkanen, "Efficiency of various chemical cleanings for nanofiltration membrane fouled by conventionally-treated surface water," *Journal of Membrane Science,* vol. 195, no. 2, pp. 265-276, 2002.

[72] S. Madaeni and S. Samieirad, "Chemical cleaning of reverse osmosis membrane fouled by wastewater," *Desalination,* vol. 257, pp. 80-86, 2010.

[73] DOW Water & Process Solutions, [Online]. Available:

http://msdssearch.dow.com/PublishedLiteratureDOWCOM/dh_0885/0901b8038088586b.pdf?filepath=/609-00071.pdf&fromPage=GetDoc. [Accessed 6 February 2012].

[74] K. G. Tay and L. Song, "A more effective method for fouling characterization in a full-scale reverse osmosis process," *Desalination,* vol. 177, pp. 95-107, 2005.

[75] M. Pilutti and J. Nemeth, "Technical and Cost Review of Commercially Available MF/UF Membrane Products," International Desalination Association, 2003.

[76] S. Sablani, M. Goosen, R. Al-Belushi and V. Gerardos, "Influence of spacer thickness on permeate flux in spiral-wound seawater reverse osmosis systems," *Desalination,* vol. 146, pp. 225-230, 2002.

[77] RosTek Associates, Inc., Tampa, Florida in association with DSS Consulting, Inc., Blue Ridge, Georgia and Aqua Resources International, Inc., Evergreen, Colorado and in cooperation with U.S. Department of the Interior - Bureau of Reclamation, "Chapter 9: Cost Estimating Procedures in Desalting Handbook for Planners, 3rd Edition," Desalination Research and Development Program, 2003.

[78] A. M. Bilton and S. Dubowsky, "The modular design of photovoltaic reverse osmosis systems: making technology accessible to nonexperts," *Desalination and Water Treatment,* 2012.

[79] H. M. Ettouney, H. T. El-Dessouky, R. S. Faibash and P. T. Gowin, "Evaluating the economics of Desalination," *Chemical Engineering Progress,* no. 8, pp. 12-32, 2002.

[80] A. Hafez and S. El-Manharawy, "Economics of seawater RO desalination in the Red Sea region, Egypt. Part 1. A case study," *Desalination,* no. 153, pp. 335-347, 2002.

[81] A. M. Helal, S. A. Al-Malek and E. S. Al-Katheeri, "Economic feasibility of alternative designs of a PV-RO desalination unit for remote areas in the United Arab Emirates," *Desalination,* no. 221, pp. 1-16, 2008.

[82] H. M. Ettouney, H. T. El-Dessouky, R. S. Faibash and P. Gowin, "Evaluating the economis of desalination," *CEP magazine,* December 2002.

[83] Solarbuzz, "Inverter price environment," Solarbuzz, 2012. [Online]. Available: http://www.solarbuzz.com/facts-and-figures/retail-price-environment/inverter-prices. [Accessed 9 September 2012].

[84] F. Evangelista, "A short-cut method for the design of reverse osmosis desalination plant," *Industrial & Engineering Chemistry Process Design and Development,* vol. 24, pp. 211-223, 1985.

[85] M. M. El-Halwagi, "Synthesis of reverse osmosis networks for waste reduction," *Journal for the American Institute of Chemical Engineers (AIChE),* vol. 38, no. 8, pp. 1185-1198, 1992.

[86] O. Barron, "Desalination Options and their possible implementation in Western Australia: Potential Role for CSIRO Land and Water," CSIRO: Water for a Healthy Country National Research Flagship, Canberra, 2006.

[87] A. Bhujle* and J. Thangavelautham*, "Maximizing Clean Water Production Through Power Modeling and Control of PVRO, FSRL Technical Report," Cambridge, 2012.

[88] K. K. Turekian, Oceans, Prentice-Hall, 1968.

[89] World Health Organization, "Guidelines for Frinking Water Quality, 3rd edition," 2006. [Online]. Available: http://www.who.int/water_sanitation_health/dwq/gdwq0506.pdf.

[90] Council of the European Union, ""Council directive 98/83/EC of 3 november 1998 on the quality of water intended for human consumption," 1998. [Online]. Available: http://eurlex.europa.eu/LexUriServ/LexUriServ.do?uri=OJ:L:1998:330:0032:0054:EN:PDF.

[91] Illinois Department of Public Health, "Commonly found substances in drinking water and available treatment," 2002. [Online]. Available: http://www.idph.state.il.us/envhealth/pdf/DrinkingWater.pdf.

[92] Agency for toxic substances and disease registry, "ToxFAQs™ for Strontium," 2004. [Online]. Available: http://www.atsdr.cdc.gov/toxfaqs/tfacts159.pdf. [Accessed February 2012].

[93] United States Environmental Protection Agency, "National Primary Drinking Water regulations," May 2009. [Online]. Available: http://water.epa.gov/drink/contaminants/upload/mcl-2.pdf. [Accessed February 2012].

[94] Nitto Denko - Hydranautics, "Technical: membrnes.com," December 2008. [Online]. Available: http://www.membranes.com/docs/tab/TAB111.pdf. [Accessed 30 January 2012].

[95] A. Gambier, A. Krasnik and E. Badreddin, "Dynamic Modelling of a Simple Reverse Osmosis Desalination Plant for Advanced Control Purposes," in *American Control Conference*, New York City, 2007.

[96] A. Gambier, E. Miksch and E. Badreddin, "A Reverse Osmosis Laboratory Plant for Experimenting with Fault-Tolerant Control," in *American Control Conference*, St. Louis, 2009.

[97] A. Gambier, E. Miksch and E. Badreddin, "Fault-Tolerant Control of a Small Reverse Osmosis Desalination Plant with Feed Water Bypass," in *American Control Conference*, Baltimore, 2010.

[98] "Photovoltaic reverse osmosis - Feasibility and a pathway to develop technology," *Desalination and Water Treatment*, 2011.

[99] Green, M. A., Emery, K., Hishikawa, Y. and Warta, W., "Solar cell efficiency tables (version 37)," *Progress in Photovoltaics: Research and Applications*, vol. 19, no. 1, pp. 84-92, 2011.

[100] J. Lienhard, *2.500: Desalination and Water Purification - Class notes*, Cambridge, 2010.

[101] P. Castro and M. Huber, Marine Biology, McGraw-Hill Higher Education, 2005.

[102] J. F. Anthoni, "Composition of seawater," Seafriends Marine Conservation and Education Centre, 2006. [Online]. Available: http://www.seafriends.org.nz/oceano/seawater.htm. [Accessed 25 November 2012].

[103] Saehan Industries, Inc., "Technical Manual - Reverse Osmosis Membrane," August 2006. [Online]. Available: http://www.csmfilter.com/searchfile/file/tech_manual.pdf. [Accessed 25 November 2012].

[104] H. Qiblawey, F. Banat and Q. Al-Nasser, "Performance of reverse osmosis pilot plant powered by Photovoltaic in Jordan," *Renewable Energy*, vol. 36, no. 12, pp. 3452-3460, 2011.

[105] S.-F. Cheah, "Photovoltaic Reverse Osmosis Desalination System," ITN Energy Systems, Inc, Littleton, CO, 2004.

[106] Spectra Watermakers, Inc, "Spectra Watermakers: Land Based Technology - The Solar Cube," [Online]. Available: http://www.spectrawatermakers.com/landbased/technology_solarcube.php. [Accessed 30 November 2012].

[107] D. Herold and A. Neskakis, "A small PV-driven reverse osmosis desalination plant on the island of Gran Canaria," *Desalination*, vol. 137, pp. 285-292, 2001.

[108] K. Zweibel, J. Mason and V. Fthenakis, "A Solar Grand Plan," *Scientific American*, January 2008.

APPENDIX

A

POWER MODELING, CONTROL AND OPTIMIZATION OF PVRO SYSTEMS

This part of the research focuses on developing real-time control systems to optimize the water produced by PVRO systems, based on the available power from the solar panel. Such a control system will maximize water output, prolong system life and decrease the cost of desalination. As the amount of incoming power (i.e. sunlight) varies over time, the PVRO system must respond to such changes in input to achieve maximum performance. In such a system, all available energy is used to produce clean water and the excess product water is stored instead of using conventional energy storage. This is advantageous as it eliminates the excess costs and power losses associated with energy storage systems such as batteries. However, the absence of an energy storage system requires optimal power management by adaptive controllers, which imposes an added level of complexity in design and implementation.

The feasibility of a physics-based controller is desired. A physics-based controller required a physical model, and so the fundamental physics of the system and the surroundings are modeled. The subsystem or component models already developed are used to model the dynamics of the system. The system configuration analyzed here is that of the MIT experimental PVRO system, which will be used for experimental validation and testing.

A.1 Steady-State PVRO System Model and Analysis

A high-level, steady state model of the PVRO system that does not include the physics and behavior of individual components is used to demonstrate the need for a controllable PVRO system. It is based on simple power flow optimizations. The general representative system considered for this analysis is shown in Figure A-1. Here, the power electronics take electrical

power from the solar panel, P, and the power recovered by the energy recovery device is fed to a motor at an optimum voltage, V_1 and corresponding current, I_1. The motor then applies a torque, T on the pump that delivers the pressurized feed water to the RO system at feed pressure, P_f.

Assumptions: The following assumptions have been made:

- The energy recovery extracts a fraction of the power in the brine stream and its efficiency does not vary with the flow rate. Although this may not hold for certain types of energy recovery devices, this is a valid assumption around a fixed operating point at steady state.
- The efficiencies used are as follows:
    - Motor efficiency (η_{motor}): 80% [81]
    - Mechanical efficiency of the pump (η_{pump}): 80% [81]
    - Energy recovery device efficiency (η_{ERD}): 85% [81]
    - Power electronics (η_{elec}): 95%
- The permeate is discharged at atmospheric pressure P_0. All pressures are gauge pressures, hence $P_0=0$
- The temperature and salt distribution is uniform in the feed water and along the membrane
- Heat losses in the RO system components don't affect the temperature of the feed water
- No salt is transmitted across the membrane

The conservation of power for this system is expressed by:

$$Q_f P_f = \eta_{elec}\eta_{motor}\eta_{pump}(\eta_{ERD} Q_b P_f + P) \quad \textbf{(48)}$$

where, Q_f is the flow rate of the feed water, Q_b is the flow rate of the brine and Q_p is the flow rate of the clean product water, P_f is the pressure of the feed water and P_0 is the atmospheric pressure.

This, the power gained by the feed water, Θ_f is:

$$\Theta_f = \Theta_b + \Theta_p \quad \textbf{(49)}$$

where Θ_b is the power recovered from the brine and Θ_p is the power used by the pump.

The input flow rate is:

$$Q_f = Q_p + Q_b \quad \textbf{(50)}$$

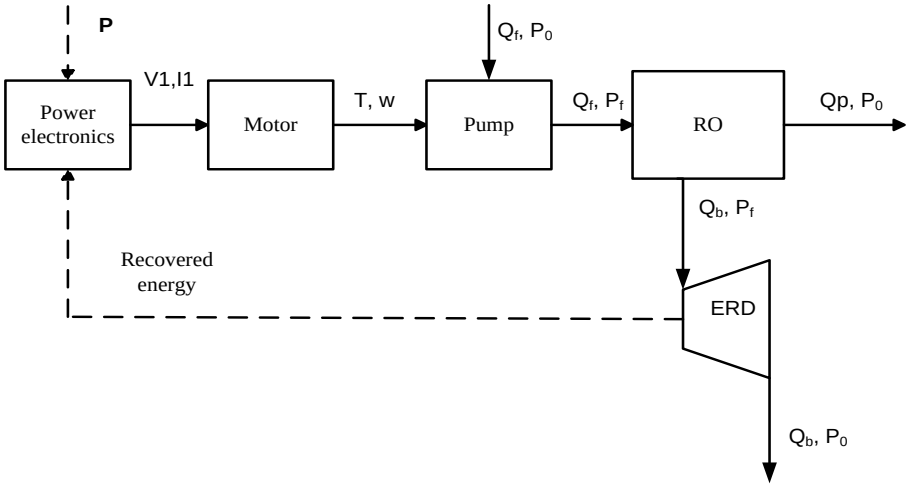

Figure A-1: Power flow schematic for a PVRO system

Rearranging to obtain the expression for feed water flow rate yields,

$$Q_p = \frac{\eta_{elec}\eta_{motor}\eta_{pump}Pr}{P_f[1-\eta_{elec}\eta_{motor}\eta_{pump}\eta_{ERD}(1-r)]} \quad \textbf{(51)}$$

where *r* is the recovery ratio and is given by:

$$r = \frac{Q_p}{Q_f} \quad \textbf{(52)}$$

and

$$1 - r = \frac{Q_b}{Q_f} \quad \textbf{(53)}$$

The efficiency of the energy recovery device is given by:

$$\eta = \frac{Energy\ recovered\ from\ the\ brine}{Energy\ in\ the\ brine} = \frac{Q_b(P_f - P_e)}{Q_b P_f} = \frac{(P_f - P_e)}{P_f} \quad \textbf{(54)}$$

Thus the product flow rate is given by [2]:

$$Q_p = AS_E(TCF)(P_f - \Delta\bar{\pi}) \quad \textbf{(55)}$$

where $\Delta\bar{\pi}$ is the average osmotic pressure of the feed water in the RO chamber, *A* is the membrane permeability of water in liters per m^2-bar-sec, S_E is the membrane area in m^2, and *TCF* is the temperature correction factor.

Assuming no salt is transmitted across the membrane, the average osmotic pressure is given by:

$$\Delta\bar{\pi} = \frac{k(C_f+C_b)T}{2} \quad \textbf{(56)}$$

where C_f is the concentration of the feed water in ppm, C_b is the concentration of the brine leaving the RO chamber in ppm, k is a proportionality constant in bar per Kelvin per ppm and T is the temperature of the feed water in Kelvin.

On the feed side of the RO membrane the total amount of salt remains constant. Hence,

$$C_f Q_f = C_b(r)Q_b + C_p Q_p \quad \textbf{(57)}$$

However, since it is assumed that no salt is transmitted across the membrane,

$$C_f Q_f = C_b(r)Q_b \quad \textbf{(58)}$$

$$\therefore C_b = \frac{C_f}{1-r} \quad \textbf{(59)}$$

$$\therefore \Delta\bar{\pi} = \frac{kC_fT}{2}\left(\frac{2-r}{1-r}\right) \quad \textbf{(60)}$$

Considering the effects of the concentration polarization, the average osmotic pressure is expressed by [2]:

$$\Delta\bar{\pi} = \frac{k(C_f+C_b)T}{2}e^{0.7r} \quad \textbf{(61)}$$

$$\therefore \Delta\bar{\pi} = \frac{kC_fT}{2}\left(\frac{2-r}{1-r}\right)e^{0.7r} \quad \textbf{(62)}$$

Thus the feed pressure can be expressed as:

$$P_f = \frac{kC_fT}{2}\left(\frac{2-r}{1-r}\right) + \frac{Q_p}{AS_E(TCF)} \quad \textbf{(63)}$$

and the clean product flow rate is given by:

$$Q_p = \frac{\eta_{elec}\eta_{motor}\eta_{pump}Pr}{\left[\frac{kC_fT}{2}\left(\frac{2-r}{1-r}\right)e^{0.7r}+\frac{Q_p}{AS_E(TCF)}\right]\left[1-\eta_{elec}\eta_{motor}\eta_{pump}\eta_{ERD}(1-r)\right]} \quad \textbf{(64)}$$

which can be rearranged as

$$\frac{{Q_p}^2}{AS_E(TCF)} + Q_p\frac{kC_fT}{2}\left(\frac{2-r}{1-r}\right)e^{0.7r} - \frac{\eta_{elec}\eta_{motor}\eta_{pump}Pr}{\left[1-\eta_{elec}\eta_{motor}\eta_{pump}\eta_{ERD}(1-r)\right]} = 0 \quad \textbf{(65)}$$

Assuming the recovery ratio is controllable, the optimal value of the recovery ratio that maximizes the product water produced for a given amount of power fed to the pump is desired. At maximum water production,

$$\frac{\partial Q_p}{\partial \mathrm{r}} = 0 \qquad \textbf{(66)}$$

Table A-1: Parameters used in steady-state PVRO system model and analysis

Parameter	**Variable**	**Type**	**Value (if Constant)**	**Units**
Feed pump displacement	D_x	Constant	10	cm^3/rev
Membrane permeability for water	A_m	Constant	3.3492e-13	l/m2/bar/sec
Membrane Surface Area	S_e	Constant	7.4	m^2
Temperature correction factor	*TCF*	Constant	1 @ T = 298 K	unitless
Salt proportionality constant	*Ks*	Constant	0.2654	bar/ ^oK/ ppm
Feed water concentration	*Cf*	Constant	35000	ppm
Temperature of feed water	*T*	Constant	298	K
Density of water	*rho*	Constant	1000	Kg/m^3

First, the effect of panel power on the optimal recovery ratio is examined. Figure A-2 shows the product flow rate plotted against the recovery ratio for varying levels of input power while Figure A-4 shows the corresponding feed pressures. A feed water salinity of 35000 ppm at a temperature of 25 ^oC was assumed. As the power increases, the product flow rates increase and so does the corresponding feed pressure. As the recovery ratio approaches one, the feed pressure becomes infinite since 100% of the water can never be recovered from salty feed water. The horizontal line on the feed pressure plot is the 70 bar limit, which is typical of most membrane manufacturers' recommendations. From Table A-2, the optimal recovery ratio varies from about 41% to 46% as the power from the panel varies from 25 W to 250 W.

Next, the effect of salinity on the optimal recovery ratio is examined. Figure A-3 shows the product flow rate plotted against the recovery ratio for varying levels of feed water salinity while Figure A-5 shows the corresponding feed pressures. An energy recovery device with 85 % efficiency, input power of 200 W and temperature of 25 ^oC is assumed. The product flow rates

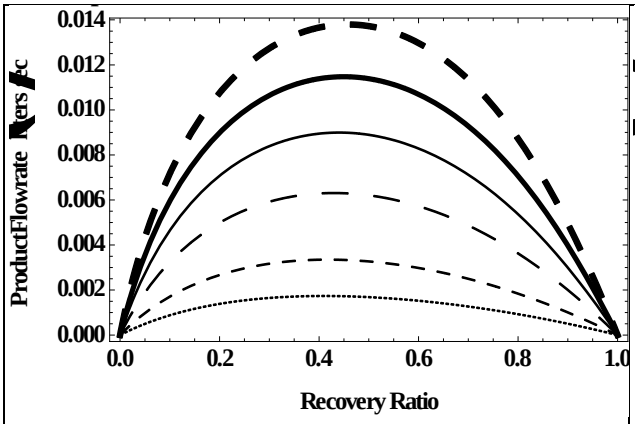

Figure A-2: Product flow rate vs recovery ratio for varying solar panel power: 25W, 50W, 100W, 150W, 200W and 250W

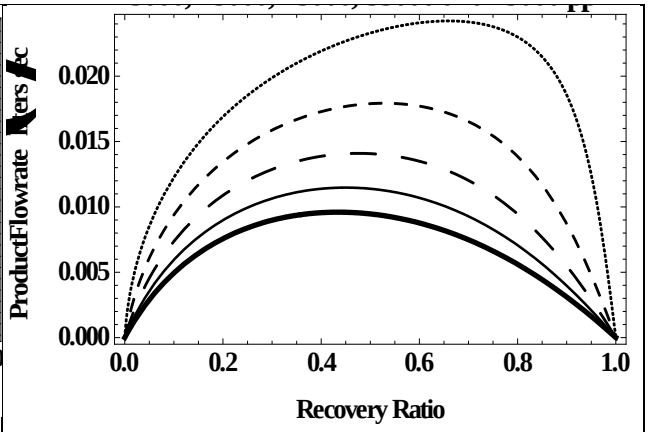

Figure A-3: Product flow rate vs recovery ratio for varying salinity: 5000 ppm, 15000 ppm, 25000 ppm, 35000 ppm and 45000 ppm

Legend for Figure A-2 and Figure A-4

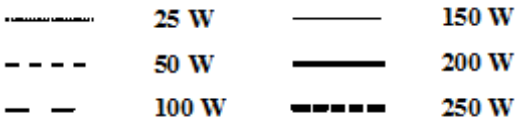

Legend for Figure A-3 and Figure A-5

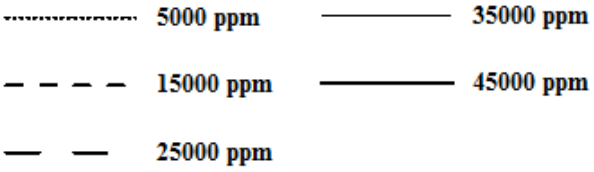

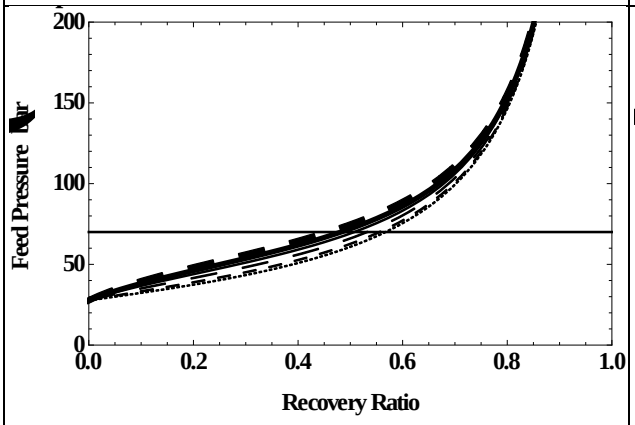

Figure A-4: Feed pressure vs recovery ratio for varying solar panel power: 25W, 50W, 100W, 150W, 200W and 250W

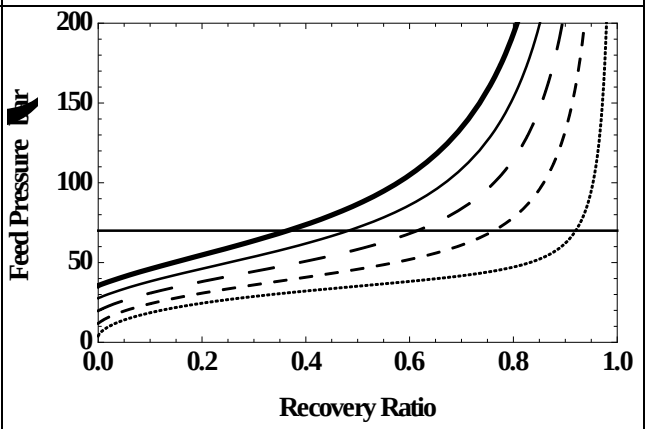

Figure A-5: Feed pressure vs recovery ratio for varying salinity: 5000 ppm, 15000 ppm, 25000 ppm, 35000 ppm and 45000 ppm

increase as the salinity decreases. This is because the osmotic pressure of the feed water decreases as the salinity decreases, so reverse osmosis happens at lower applied pressures. The product flow rate curves show a significant variation in the optimal recovery ratio ranging from 66% for feed water at 5000 ppm to 44% for feed water at 45000 ppm. However, in the 45000

ppm case, the feed pressure goes above 70 bar. Therefore the feed pressure will have to be limited to 70 bar, and the optimal recovery ratio for that feed pressure is selected as 35%.

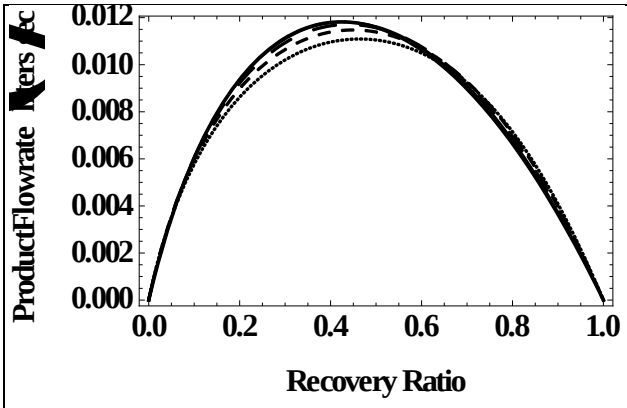

Figure A-6: Product flow rate vs recovery ratio for varying temperatures of 15, 25, 35, 45 and 55 C

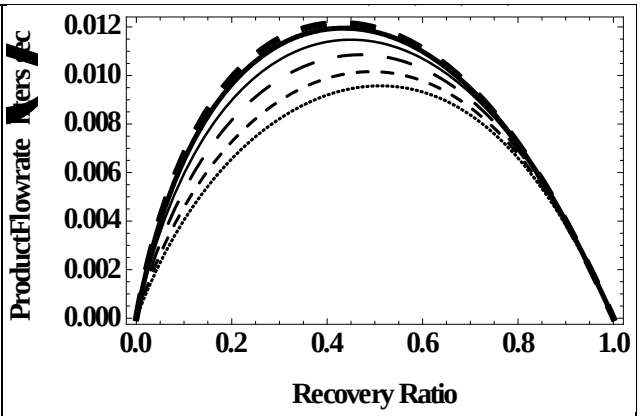

Figure A-7: Product flow rate vs recovery ratio for ERD efficiencies of 30, 50, 70, 54, 95 and 99%

Legend for Figure A-6 and Figure A-8

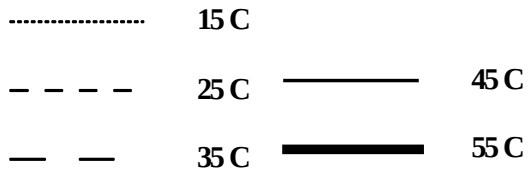

Legend for Figure A-7 and Figure A-9

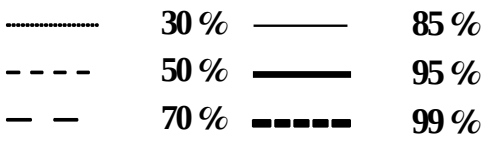

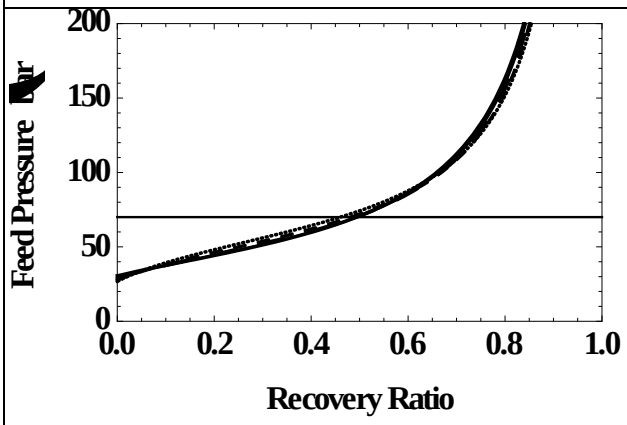

Figure A-8: Feed pressure vs recovery ratio for varying temperatures of 15, 25, 35, 45 and 55 C

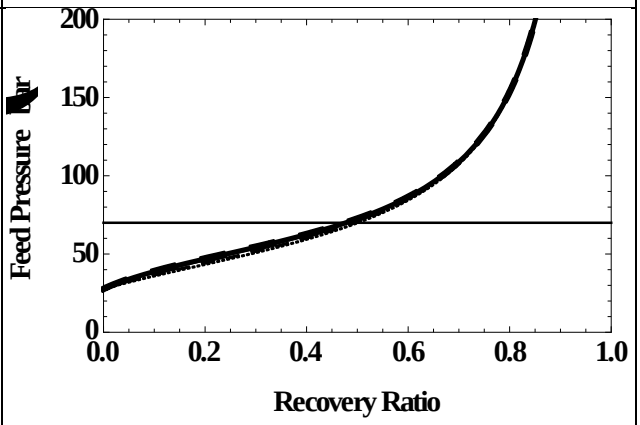

Figure A-9: Feed pressure vs recovery ratio for ERD efficiencies of 30, 50, 70, 54, 95 and 99%

The effect of feed water temperature on the optimal recovery ratio is studied. Figure A-6 shows the product flow rate plotted against the recovery ratio for varying feed water temperatures while Figure A-8 shows the corresponding feed pressure. A feed water salinity of 35000 ppm is assumed and the power from the panel is assumed to be 200 W. The variability in recovery ratio is not significant when the temperature varies from 15 ^{o}C to 45 ^{o}C, although the water produced increases slightly. For a certain feed pressure, the clean water produced increases with temperature as the water can go across the membrane more easily [3].

Finally, the effect of energy recovery device efficiency on the optimal recovery ratio is studied. Figure A-7 shows the product flow rate plotted against the recovery ratio for the varying energy recovery efficiencies while Figure A-9 shows the corresponding feed pressures. The efficiency of the ERD influences the choice optimal recovery ratio significantly, since a very efficient ERD allows a low recovery ratio that does not waste too much power in the energy recovery loop and enables operation at lower pressures. However, if the ERD is very inefficient, then the recovery ratio must be kept high, since a lot of the energy is wasted by the ERD and it is better to use the pressurized feed water to produce relatively lower amounts of clean water than lose the considerable energy in the energy recovery loop. Therefore, the optimal recovery ratio varies from about 42 % to 51 % when the efficiency of the ERD varies from 99 % to 30 %.

Table A-2: Parametric analysis of Steady-state RO membrane system model for varying panel power, feed water salinity, feed water temperatures and ERD efficiencies

RO membrane system optimal performance for varying solar panel power output			
Power (W)	**Max Q_p (l/sec)**	**Recovery ratio, r (%)**	**SEC (kWh/m^3)**
25	0.0017	40.97	4
50	0.0033	41.72	4.15
100	0.0063	43	4.40
150	0.0091	44.06	4.63
200	0.0115	45	4.84
250	0.0138	45.77	5.03
RO membrane system optimal performance for varying feed water salinity			
Salinity (ppm)	**Max Q_p**	**Recovery ratio, r**	**SEC (kWh/m^3)**

	(liters/sec)	(%)	
5000	0.0242	66	2.293
15000	0.0179	52.81	3.098
25000	0.0141	47.62	3.941
35000	0.0115	45	4.842
45000	0.0096	43.46	5.789
RO membrane system optimal performance for varying feed water temperatures			
Temperature (C)	**Max Q_p (liters/sec)**	**Recovery ratio, r (%)**	**SEC (kWh/m^3)**
15	0.0110	46.36	5.009
25	0.0115	45	4.842
35	0.0117	43.87	4.745
45	0.0118	43	4.702
55	0.0118	42.35	4.701
RO membrane system optimal performance for varying energy recovery device (ERD) efficiencies			
ERD efficiency (%)	**Max Q_p (liters/sec)**	**Recovery ratio, r (%)**	**SEC (kWh/m^3)**
30	0.0096	51.14	5.803
50	0.0102	49.25	5.468
70	0.0109	47	5.118
85	0.0115	45	4.842
95	0.0120	43.4	4.649
99	0.0122	42.72	4.57

This simple PVRO system analysis shows that there is a need for actively controlling the recovery ratio and pressure in a PVRO system, especially when the panel power and feed water salinity vary considerably and when the ERD has a variable efficiency profile over the operating range of the system.

A.2 Pelton Wheel Generator Efficiency

The efficiency of the pelton wheel generator combination varies with the brine flow rate and input mechanical power. The efficiency of the energy recovery system for a range of input mechanical power and corresponding operating conditions is shown in Figure A-10.

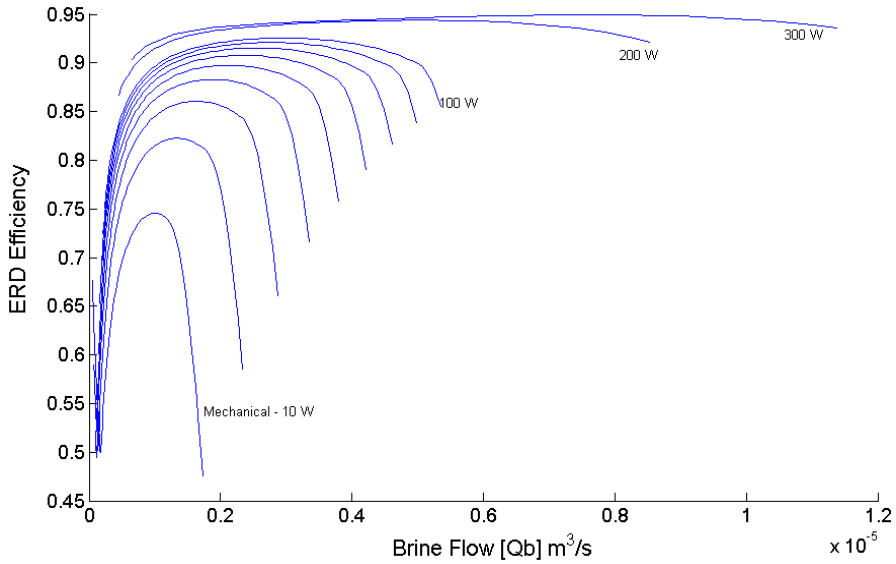

Figure A-10: Pelton wheel generator efficiency as a function of brine flow rate and input mechanical power [87]

A.3 Compliance Modeling of a PVRO System for Optimal Power Control

In this section, a PVRO steady state compliance energy model is presented that accounts for the transient and steady state behavior of the PVRO system by modeling the compliant energy stored in the various components of the PVRO system. Experimental data from the MIT PVRO experimental system is used to determine certain empirical parameters in the model. This model is then experimentally validated using data from a summer day in Boston. A concept system with a controllable energy recovery is presented. Next, the feasibility of a novel physics based controls approach that maximizes the clean water produced is presented and the performance of this controlled concept system are compared with the fixed recovery MIT PVRO experimental system.

There are several non-linearities in the PVRO system. A set of experiments were carried out to analyze and model these behaviors.

During peak sunlight hours, the computer controlled DC to DC converter was set at the maximum power transfer point and panel tilted towards the sun. The system was shut down

completely by switching off the panel, and the pressure in the RO chamber was bled down to zero by releasing the pressure relief valve. Once the system reached its lowest energy state, the panel was switched back on and the panel instantly resumed peak power production levels. The pressure, feed flow rates and clean water flow rates were recorded and some interesting features were noted. The first interesting feature was that even though the feed flow had started increasing from zero, there wasn't any permeate flow until the feed pressure had reached about 28 bar. This is unsurprising, since the feed pressure was unable to overcome the osmotic pressure which was 28 bar for feed water salt concentration of 35,000 ppm. After the panel was shut down, the feed flow rate decreased rapidly to zero as the pumps stopped rotating, the feed pressure dropped and consequently the clean water flow rate dropped as well. Interestingly, the rate at which the feed flow rate fell was far higher than the rate at which the permeate flow fell. This meant that the pressure that was building up on the feed side of the system when the panel was switched on was accumulating. This is due to the compliance of the system components. During shut off, when the panel was switched off, the pressure stored in the compliance of the system gradually dropped while continuing to drive some of the permeate flow. Thus it can be observed that the feed side of the PVRO system starting from the filters onwards to the RO membrane stores energy.

The energy stored in a spring is given by $E = \frac{1}{2} k \Delta x^2$ where k is the spring constant and Δx is the length of compression or extension of the spring. The inverse of the spring constant is the compliance, $1/k$. The corresponding force that was applied to produce this compression or extension is given by $F = k\Delta x$. The energy stored in the spring can also be written as:

$$E = \frac{1}{2k} F^2 = \frac{1}{2} C F^2 \qquad \textbf{(67)}$$

The system compliance can be modeled in a similar way using a system compliance parameter, C and an effective expansion of the materials of the components: $P = C\Delta V$. These components exhibit a volumetric displacement ΔV as pressure builds up on the feed side of the RO system and in the components upstream of the RO membrane. Since the displacement of a spring is proportional to the corresponding force, the change in volume is proportional to the applied pressure. Therefore, the energy stored in the PVRO system is hypothesized to be proportional to the square of the applied pressure as shown below.

$$\text{Pressure } \alpha \text{ Force } \alpha \ \Delta x \tag{68}$$

$$\therefore \text{Energy } \alpha \text{ Pressure}^2 \tag{69}$$

$$\text{Energy } = constant * \text{Pressure}^2 \tag{70}$$

This internal pressure is equal to the feed pressure that is measured on the feed side of the RO membrane. The feed pressure and consequently the compliance energy vary as a function of time and can be written as:

$$E(t) = \frac{1}{2} C P_f^2(t) \tag{71}$$

where *E(t)* is the compliance energy stored in the system, *C* is the system compliance parameter, and $P_f(t)$ is the feed pressure.

The system compliance parameter is not known and is determined empirically from the experiment step response data. The feed pressure is measured using a pressure gauge. The compliance energy is the energy that builds up as result of the difference in the power coming in to the system and the power out of (leaving) the system. The instantaneous power balance of the system is:

$$\theta_{net} = P_f Q_f - P_b Q_b - P_f Q_c \tag{70}$$

The system under consideration here from the compliance perspective is defined as the components in between the feed pump and the RO chamber exit. Thus, the compliance energy is calculated using the following equation:

$$E(t) = \int \left(P_f Q_f - P_b Q_b - P_f Q_c \right) dt \tag{72}$$

where q_p is the clean permeate flow rate, q_b is the brine stream flow rate, P_b is the brine stream pressure. Assuming $P_f = P_b$,

$$E(t) \approx \int P_f q_{net} dt \tag{73}$$

where q_{net} is given by

$$q_{net} = q_f - q_p - q_b \tag{74}$$

Therefore,

$$\frac{1}{2}kP_f^2 \approx \int P_f q_{net} dt \quad \textbf{(75)}$$

Using the series of step response experiments, an empirical value of 1.34 was determined for *C*. This value of *C* is system specific and will vary from system to system. Using this *C* value and the calculated instantaneous system compliance energy, the instantaneous feed pressure can be obtained. Alternatively, if the feed pressure is known, then the system compliance energy can be calculated. From Figure A-11, the measured system compliance energy and the calculated system compliance energy using the instantaneous feed pressure and empirically determined compliance parameter match well. This shows that the hypothetical relation between feed pressure and system compliance energy is valid and can be used to model the transient behavior of the PVRO system.

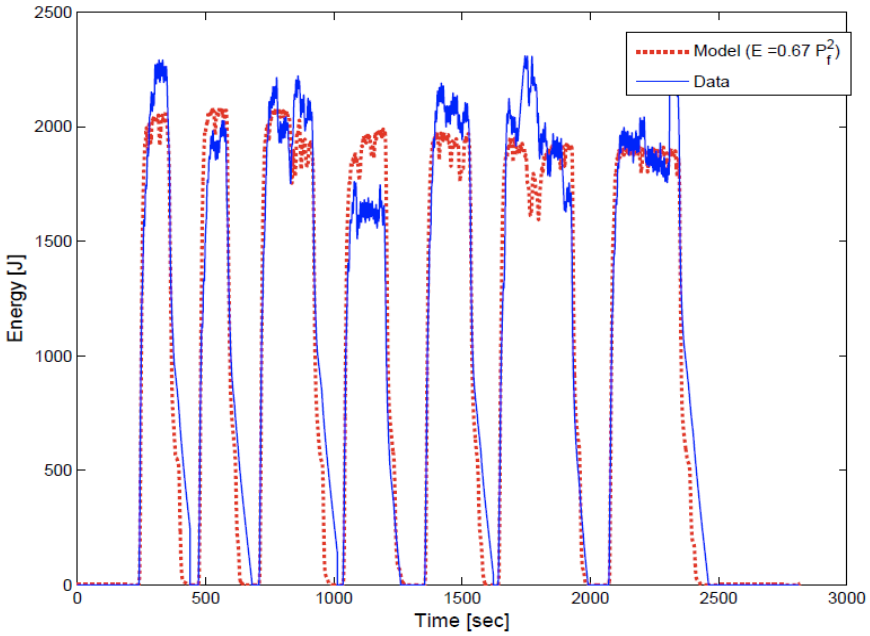

Figure A-11: Comparison of compliance energy calculated from experimental data and the compliance energy predicted by the model

A.3.1 Experimental Validation of Energy Model

The MIT PVRO experimental system described in Chapter 2 was used to validate the RO compliance model. Figure A-12 shows a schematic of the MIT PVRO experimental system with the efficiencies of the components. The solar panel efficiency varies from 10% to 20% depending on the available sunlight and temperature. The power electronics have an efficiency of

79% and the boost pumps, including the motors used to drive the pumps, have an efficiency of 51%. The Clark pump has an efficiency of 95%. An additional 1 % loss is assumed in the energy recovery loop. The sensors shown in Figure A-13 are used to determine these efficiencies and the power flowing through the system at the various stages.

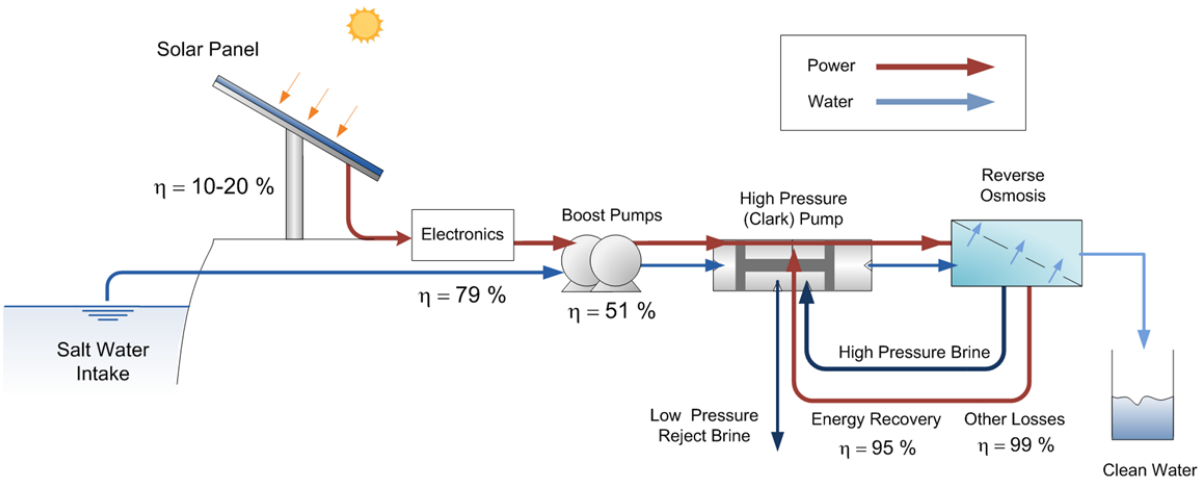

Figure A-12: Experimental Validation Using MIT PVRO experimental system [87]

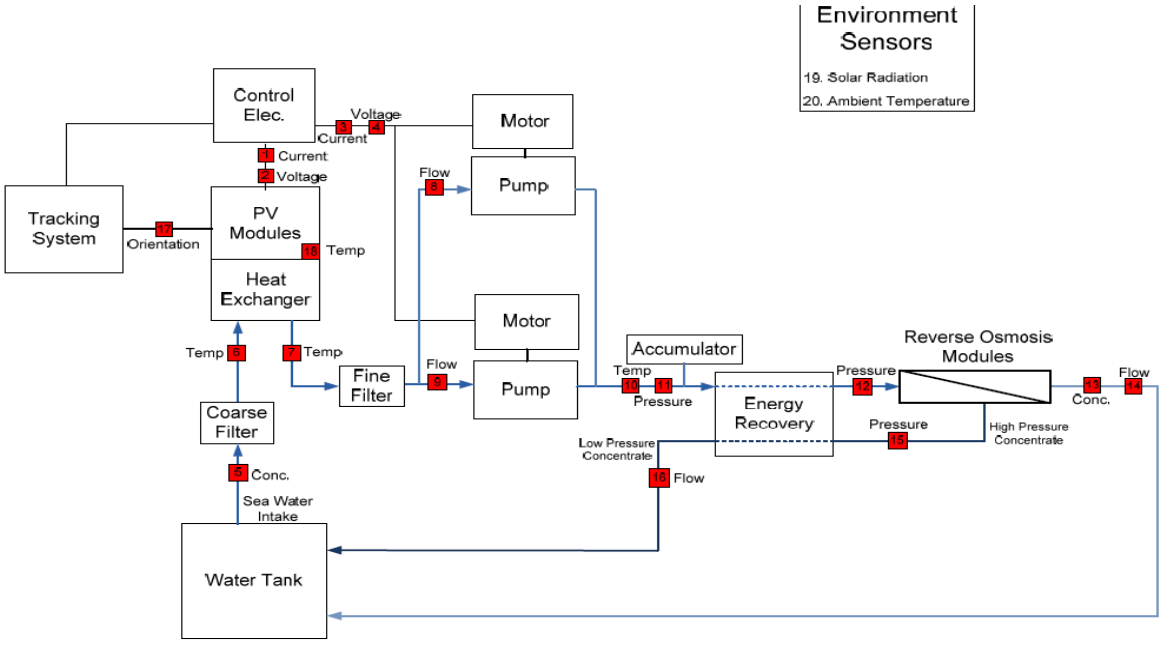

Figure A-13: MIT PVRO experimental system sensor layout [26]

A MATLAB/Simulink model of the experimental system along with the compliance energy model was created to simulate the behavior of the system. The inputs to the model include solar

insolation, feed water salinity, temperature and system parameters such as the membrane area and the fouling factor. The model outputs are clean water produced, the pressures in the feed stream and brine stream, the power flow through the different sections of the system and the stored compliance energy. The efficiencies of the motor, pump and power electronics are assumed to be constant. Solar radiation data recorded in July 2010, Boston is used for the inputs. The water produced and the feed pressure predicted by the model is compared to the experimental values as shown in Figure A-14 and Figure A-15 respectively. The model predicts clean water production of 318 liters and the actual experimental result was 324 liters. This is a difference of about 2% and shows that the model is in good agreement with the experimental data. From Figure A-15, the model and data show good correlation. However, when there are drastic changes in the input power on account of clouds passing over, the difference between the experimental data and the model is considerably higher at around 20%. This difference is due to a higher compliance assumed by the model than in the system. Over time, the difference in the pressure predicted by the model and the data diminishes. Another possible explanation is that the water flow measurements are somewhat filtered and thus the higher frequency variations are cut off. The initial discrepancies could indicate additional nonlinearities in the system compliance. When the system reaches steady state, the theoretical compliance energy is in agreement with the system compliance used in the model.

In summary, the model shows good agreement with the data as the water produced in a day predicted by the model is within 2% of the experimental value. When the power fluctuates, the instantaneous pressure values predicted by the model can be off by about 20%. However, the steady state values are within 2-5%.

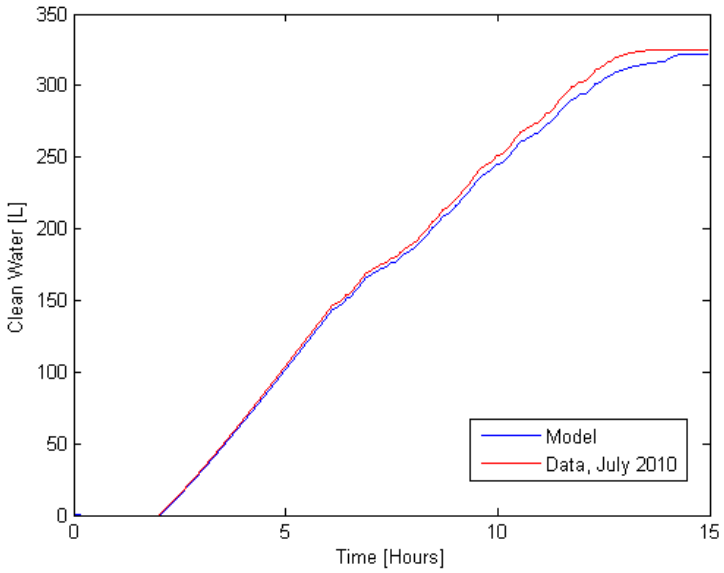

Figure A-14: Comparison of compliance energy model with experimental data for the clean water produced by the MIT PVRO system on summer day in Boston [87]

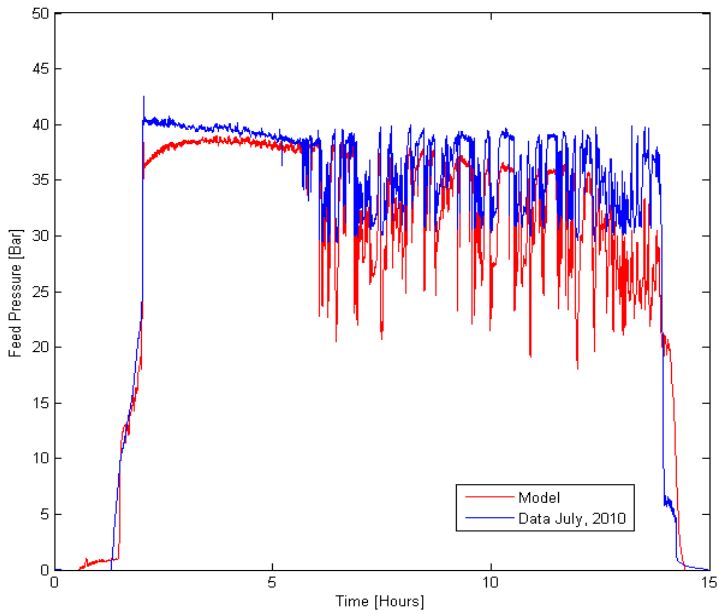

Figure A-15: Comparison of compliance energy model with experimental data for the feed pressure by the MIT PVRO system on summer day in Boston [87]

A.3.2 Control Feasibility

To effectively control a PVRO system to maximize the clean water produced, a controllable energy recovery device is needed because the energy used to pressurize the input stream cannot all be used to produce clean water at once. Hence some of the energy used to pressurize needs to be recovered and reused. The controllable energy recovery device is needed to maximize the

energy recovered at different pressures. Unlike the fixed recovery MIT PVRO experimental system, a concept system has been proposed that is comprised of solar panels mounted on a tracker, power electronics, higher pressure boost pump, check valve, RO chamber, controllable nozzle, pelton wheel and generator. This is shown in Figure A-16. Using the controllable nozzle on the brine stream, the recovery ratio can be controlled. The jet exiting the nozzle hits the cup of the pelton wheel at a certain velocity. The impact of the jet on the cup rotates the pelton wheel which is coupled to a generator. The generator feeds the power back into the power electronics and this completes the energy recovery loop. The check valve in combination with the nozzle is used to maintain a threshold pressure within the RO chamber to keep the system in an energized state.

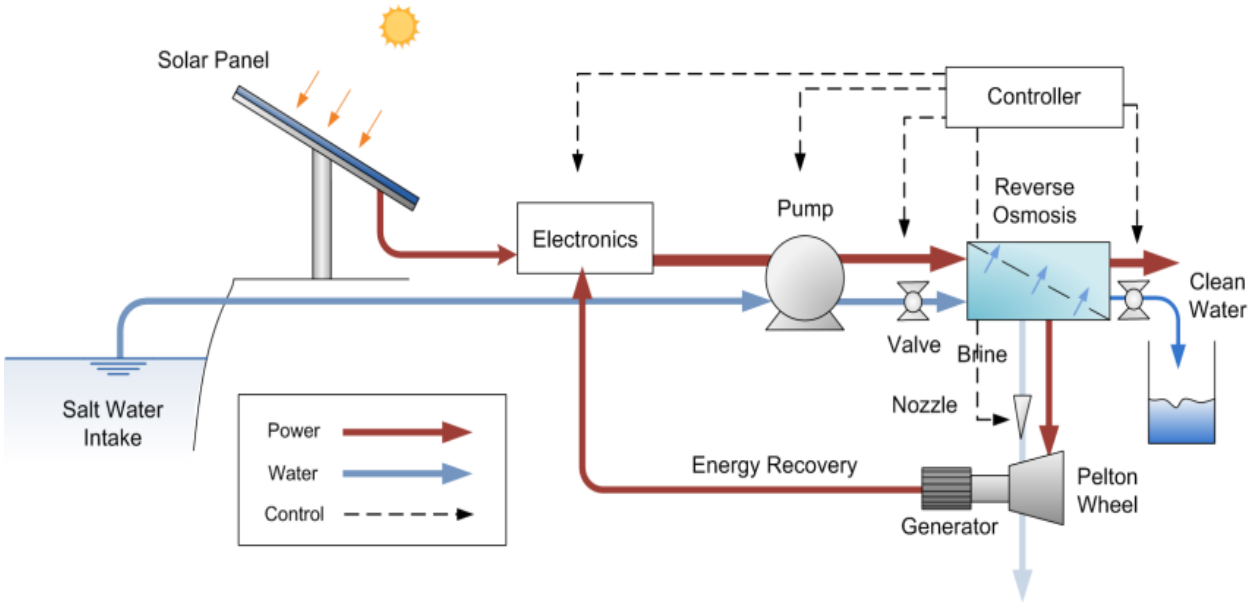

Figure A-16: Concept system with controllable energy recovery.

This system now has the following control variables:

- The DC-DC converter – This is set using the peak power tracking algorithm that maximizes the power out of the panel.
- The pump voltage – This sets the power into the pump to obtain desired pressure.
- The valve position – This maintains the pressure within the RO chamber
- The nozzle position – This is used to determine recovery ratio and jet velocity of the brine stream

- The effective load on the generator

The system is composed of four major controllers (Figure A-17). The controllers include the pump controller that throttles the pump used to pressurize the feed stream. The input variables to the pump controller are the total electrical power: the power from the panel and recovered power from the ERD, and the current pressure. The pump controller outputs a voltage to the pump to achieve a set point pressure (Figure A-18). The next controller is the minimal pressure controller, which maintains a minimal pressure with the Reverse Osmosis chamber. Its input variable is the RO chamber pressure and its output is the valve position. The next controller is the recovery ratio controller, which uses the total pressure and feed pressure (Figure A-19) measurements as inputs, and outputs a nozzle position that determines the recovery ratio, jet velocity and brine flow. The fourth controller is the generator voltage controller (Figure A-20) that sets the generator voltage. Its inputs are the turbine/generator angular velocity, nozzle jet velocity, the brine flow rate and total power to the pumps. These variables are used to determine the generator voltage. The controllers as can be seen are cascaded: the output of one controller is the input to the next one. They are designed to work concurrently to optimize water production.

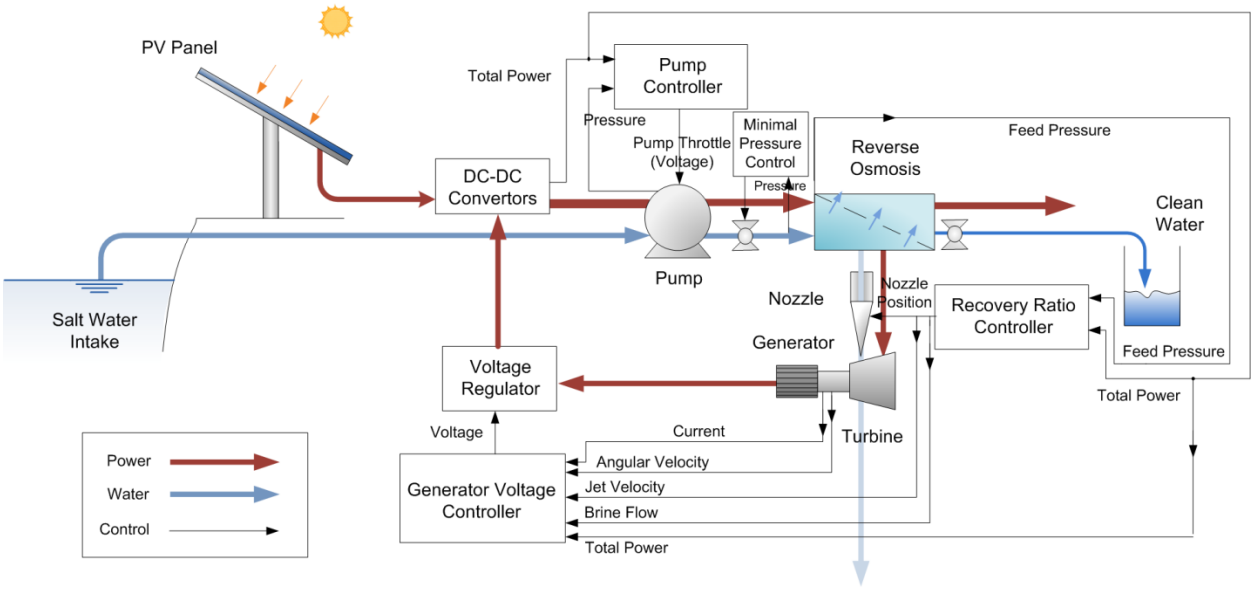

Figure A-17: Concept system showing a series of controllers used to maximize water production

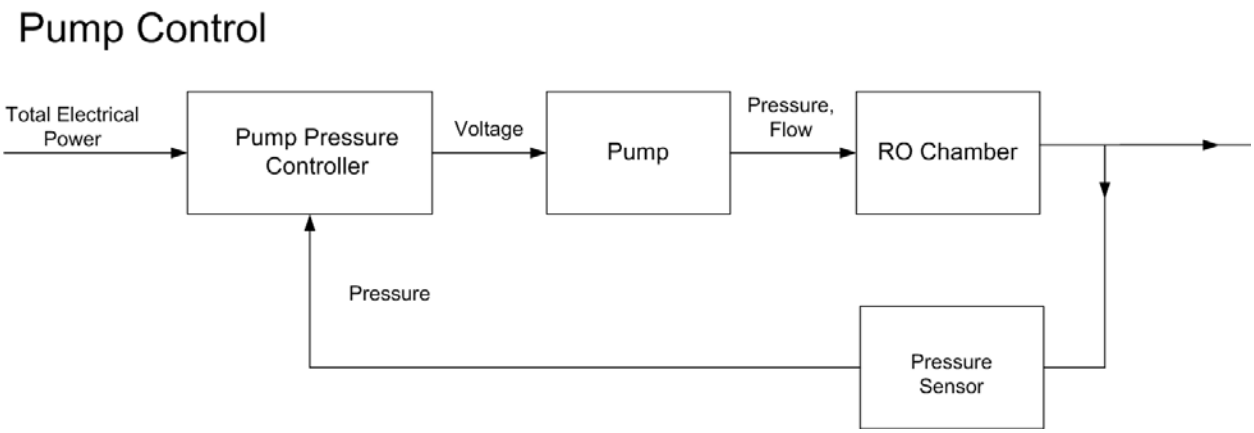

Figure A-18: Pump controller block diagram

The pump controller operates the pump by varying the voltage to achieve a desired set point pressure of the feed stream, based on current feed stream pressure and total electrical power being fed to the pumps.

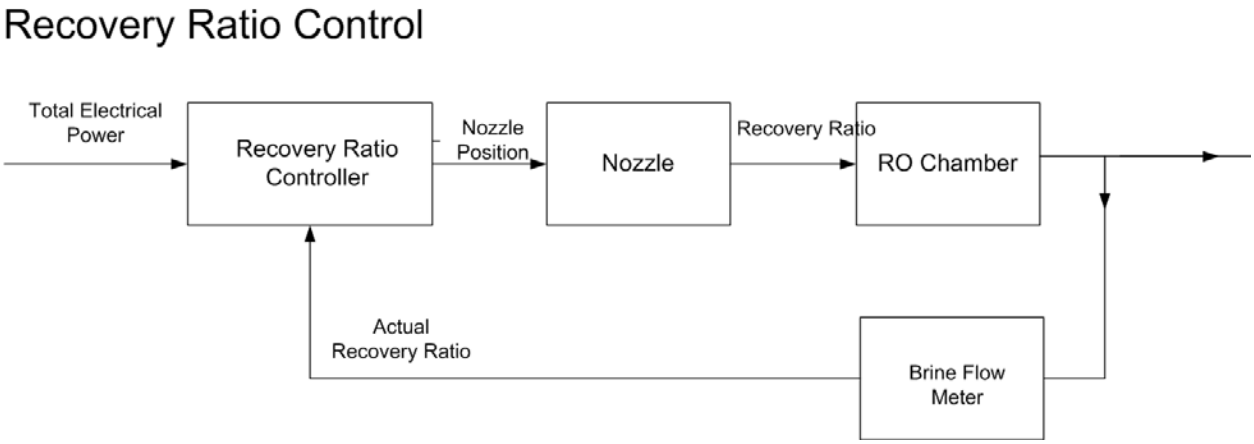

Figure A-19: Recovery ratio controller block diagram

The recovery ratio controller operates the position of the nozzle, based on the total electrical power being fed to the pumps and the current recovery ratio.

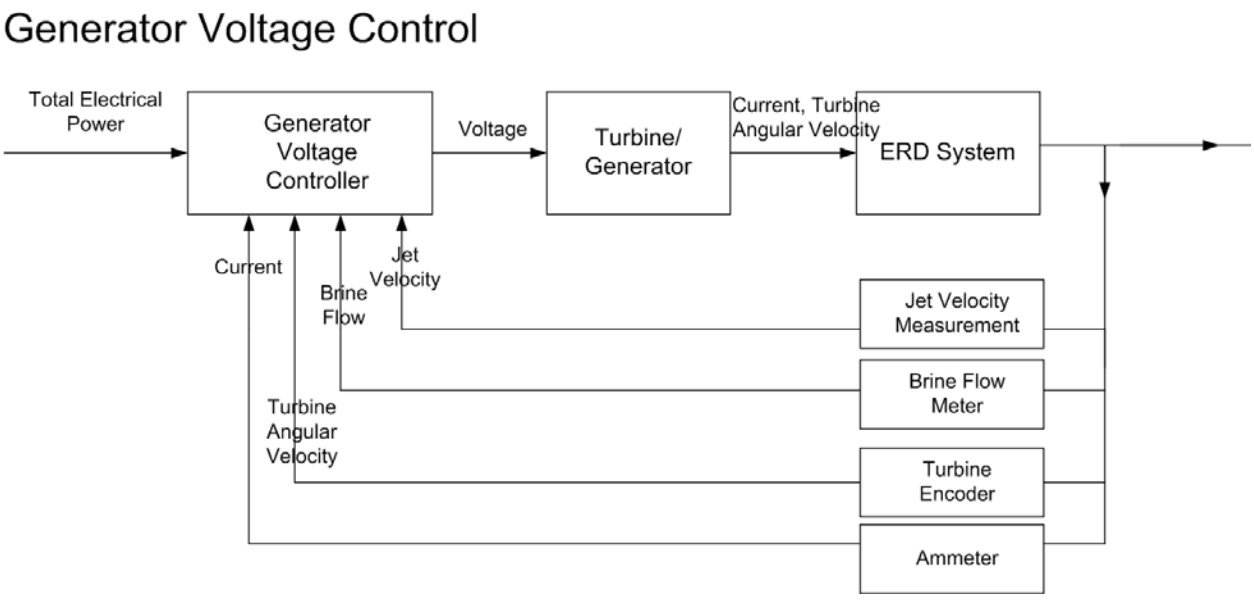

Figure A-20: Generator controller block diagram

The generator voltage is set based on the total electrical power being fed to the pumps and other variables such as the brine flow rate and jet velocity from the nozzle. In addition, other variables include the turbine angular velocity and current output from the generator.

An effective control strategy is necessary that controls recovery ratio and pressure to maximize clean water production. Once the input power from the panel and the energy recovery stream is determined, the optimal combination of recovery ratio and pressure is calculated.

At steady state, the power used to produce clean water P_{clean} is given by:

$$P_{clean} = P_{mech} - P_{brine} \quad \textbf{(76)}$$

where P_{mech} is the hydraulic power in the feed water once it has been pressurized by the pumps and P_{brine} is the hydraulic power in the brine stream. This equation can be further expanded in terms of the product q_p flow rate, q_b, brine flow rate, P_f feed pressure, P_b brine pressure as shown below:

$$q_p P_f = P_{mech} - q_b P_b \quad \textbf{(77)}$$

The brine pressure, P_b can be expressed as a function of feed pressure, P_f. There is a small difference (less than 2%) on account of losses in the RO module and this has been modeled using a pressure drop constant, k_l as follows:

$$P_b = P_f k_l \tag{78}$$

The term for the hydraulic power in the feed is expanded as the sum of the power from the panel and the power from the energy recovery stream as follows:

$$q_p P_f = P_{mech\_panel} + k_m \eta_{ERD} q_b P_b - q_b P_b \tag{79}$$

The product flow, q_p can be expressed as a function of the feed pressure, P_f, RO parameter $k(T)$ and osmotic pressure, π.

$$q_p = k\left(P_f - P_{Osm}\right) \tag{80}$$

The $k(T)$ parameter is given as follows:

$$k = A_{RO} S \tau F \tag{81}$$

where, A is the membrane area, S is the hydraulic permeability of water, τ is the TCF factor and F is the fouling factor.

The osmotic pressure, π, as a function of $k_l(T,C)$ and recovery ratio, r is given as follows:

$$P_{Osm} = k_1(T,C) \cdot e^{0.7r}\left(\frac{2-r}{1-r}\right) \tag{82}$$

where $k_1(T,C)$ is given as follows:

$$k_1(T,C) = \frac{k_s TC}{2} \tag{83}$$

where k_s is the salt concentration coefficient, C is the salt concentration and T is temperature.

The feed pressure is expressed in terms of the product flow, q_p and the recovery ratio, r. On substitution and simplification, the following quadratic equation is obtained:

$$q_p^2 + \left(k k_1(T,C) \cdot e^{0.7r}\frac{2-r}{1-r}\right) q_p - \frac{krP_{mech\_panel}}{\left[\left(1-\eta_m\eta_{ERD}\right)\left(1-r\right)k_l + r\right]} = 0 \tag{84}$$

Solving for q_p yields the following expression:

$$q_p = \frac{-kk_1 e^{0.7r}\dfrac{2-r}{1-r} \pm k\sqrt{\dfrac{k_1^2 e^{1.4r}(2-r)^2}{(1-r)^2} + \dfrac{4P_{mech\_panel}\, r}{k\left[r + k_l(1-r)(1-k_m\eta_{ERD})\right]}}}{2} \quad \textbf{(85)}$$

Thus the instantaneous steady state product flow rate can be maximized by selecting the optimal recovery ratio for a given amount of input power from the panel, temperature and salinity. However, this alone does not achieve the maximum amount of water that the system can produce over a longer duration of as little as a few minutes to a few days. To achieve this, the pressure of the feed stream must be controlled and maintained at an optimal energized level, especially when the solar insolation fluctuates or drops. Using the expression obtained for q_p , the following expression relates the feed pressure and recovery ratio for a given power produced by the panel:

$$p_{feed} = \frac{p_{critical} \pm \sqrt{p_{critical}^2 + \dfrac{4P_{mech\ panel}\, r}{k_2 k\left[r + k_l(1-r)(1-k_m\eta_{ERD})\right]}}}{2} \quad \textbf{(86)}$$

For a salt concentration of 42,000 ppm and a feed water temperature of 25 ^{o}C, the relationship between the optimal feed pressure and the panel power is shown in Figure A-21. The relationship between the optimal recovery ratio for the same conditions and panel power is shown in Figure A-22. At about 120 Watts, the pressure and recovery ratio is limited to a certain value such that the pressure is below 70 bar, the safe operating limit for most RO membranes.

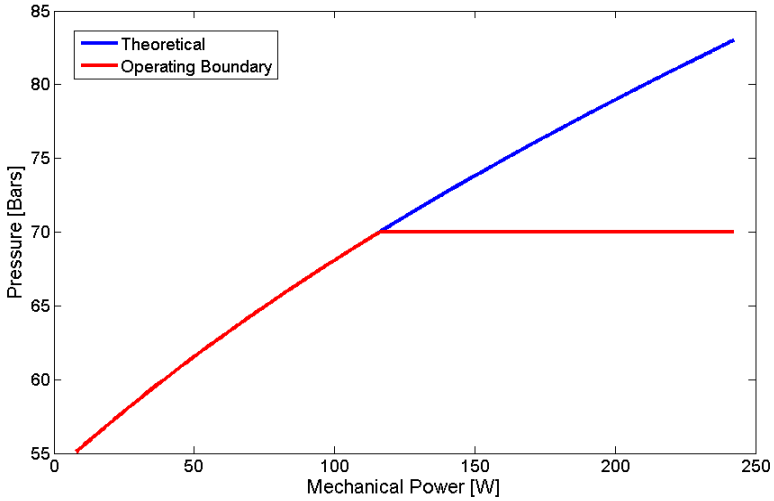

Figure A-21: Optimal pressure for input panel power [87]

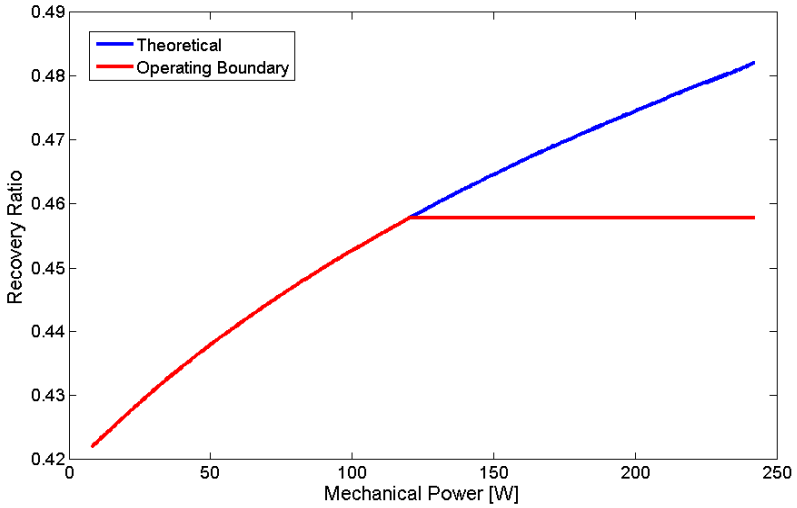

Figure A-22: Optimal recovery ratio for input panel power [87]

The optimal pressure and the optimal recovery ratio are used to maximize the amount of water produced. An important part of the system is controlling the energy recovery device. The operation of the ERD is concurrently controlled together with the pumps and recovery ratio to maximize the overall water production. This is done by setting the voltage of the voltage regulator based on the total power entering the pumps and other variables dependent on the recovery ratio, including the brine flow rate and nozzle jet velocity.

The feed pressure and recovery ratio is influenced by the feed water temperature and salinity. The effect of temperature on the operating pressure and recovery ratio used to maximize clean water is shown in Figure A-23 and Figure A-24 respectively. As the temperature increases, both the optimal feed pressure and optimal recovery ratio decreases. This can be attributed to the hydraulic permeability of RO membranes increasing as the temperature of the feed water increases. Thus, it becomes easier to push the water across the membrane at a lower feed pressure. For increased temperatures, the optimal recovery ratio and pressure drops because additional thermal energy which is microscopically kinetic energy is added to the system. This is logical, because there is no need to add additional kinetic energy, in terms of higher pressure and a corresponding recovery ratio to maximize water production.

The effect of salinity on the operating pressure and recovery ratio used to maximize clean water is shown in Figure A-25 and Figure A-26 respectively. As the salinity increases, the optimal

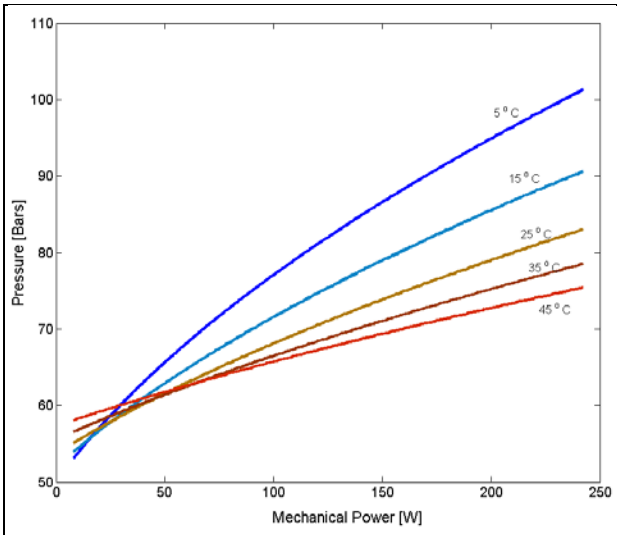

Figure A-23: Effect of temperature on operating pressure to maximize water production [87]

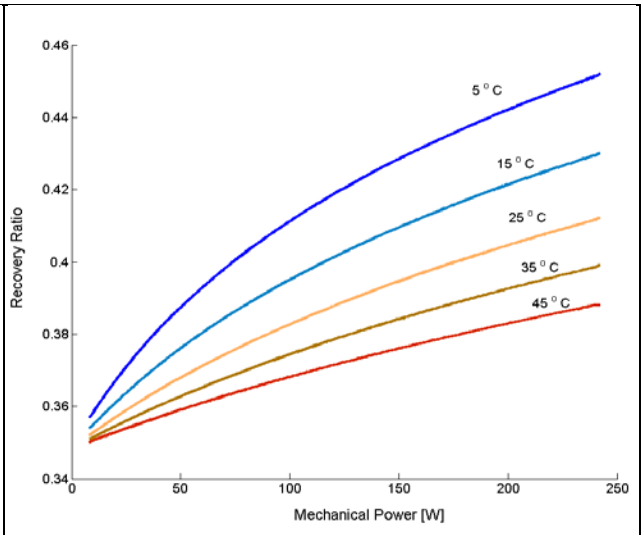

Figure A-24: Effect of temperature on recovery ratio to maximize water production [87]

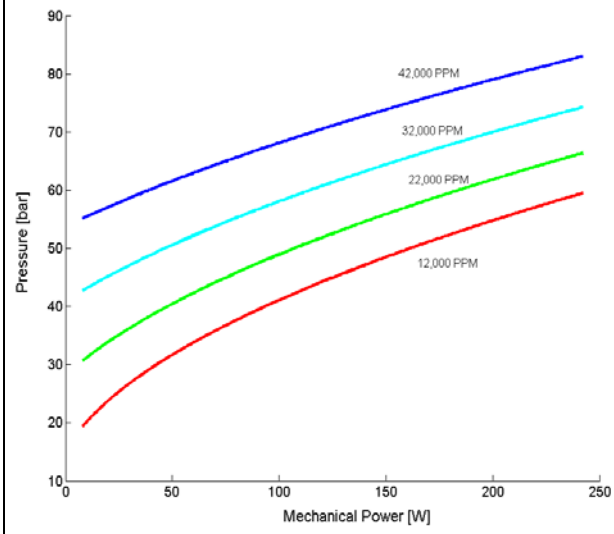

Figure A-25: Effect of salinity on operating pressure to maximize water production [87]

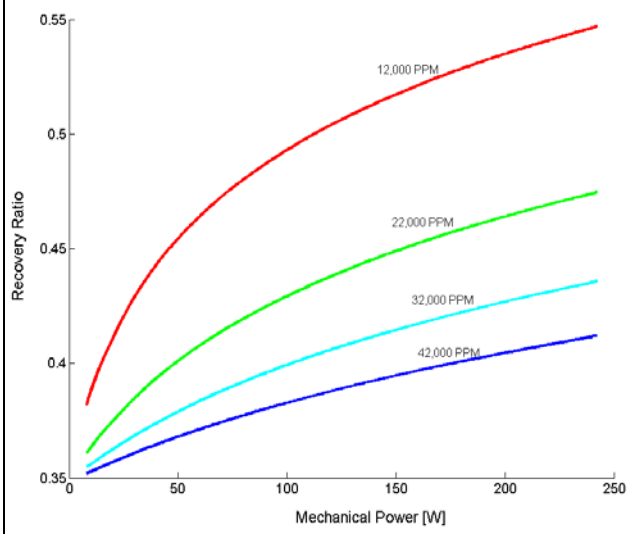

Figure A-26: Effect of salinity on recovery ratio to maximize water production [87]

pressure increases while the optimal recovery ratio decreases. Higher salinities have higher osmotic pressures, so the pressure required to overcome the osmotic pressures will be higher. This means that the optimal recovery ratios have to be lower since there is more salt in the water.

There are two principle ways of controlling the concept system based on the principles discussed in this section:

- Setting the optimal recovery ratio and feed pressure once a day such that it maximizes the water produced for an expected daily solar insolation profile.
- Actively control elements of the system to maximize the instantaneous water production

In the first approach, once the optimal recovery ratio and pressure are determined, the system is operated at this recovery ratio and pressure as long as there is sufficient power from the panels. When the power drops on account of fluctuations in the solar insolation, the pressure in the system is maintained using the valve and controllable nozzle. This reduces the energy wasted in energizing the system on account of compliance energy storage within the system. By doing this, water can be produced as soon as the power within the system is high enough to maintain the optimal pressure and recovery ratio. This approach shows an improvement of 21% over the MIT PVRO experimental system with a total clean water production of 385 liters for a July day in Boston, Massachusetts (Figure A-27).

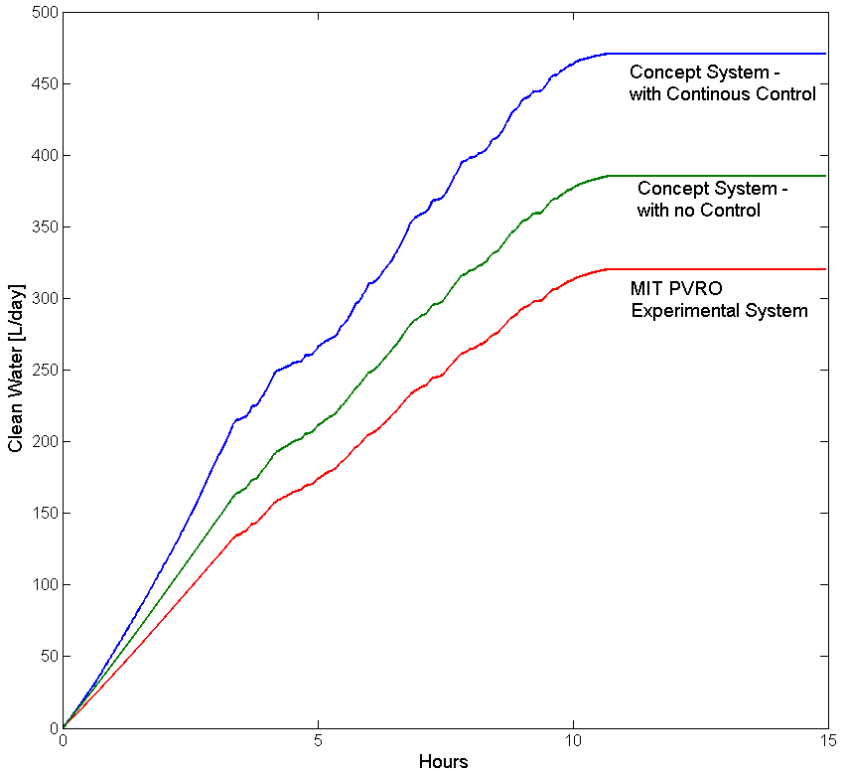

Figure A-27: Comparison of concept system performances with and without control with the MIT PVRO experimental system

The total water production for the three control approaches was simulated using Boston insolation data for an entire day in July, 2010. One is the concept system, with a controller that

maximizes instantaneous water production. Next is the controller that sets the recovery ratio and minimal threshold pressure once a day based on expected solar insolation. The third is the current MIT PVRO Experimental system.

In the second approach, the system is actively controlled depending on the fluctuations in power, temperature and salinity. This approach results in a total water production of 471 liters which is an increase of 47% over the 318 liters produced by the MIT PVRO experimental system (Figure A-27). The active control approach is the best way to operate the controllable PVRO concept system as the synchronization of all the components in the system is necessary to maximize the water produced. A key feature of this approach is the exploitation of the compliance energy storage. This compliance energy is a type of capacitance that causes delays and wasted power in energizing the system when the solar power fluctuates causing the system to start and stop. By maintaining the pressure within the RO chamber at an optimal threshold value, these delays of reenergizing of the RO system are eliminated.

This appendix presented a steady state PVRO system model that can be used to find the optimal recovery ratio that minimizes the specific energy consumption when the system is subjected to varying solar panel power, feed water salinity, feed water temperature and ERD efficiency. A comprehensive model that captures the steady state and the dynamics while accounting for the system energy compliance was also presented. The phenomenon of energy compliance in PVRO systems was identified, modeled and experimentally validated using the MIT PVRO system. Two control strategies were presented that exploit the dynamics in the system on account of energy compliance and latencies within the system. The first method requires setting the optimal recovery ratio and feed pressure for an entire day based on an expected daily solar insolation profile. The second method involves the active control of the system to maximize the instantaneous water production of the system. An improvement of 47 % over the existing MIT PVRO experimental system performance was shown using the controller simulation for the water produced by the system on a July day in Boston, Massachusetts.

Significant work still needs to be done in this area. A better understanding of the dynamics of the energy recovery loop and its interaction with the power electronics is required. This work is currently being done in the FSRL at MIT. Experimental validation of this control approach

shown in these feasibility studies is necessary. This involves the detailed design and selection of appropriate actuators, instrumentation and controller.

An important area of research once the concept experimental system is constructed is its integrity with the energy compliance model. The effect of changing the components on the dynamics of the system needs to be understood. Finally, the impact of component degradation and reliability on the system dynamics and controller performance needs to be understood.

APPENDIX

B

WATER QUALITY

Table B-1: Detailed composition of seawater at 35000 ppm salinity [88]

Element	At. weight	ppm		Element	At. weight	ppm
Hydrogen	1.00797	110,000		Molybdenum	0.09594	0.01
H2O	15.9994	883,000		Mo	101.07	0.0000007
Oxygen H2O	22.9898	10,800		Ruthenium Ru	102.905	.
Sodium NaCl	35.453	19,400		Rhodium Rh	106.4	.
Chlorine NaCl	24.312	1,290		Palladium Pd	107.870	0.00028
Magnesium	32.064	904		Argentum	112.4	0.00011
Mg	39.102	392		(silver) Ag	114.82	.
Sulfur S	40.08	411		Cadmium Cd	118.69	0.00081
Potassium K	79.909	67.3		Indium In	121.75	0.00033
Calcium Ca				Stannum (tin) Sn		
Bromine Br				Antimony Sb		
Helium He	4.0026	0.0000072		Tellurium Te	127.6	.
Lithium Li	6.939	0.170		Iodine I	166.904	0.064
Beryllium Be	9.0133	0.0000006		Xenon Xe	131.30	0.000047
Boron B	10.811	4.450		Cesium Cs	132.905	0.0003
Carbon C	12.011	28.0		Barium Ba	137.34	0.021
Nitrogen ion	14.007	15.5		Lanthanum La	138.91	0.0000029
Fluorine F	18.998	13		Cerium Ce	140.12	0.0000012
Neon Ne	20.183	0.00012		Praesodymium	140.907	0.00000064
Aluminium Al	26.982	0.001		Pr	144.24	0.0000028
Silicon Si	28.086	2.9		Neodymium Nd	150.35	0.00000045
Phosphorus P	30.974	0.088		Samarium Sm	151.96	0.0000013
Argon Ar	39.948	0.450		Europium Eu	157.25	0.0000007
Scandium Sc	44.956	<0.000004		Gadolinium Gd	158.924	0.00000014
Titanium Ti	47.90	0.001		Terbium Tb	162.50	0.00000091
Vanadium V	50.942	0.0019		Dysprosium Dy	164.930	0.00000022
Chromium Cr	51.996	0.0002		Holmium Ho	167.26	0.00000087
Manganese	54.938	0.0004		Erbium Er	168.934	0.00000017
Mn	55.847	0.0034		Thulium Tm	173.04	0.00000082
Ferrum (Iron)	58.933	0.00039		Ytterbium Yb	174.97	0.00000015
Fe	58.71	0.0066		Lutetium Lu	178.49	<0.000008
Cobalt Co				Hafnium Hf		
Nickel Ni						

Copper Cu	63.54	0.0009		Tantalum Ta	180.948	<0.0000025
Zinc Zn	65.37	0.005		Tungsten W	183.85	<0.000001
Gallium Ga	69.72	0.00003		Rhenium Re	186.2	0.0000084
Germanium	72.59	0.00006		Osmium Os	190.2	.
Ge	74.922	0.0026		Iridium Ir	192.2	.
Arsenic As	78.96	0.0009		Platinum Pt	195.09	.
Selenium Se	83.80	0.00021		Aurum (gold)	196.967	0.000011
Krypton Kr	85.47	0.120		Au	200.59	0.00015
Rubidium Rb	87.62	8.1		Mercury Hg	204.37	.
Strontium Sr	88.905	0.000013		Thallium Tl	207.19	0.00003
Yttrium Y	91.22	0.000026		Lead Pb	208.980	0.00002
Zirconium Zr	92.906	0.000015		Bismuth Bi	232.04	0.0000004
Niobium Nb				Thorium Th	238.03	0.0033
				Uranium U	(244)	.
				Plutonimu Pu		

ppm= parts per million = mg/litre = 0.001g/kg.

Source: Karl K Turekian: *Oceans*. 1968. Prentice-Hall

Table B-2: Concentration limits for typical constituents in seawater and reasons for the same

Chemical	Typical concentration in Seawater (mg/l)	Concentration limit	Reason for limit
Sodium, Na^{+}	10900	No limit. 200 mg/l is a guideline set since excess may give rise to unacceptable taste.[89][90]	No firm conclusions can be drawn about the role of Sodium on health
Magnesium, Mg^{++}	1310	Calcium and Magnesium salts cause hardness in water. No limit. 200 mg/l is suggested to limit scale deposition in the distribution system[89][91]	No hard evidence of adverse effects on human health although statistically significant relationship with cardiovascular disease exists. [89]
Calcium, Ca^{++}	410		
Potassium, K^{+}	390	No limit.	Potassium is an essential dietary constituent and hence potassium water softeners are being used as an alternative to sodium water softeners. However, some people with specific diseases or on certain medications are susceptible to hyperkaelaemia.
Strontium, Sr^{++}	13	EPA has set a limit for strontium of 4 mg/l.[92]	"Exposure to low levels of stable strontium has not been shown to affect adult health, but may harm children. Breathing or ingesting low

			levels of radioactive strontium have not been shown to affect health. High levels of radioactive strontium can damage bone marrow and cause anemia and prevent the blood from clotting properly."[92]
Barium, Ba^{++}	0.05	2 mg/l[93]	Long term exposure above the limit can cause an increase in blood pressure.[93]
Iron, Fe^{++}	<0.02	0.3 mg/l[93]	This is a secondary water regulation that may or may not be enforced.
Manganese, Mn^{++}	<0.01	0.05 mg/l [93]	This is a secondary water regulation that may or may not be enforced.
Chloride, Cl^{-}	19700	250 mg/l [93]	This is a secondary water regulation that may or may not be enforced. However, this affects the taste of the water.
Sulfate, SO_4^{-2}	2740	250 mg/l [93]	This is a secondary water regulation that may or may not be enforced.
Bicarbonate, HCO_3^{-}	152	30 mg/ minimum. 250 – 500 mg/l permissible.[89]	
Bromide, Br^{-}	65	0.01 mg/l for bromated.[93]	Long-term exposure above the specified limit increases the risk of cancer.[93]
Fluoride, F^{-}	1.4	4 mg/l. [93]	Long-term exposure above the specified limit causes bone disease (pain and tenderness of the bones); children may get mottled teeth[93]
Nitrate, NO_3^{-}	<0.7	10 mg/l [93] 50 mg/l, short term exposure. [89]	Long-term exposure above the specified limit affects infants below the age of six months and they can become seriously ill and, if untreated, may die. Symptoms include shortness of breath and blue-baby syndrome. [93]
Silica, SiO_2	0.04~8	No limit.	
Boric Acid, $B(OH)_3$ or Borate, BO_3^{-}	4-5	0.5 mg/l [89]	Can be toxic. Tests have shown toxicity in reproductive areas of male rats and decreased fetal body weights in rats.
Total dissolved solids, TDS	0	500 mg/l[93]	Excessive TDS can have laxative effects.